DOE/JPL/954465-2

SILICON SHEET GROWTH BY THE INVERTED STEPANOV TECHNIQUE

Final Report

By
K. M. Kim
S. Berkman
M. T. Duffy
A. E. Bell
H. E. Temple
G. W. Cullen

June 1977

Work Performed Under Contract No. NAS-7-100-954465

RCA Laboratories
Princeton, New Jersey

U.S. Department of Energy

Solar Energy

DISCLAIMER

NOTICE

DOE/JPL/954465-2
Distribution Category UC-63b

PRRL-77-CR-22

SILICON SHEET GROWTH BY THE INVERTED STEPANOV TECHNIQUE

K. M. Kim, S. Berkman, M. T. Duffy, A. E. Bell,
H. E. Temple, and G. W. Cullen

RCA Laboratories
Princeton, New Jersey 08540

FINAL REPORT

JUNE 1977

This work was performed for the Jet Propulsion Laboratory, California Institute of Technology, under NASA Contract NAS7-100 for the U. S. Department of Energy (DOE).

The JPL Low-Cost Silicon Solar Array Project is funded by DOE and forms part of the Photovoltaic Conversion Program to initiate a major effort toward the development of low-cost solar arrays.

Prepared Under Contract No. 954465 For
JET PROPULSION LABORATORY
CALIFORNIA INSTITUTE OF TECHNOLOGY
Pasadena, California 91103

RCA

PREFACE

This Final Report was prepared at RCA Laboratories, Princeton, New Jersey, under JPL Contract No. 954465. The work performed in the period March 22, 1976 to May 31, 1977 is described. The work was carried out in the Materials and Processing Research Laboratory. P. Rappaport was the Director to May 1, 1977. Subsequent to this date, H. Kressel is the Director of this Laboratory. G. W. Cullen is the Project Manager. The contributors to this report are as follows:

S. Berkman, K. M. Kim, and H. E. Temple — silicon ribbon growth studies

A. E. Bell — thermal analysis

M. T. Duffy — reactivity studies

S. Berkman and M. T. Duffy — CVD of Si_3N_4 and $Si_3O_xN_y$

S. H. McFarlane — x-ray topography

R. V. D'Aiello and P. H. Robinson — fabrication and measurement of the epitaxial solar cell

G. W. Cullen and R. E. Novak — technical consultation on the silicon ribbon growth

K. M. Kim and G. W. Cullen — report editing

The JPL Project Monitor is K. M. Koliwad.

This report was submitted by the authors in June 1977.

TABLE OF CONTENTS

TABLE OF CONTENTS (Cont'd.)

LIST OF ILLUSTRATIONS

LIST OF ILLUSTRATIONS (Continued)

LIST OF TABLES

SECTION I

SUMMARY

The feasibility of growing silicon ribbons by the inverted ribbon growth process has been established using both nonwetting boron nitride (BN) dies as well as wetting composite dies coated with chemically vapor deposited silicon nitride (CVD Si_3N_4). The former can be termed as the inverted Stepanov process, the latter as the inverted edge-defined film-fed growth (EFG) process. Flat die and V-shaped crucible-die configurations have been employed.

The shift of the die material from nonwetting BN to nonwetting SiO_2 was more difficult than anticipated. Even though a SiO_2 die was readily filled with the liquid silicon to the edge of the die slot, ribbon growth was not stable. The growth instabilities are associated primarily with the formation and evolution of the silicon monoxide; the escape of the gas causes hysteresis of the contact angle and mechanical vibration of the melt. As a result of this, the meniscus during the ribbon growth is not "pinned" at the die edge but is in constant motion, and growth is difficult to initiate.

The V-shaped susceptor has been modified to decrease the vertical gradient inside the susceptor in order to minimize the SiO formation and the related hysteresis. Furthermore, in an effort to improve "pinning" the meniscus at the die edge, three different die designs were used. A pressure differential has also been applied across the melt in an effort to suppress the hysteresis. Various types of thermal trimmers have been used in an attempt to provide suitable thermal gradients at the solid-liquid ribbon growth interface. Although real progress was made, the instabilities have not been suppressed sufficiently to allow for initiation of ribbon growth.

Preliminary evaluation of the reactivity of liquid silicon with CVD Si_3N_4 and CVD $Si_3O_xN_y$ indicated that these materials are considerably more resistant to reaction with and/or dissolution in silicon than other materials examined to date. Reaction-sintered (RS) Si_3N_4 and UT-8 (AG) graphite were found suitable, in ribbon growth tests, as the die material to be coated with CVD Si_3N_4. The contact angle of CVD Si_3N_4 with liquid silicon is 53°.

Silicon ribbon growth was carried out using CVD Si_3N_4 coated composite dies in the V-shaped crucible-die configuration. Stable growth of silicon ribbons (2 cm wide, ~0.05 cm thick) was achieved by using curved dies

coated with CVD Si_3N_4; the radius of curvature at the die edge was 8.9 cm. The growth orientation was (011)[$\overline{2}$11]. The crystallinity and defect structures were characterized by x-ray topography. The ribbons were, in general, composed of long grains and twins aligned with the growth direction. The misorientation between grains was ~0.1°. The resistivity of the ribbons was low, i.e., ~0.020 ohm-cm, because of the contamination in the growth system. It was not feasible to fabricate solar cells in the ribbons because of the low resistivity. More recent elimination of BN parts has led to the maintenance of the melt at a level of 80 ohm-cm p-type.

Solar cells made in the epitaxially deposited silicon on a silicon ribbon grown by the inverted Stepanov process with the BN flat die had an efficiency of 8.2% (AM1). At the time these measurements were made, the CVD silicon overlayer had not been optimized by grading the dopant level. Under these circumstances, similar efficiencies were observed in CVD silicon on EFG ribbon.

The stability of seeding with pyrolytic BN die has been analyzed by evaluating the surface-free energy of the system prior to and after the seeding. The interfacial free energy between the liquid and solid silicon is less than one-half the liquid surface tension; this enhances the stability of seeding and supplies a driving force to overcome the capillary depression in the pyrolytic BN die with a contact angle of 110°. Using the proper melt height, the hydrostatic pressure in the melt due to the gravitation contributes to this driving force in the inverted Stepanov configuration. It is of interest to note that stability of the ribbon growth, in terms of the dependence of the ribbon thickness on the change in the meniscus height, is theoretically greater in the inverted Stepanov or inverted EFG than in Stepanov or EFG process.

A one-dimensional heat flow model has been developed to simulate numerically the major thermal aspects of the inverted Stepanov growth process. Our results show that for a given ribbon geometry, die temperature and ambient configuration, the height of the molten zone increases as the growth velocity is increased. At the critical maximum velocity, where the rate of generation of latent heat of fusion approaches the total heat energy which can be dissipated from the ribbon to its ambient, the zone height diverges rapidly and growth will be terminated. The highest growth

velocities are therefore achieved with the lowest ambient temperatures coupled with experimental configurations which maximize the convective heat transfer coefficient as well as the conducted heat loss to the ribbon support clamp. We have investigated the curvature in the temperature profile along the growing ribbon as a function of the ambient configuration and demonstrate a particular case where the profile is substantially linearized while still maintaining a reasonable growth velocity. Such a linearized temperature profile is important in keeping the thermal stresses along the growing ribbon to a minimum.

SECTION II

INTRODUCTION

A. OBJECTIVE

The inverted ribbon growth program was originally started to provide shaped crystal growth by use of nonwetting dies as an alternative method to the conventional Stepanov [1] and edge-defined film-fed growth (EFG) or capillary action shaping technique (CAST) [2,3] processes. Figure 1 is a schematic representation of silicon ribbon growth in the inverted ribbon growth configuration. Using this setup, die liner materials can readily be employed which have contact angles spanning those required for either EFG (wetting) or Stepanov growth (nonwetting). Ribbon growth with the wetted and nonwetted die in the inverted configuration can be identified as the inverted EFG and inverted Stepanov processes, respectively.

The overall objective of the inverted ribbon growth program is to maintain the potential for economical silicon sheet growth characteristic of the EFG (or CAST) process [2,3] while minimizing the interference with crystal growth which results from the reaction between the die and the molten silicon.

B. BACKGROUND

The conventional silicon ribbon growth methods employing a shaping guide or die are the Stepanov technique [1] and the edge-defined film-fed growth (EFG) [2]. The latter process has also been referred to as the capillary action shaping technique (CAST) [3]. The ribbon growth arrangements by Stepanov and EFG process are shown schematically in Fig. 2. The shaping of the meniscus for the ribbon geometry is controlled by the

1. A. V. Stepanov et al., Bull. Acad. Sci. USSR, Phys. Series 33, 1826 (1969); A. V. Stepanov, Transl. Soviet Phys. Technical Physics 29, 339 (1959).
2. J. C. Schwartz, T. Surek, and B. Chalmers, J. Electronic Mat. 4, 255 (1975); H. E. Bates, F. H. Cocks, and A. I. Mlavsky, "Thick Film Silicon Growth Techniques," NAS7-100/JPL-953365, First Quarterly Progress Report, July 1972.
3. T. F. Ciszek, Mat. Res. Bull. 7, 731 (1972).

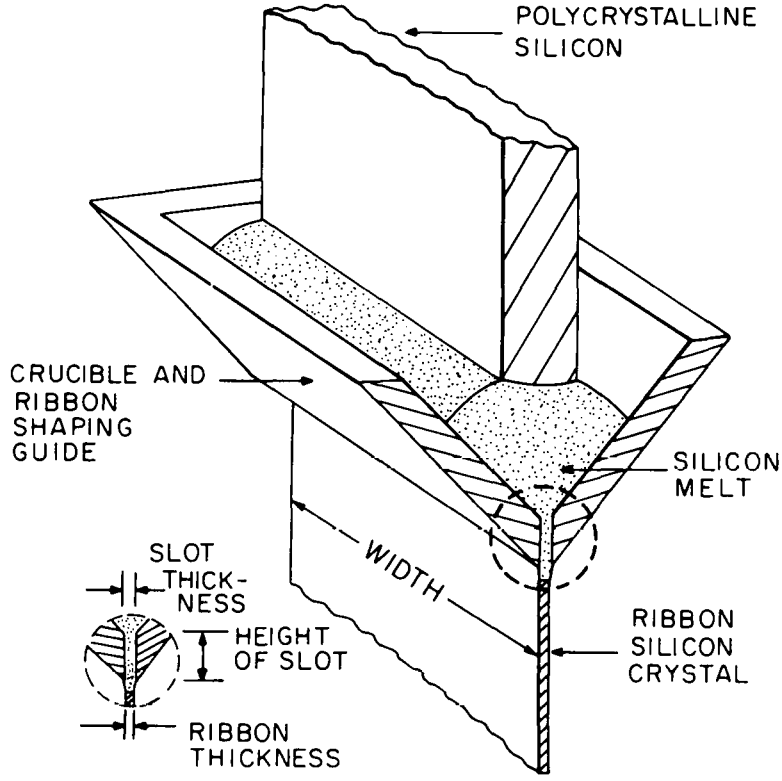

Figure 1. Schematic drawing of silicon ribbon growth by the inverted ribbon growth process.

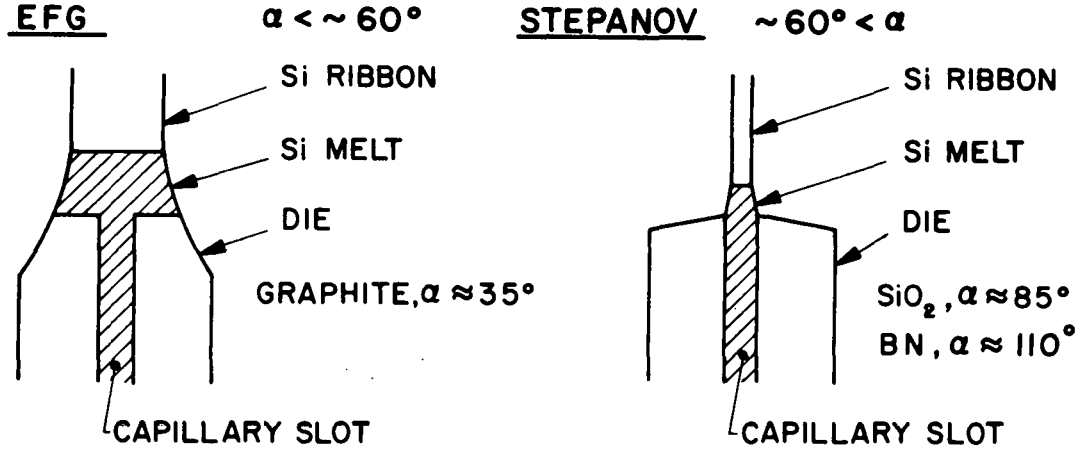

Figure 2. Schematic representation of the silicon ribbon growth with EFG and Stepanov process. α is the contact angle of the die material with the molten silicon.

capillary shape, i.e., the inner dimension of the die in the Stepanov case, while this occurs at the outer edge of the die in EFG.

The main difference in the two methods lies in the range of the applicable contact angles (α) of the die material with the liquid silicon. In EFG, the contact angle must be significantly less than 90°, which is commonly referred to as "wetting"; a typical die material is graphite with $\alpha \approx 30°$. On the other hand, in the Stepanov method a die is used with a contact angle slightly less or larger than 90°, commonly called "nonwetting" die; fused silica with $\alpha \approx 87°$ has been successfully tested as a die in a special Stepanov configuration where the capillary height was small, i.e., 0.04 cm [4].

The capillary action or capillary rise is proportional to cos α at a given capillary dimension. For materials used in EFG α is low, and thus the capillary action is sufficiently high to feed the melt to the top of the die. However, in the Stepanov case, α is close to or higher than 90°, and thus the capillary action is not sufficient to feed the melt to the die edge in practical systems used to date. For instance, the capillary rise for a 0.05 cm thick slot in quartz, assuming $\alpha \approx 87°$, is 0.6 cm. Therefore, external pressure must be applied to the melt either hydrostatically or mechanically. Alternatively, an extremely small capillary height must be used.

We have succeeded in partially compensating for the lack of capillary rise with nonwetting dies by inverting the Stepanov growth configuration, i.e., growing the silicon ribbon downward and melting the lower end of the polycrystalline silicon charge, as represented schematically in Fig. 1. The hydrostatic pressure in the melt due to the gravitation can, with sufficient melt height, enhance the feeding of the melt to the die edge. Silicon ribbons up to 2 cm in width have been grown with a pyrolytic boron nitride die with $\alpha \approx 110°$.

In EFG with the wetted graphite die, the degradation of crystalline quality is associated in part with inclusions of silicon carbide in the ribbon which result from erosion of the die by silicon. The use of a nonwetted die or wetted die of less reactivity than graphite with the molten silicon provides the possibility to minimize or eliminate the reaction between silicon and the die, and thus to minimize or eliminate the associated degradation in the crystalline quality of grown ribbons.

4. P. C. Goundry and J. C. Boatman, "Investigation of Single Crystal Si Ribbon," AFAL-TR-66-312, Part I, Sept. 1966, and Part II, Oct. 1967.

C. PROGRAM

Fused silica and pyrolytic boron nitride were employed initially as the nonwetted die materials. Silica is chosen because it contaminates silicon only with oxygen. Silicon ribbons of good crystalline quality have been grown in a Stepanov configuration using silica dies (with a small capillary height) [4]. However, the relative mechanical softness of silica at the growth temperature is of some disadvantage. The other die material, pyrolytic boron nitride, was used to investigate the important parameters in the inverted Stepanov growth and to examine any inherent limitations in ribbon thickness.

Very encouraging results have been realized in the inverted Stepanov configuration using boron nitride dies. Stable growth of 0.05-cm-thick ribbons has been achieved. It was known that the boron nitride would result in heavy doping of the silicon, but the mechanical integrity at the ribbon growth temperature and the appropriate wetting angle for Stepanov growth (110°) made it an attractive test vehicle for this process.

After initial experiments with a flat-die inverted Stepanov configuration, a V-shaped die was designed and put into use (Fig. 1). The V-shape was originally introduced to compensate for the lack of mechanical strength of silica at the temperatures required for the growth of silicon. This geometry has also proven to be useful in expediting the growth experiments since flat plates can be used as the liner of the die. Thus, the die slot dimensions and the position of the edge of the die in relation to the hot susceptor can be readily altered without the necessity for precision machining.

In light of our experience with boron nitride and the experience of other investigators with silica dies [4], we had anticipated that the use of silica in the V-shaped geometry would offer a viable solution to the boron doping problem. It was felt at that time that the major problem with silica was the softness at the growth temperature, and that the mechanical support available with the V-shaped configuration would minimize this problem. Difficulties experienced with the growth using silica dies were

initially associated with feed and/or thermal gradient problems. After a good deal of experimentation, however, it has become clear that the problems encountered have been associated mainly with the generation of silicon monoxide and the escape of the gas from the silicon-die interface. Efforts have been directed toward the suppression of the instabilities associated with the gas evolution. We have found, however, that the use of fused silica dies is comparatively difficult because of the hysteresis of the contact angle as the result of the formation and evolution of silicon monoxide at the interface between the silica die and the liquid silicon. The hysteresis prevents "pinning" the meniscus at the die edge to establish effective meniscus shaping for the initiation of ribbon growth. Even though the growth instabilities associated with the hysteresis of the contact angle do not necessarily appear to be insurmountable, it was decided that more rapid progress (in light of the JPL time goals for growth of ribbon not more than 0.025 cm thick) would be achieved using die materials other than fused silica.

Vapor-deposited silicon nitride (Si_3N_4) was evaluated as the die surface material on this program. Substrate materials such as reaction sintered Si_3N_4 and graphite were coated with Si_3N_4 by chemical vapor deposition (CVD). The CVD Si_3N_4 has a contact angle of 53°. While the contact angle between the molten silicon and the CVD Si_3N_4 is sufficiently low to provide capillary rise, the inverted V-shaped configuration was maintained, partly because of the ease of employing CVD-coated flat plates as the liner material. The possibility of employing the CVD Si_3N_4 had developed after carrying out sessile drop experiments to evaluate the reactivity of various chemically deposited materials in contact with the molten silicon. Subsequent to the work with the CVD Si_3N_4, CVD silicon oxynitride (SiO_xN_y) was examined in sessile drop experiments. This material also appears to be very promising as a die surface material. There was not time on this contract effort, however, to test the CVD SiO_xN_y (on an appropriate substrate) in ribbon growth experiments.

Since the success of this ribbon growth process is so critically dependent on the thermal configuration, a detailed theoretical thermal analysis of the method has been made. This analysis not only provides important guidance for design of the apparatus, but also brings to light what may prove to be some fundamental limitations on the growth rate. An appreciation of these limitations could lead to the configuration providing the maximum growth rate possible with this process.

SECTION III

INVERTED SILICON RIBBON GROWTH PROCESS – APPARATUS AND GROWTH PROCEDURE

A. GROWTH APPARATUS AND COMPONENTS

1. Introduction

The silicon ribbon growth in the inverted ribbon growth configuration is represented schematically in Fig. 1. The silicon ribbon is pulled downward using dies positioned inside a fused silica chamber. Induction heating is employed in conjunction with a work-coil and graphite susceptor. The titanium-gettered argon (5 ft^3/h) at atmospheric pressure provides a clean growth ambient.

The ribbon growth apparatus, Model 1, which has been employed during this contract, has a limited capability regarding the stroke (15 cm) and pull rate of the silicon ribbon (150 cm/h). The overall view of the Model 1 apparatus is shown in Fig. 3. A new ribbon growth apparatus, Model 2, was designed and built during the contract to avoid the limitations associated with the Model 1. Model 2 puller, shown in Fig. 4, has a stroke of 70 cm and a pull rate up to 400 cm/h. Furthermore, Model 2 is designed for mechanical rigidity, and the pull mechanism has a mechanical alignment within 12 μm per 30 cm stroke. This is achieved through the use of a precision-ground lead screw.

Details of the components of the Model 1 apparatus, which are also applicable to the Model 2, are presented below.

2. Power Source, Work-Coil, and Temperature Control

A 15 kVA/450 kHz rf generator (Model T-15-3-KC-EH, Lepel) is employed with a closed cooling water recirculating system. In the current ribbon growth conditions, about 50% of the output is sufficient. A five-turn coil is found to have a satisfactory impedance matching in the current growth arrangement. The coil is 10.2 cm i.d. and 11.5 cm o.d. and is made of flat copper tubing. A proportional controller with a closed loop feedback (Bruce units, NBS Associates) is used with an rf pickup as a sensor; the Bruce units are a Bruce 101 precision set point amplifier, a Bruce 410 current output controller, and a Bruce 326 control module with anode voltage

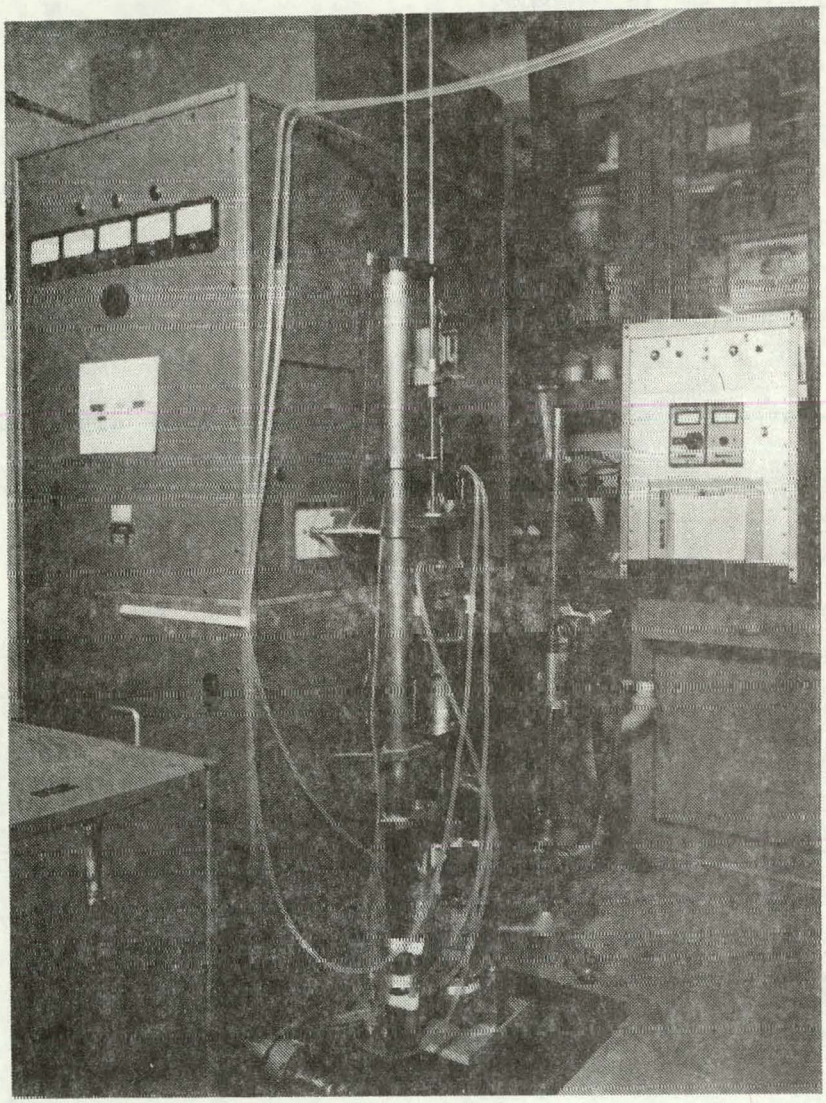

Figure 3. The inverted silicon ribbon growth apparatus (Model 1).

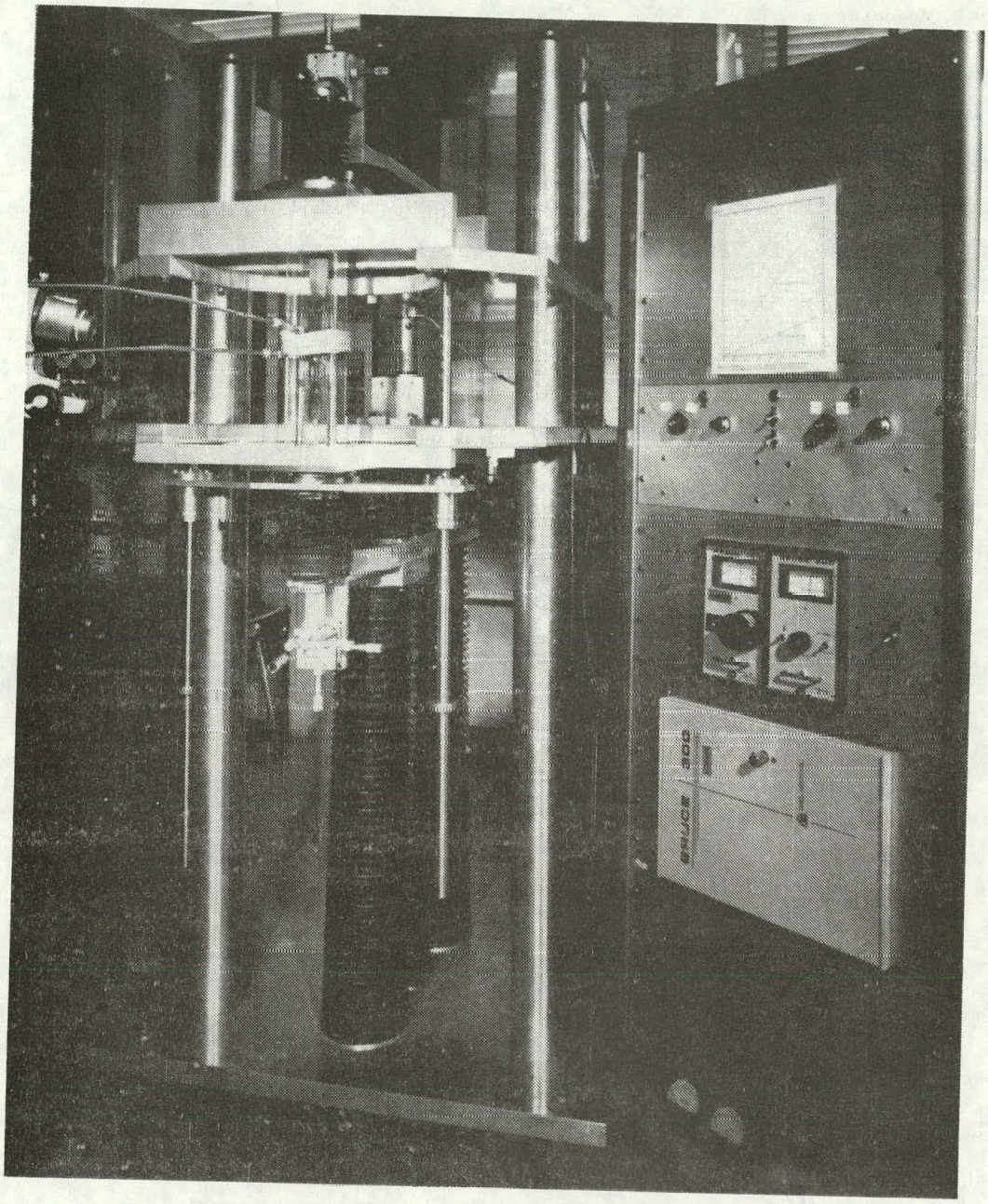

Figure 4. The inverted silicon ribbon growth apparatus (Model 2).

feedback. The power input to the load (susceptor) is controlled and kept constant.

3. Pulling Mechanism of the Silicon Ribbon and Feeding Mechanism

A Motomatic drive system (Type E-550, Electro-Craft Corp.) coupled to a linear motion assembly is employed. The Motomatic drive system consists of two basic units, i.e., a permanent magnet dc motor generator and a solid-state electronic controller. The set speed is maintained constant regardless of changes in load or line voltage fluctuation.

A calibration curve of the pull and feed rate vs the set point of the motor controller is shown in Fig. 5.

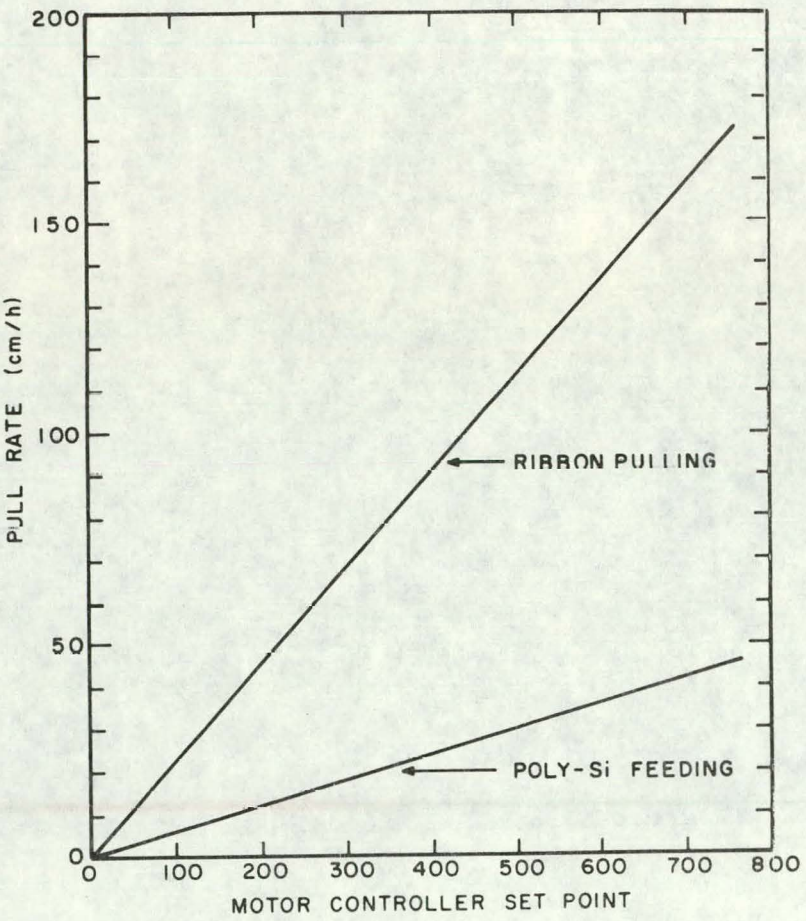

Figure 5. Calibration curve of the ribbon pull and polycrystalline silicon feed rate vs the set-point of the motor control.

An XYZ-micromanipulator (Line Tool Co.) is incorporated in the linear motion assembly. The seed is aligned exactly inside the die slot or capillary at the ambient temperature and realigned, if necessary, during the seeding or ribbon growth. For the fine alignment and observation of the meniscus height during the ribbon growth, a stereoscopic microscope (American Optical, Inc.) is used. An XYZ-micromanipulator is also built into the feeding mechanism.

4. Die and Susceptor Assembly

Two kinds of die-susceptor assembly have been employed. The first consists of a flat plate with a rectangular slot, which is positioned inside a rectangular graphite susceptor on top of a pyrolytic graphite plate with a larger slot opening than the die. The pyrolytic graphite has a relatively high and anisotropic thermal conductivity. The thermal conduction is 200 times higher on the "a-b" plane than along the c-axis. By positioning the high conductivity "a-b" plane in the horizontal direction, a flat isotherm along the die slot and a high vertical thermal gradient are established. This die-susceptor configuration has been used prior to and during the initial part of the contract effort. Stable ribbon growth with pyrolytic BN flat die was achieved, which will be described in Section IV.A.1. As the second die-susceptor assembly, a rectangular graphite susceptor with a V-shaped geometry is used. In this configuration, flat plates (two rectangular and two triangular pieces) which constitute the die are positioned inside the V-shaped susceptor as shown in Fig. 6. This die-susceptor assembly has been employed mostly during the contract. SiO_2 and composite dies coated with CVD Si_3N_4 were used.

In the case of SiO_2 die, the ends of the plates are fused to the triangular end pieces to form a crucible and thus to better contain the liquid silicon. One end of the SiO_2 plate is ground in angle, i.e., 30° in the present geometry, and is provided with a recess in the middle section which forms the capillary slot when two pieces are joined together in the V-shape. Details of the die and susceptor assembly are reproduced in Fig. 6. Ribbon growth with SiO_2 die will be described in Section IV.A.2. In the case of the composite dies coated with CVD Si_3N_4, the flat plates are positioned inside the susceptor with thin pyrolytic BN plates (0.025 cm

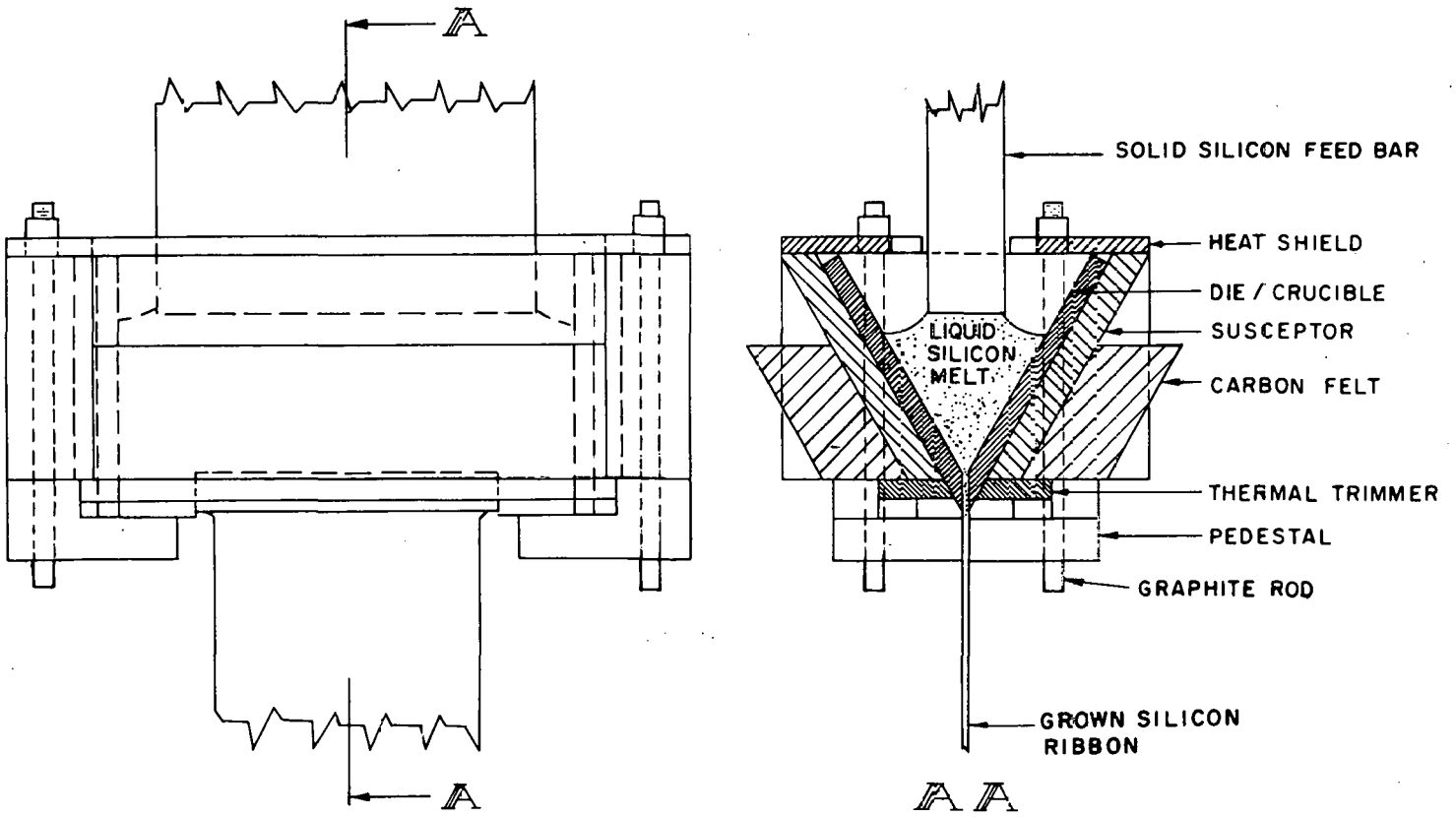

Figure 6. A schematic drawing of the V-shaped susceptor and crucible-die assembly in the inverted silicon ribbon growth process.

thick) as inserts between the die and susceptor. These inserts are necessary because the contact angle of the CVD Si_3N_4 is 53°, and thus molten silicon could leak through the joints of the die plates. A high doping level in the silicon ribbons grown with the CVD Si_3N_4 composite die is partly caused by the presence of the BN insert (see Section VI.B).

Some advantages of the V-shaped die-susceptor configuration are:

(1) The arrangement is simple, and the crucible-die can be easily assembled out of simple flat plates;

(2) Mechanical support is provided for the die, which is desirable for the die materials such as SiO_2 which soften to a certain extent at the silicon crystal growth temperature;

(3) The amount of the melt required is relatively small, and continuous charging of the polycrystalline silicon is easily implemented;

(4) The vertical temperature gradient can be high, which is desirable for the high growth rates;

(5) Thermal trimmers can be added easily to adjust the horizontal isotherm as well as the vertical thermal gradient at the solid-liquid growth interface;

(6) New die materials can be easily tested under real ribbon growth conditions.

B. EXPERIMENTAL PROCEDURES

1. Thermal Gradient Trimming

For the silicon ribbon growth, a low horizontal temperature gradient is required to maintain the width of the ribbon, and a high vertical temperature gradient is necessary to achieve a high growth rate. In the growth configuration with a flat die and rectangular susceptor, satisfactory thermal gradients were established by positioning the die plate on top of the pyrolytic graphite plate with the high conductivity "a-b" plane parallel to the die plate (see Section III.A.4).

The thermal gradients in the V-shaped die-susceptor configuration can be trimmed by adding thermal modifiers such as graphite felt insulation on the susceptor and laying graphite plates in intimate contact with the die edge and the susceptor.

A series of the thermal trimmers which have been tested to adjust the thermal gradient at the solid-liquid (s-ℓ) growth interface are shown in Fig. 7. The thermal trimmers consist of basically three types in various combinations. The first is a pyrolytic graphite (PG) plate with the low-conductivity c-axis parallel to the ribbon growth direction. The second type is a PG plate of the same orientation as the first type, which is positioned inside a rectangular graphite. The last type is an L-shaped graphite piece. The pyrolytic graphite trimmer was not as effective in the V-configuration as in the flat die geometry in providing satisfactory thermal conditions. With the SiO_2 die in the V-configuration, the ribbon width was always decreasing, while ribbon thickness was increasing continually during growth. This occurred with all combinations of thermal trimmers shown in Fig. 7. The main cause for the growth instability was found to be the hysteresis of the contact angle and the lack of "pinning" the meniscus at the die edge. But we felt at that time that unsatisfactory thermal gradients at the meniscus were responsible

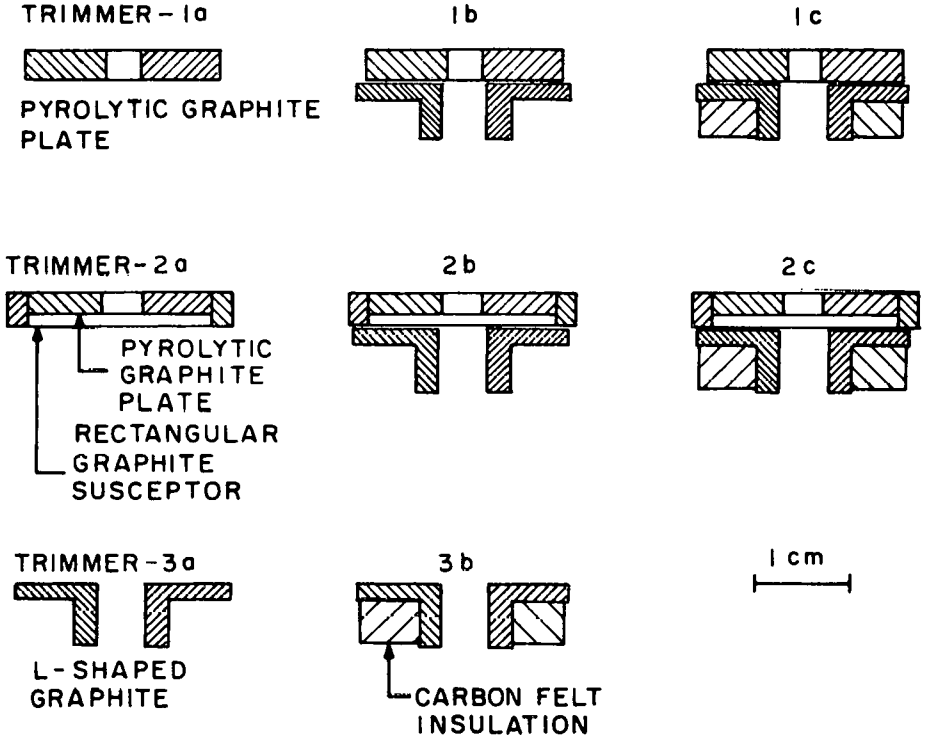

Figure 7. Cross-sectional view of the thermal trimmers used in the V-shaped configuration to control the thermal gradients at the s-ℓ ribbon growth interface.

for the instability, and thus we measured the temperature distribution at the die edge to find suitable thermal trimmers, as will be described in the next section.

2. Temperature Profiling

The thermal gradients in the V-shaped die-susceptor configuration have been measured. The ribbon growth apparatus, Model 1, was modified so that the thermocouple could be moved within the system in order to measure the horizontal and vertical temperature gradients continuously at high temperatures. By grounding the susceptor and the metal shield of the thermocouple we were able to use an unshielded thermocouple junction and to measure more realistic temperature distributions without rf interference. Two kinds of thermocouples of fine gauge wires were used: Chromel/Alumel of 0.02 cm diameter and PT-13%Rh/Pt of 0.025 cm diameter. Figure 8 is a schematic of the temperature measurement arrangement with a thermal trimmer. To simulate the growth thermal conditions, a fused silica die with a V-shaped graphite insert (1 cm high, 4.1 cm long) was positioned inside the susceptor.

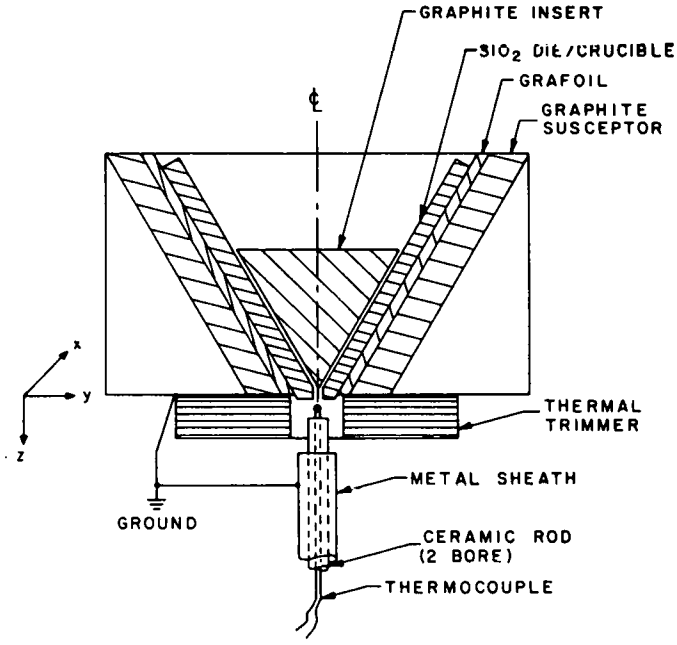

Figure 8. Schematic of the temperature measurement configuration. Note that the junction is exposed to accurately measure the temperature distribution. The susceptor and the sheath of the thermocouple are grounded.

Figure 9 shows a horizontal temperature profile as measured with the Chromel/Alumel thermocouple at three temperatures, i.e., 1038, 1188, and 1207°C at the midpoint of the die edge. The measured temperature profile at 1207°C is similar to the profile measured at 1038°C. It is therefore assumed that the profile at the silicon growth temperature is similar to the 1200°C profile. Clearly adjustments are needed, based on experience, of the profile at the growth temperature. The profiles were developed at the lower temperatures due to the limitations of the thermocouple. The thermocouple was touching the edge of the fused silica die. A pyrolytic graphite (PG) plate (5.1 x 2.0 x 2.3 cm thick) was used as the thermal trimmer (see Fig. 7, trimmer-1a); the high conductivity "a-b" plane was positioned perpendicular to the vertical axis. The temperature at the midpoint of the horizontal temperature profile is lower than along both sides of the slot. The horizontal temperature gradient at the midpoint is 2 and 8°C/mm along two directions. A similar profile was observed with an L-shaped graphite thermal trimmer. Ideally, the temperature near the midpoint should be slightly higher than the edges in order to offset the high heat loss during seeding and ribbon growth. The vertical temperature profile along the midpoint at 1188°C is reproduced in Fig. 10. The vertical gradient at the die edge is 40°C/mm.

3. Seed and Charge

The orientation of the silicon seed is $\{110\}\langle 211\rangle$ or $\{111\}\langle 211\rangle$. The silicon seed is cut out of a Czochralski crystal (p-type, 10 ohm-cm), the typical size being 1.0 to 2.0 cm wide, 0.1 cm thick, and 4 to 7 cm long. One end of the seed is etched in CP-4 silicon etchant to about 0.025 cm thick to fit into the capillary slot. The slot is 2.5 cm wide with an internal spacing of 0.05 cm. The seed is then attached to the seed holder and put in place in the ribbon growth station. The seed holder is a Lucalox alumina rod 0.6 cm in diameter with a slotted end to hold the silicon seed. The other end of the seed holder is positioned in the XYZ-micromanipulator of the ribbon pull mechanism.

The polycrystalline silicon (hyperpure silicon, Dow Corning) to be inserted into the die assembly is cut to fit into the geometry and etched in CP-4. The weight of the charge is 4 to 10 g. Additional feeding of the

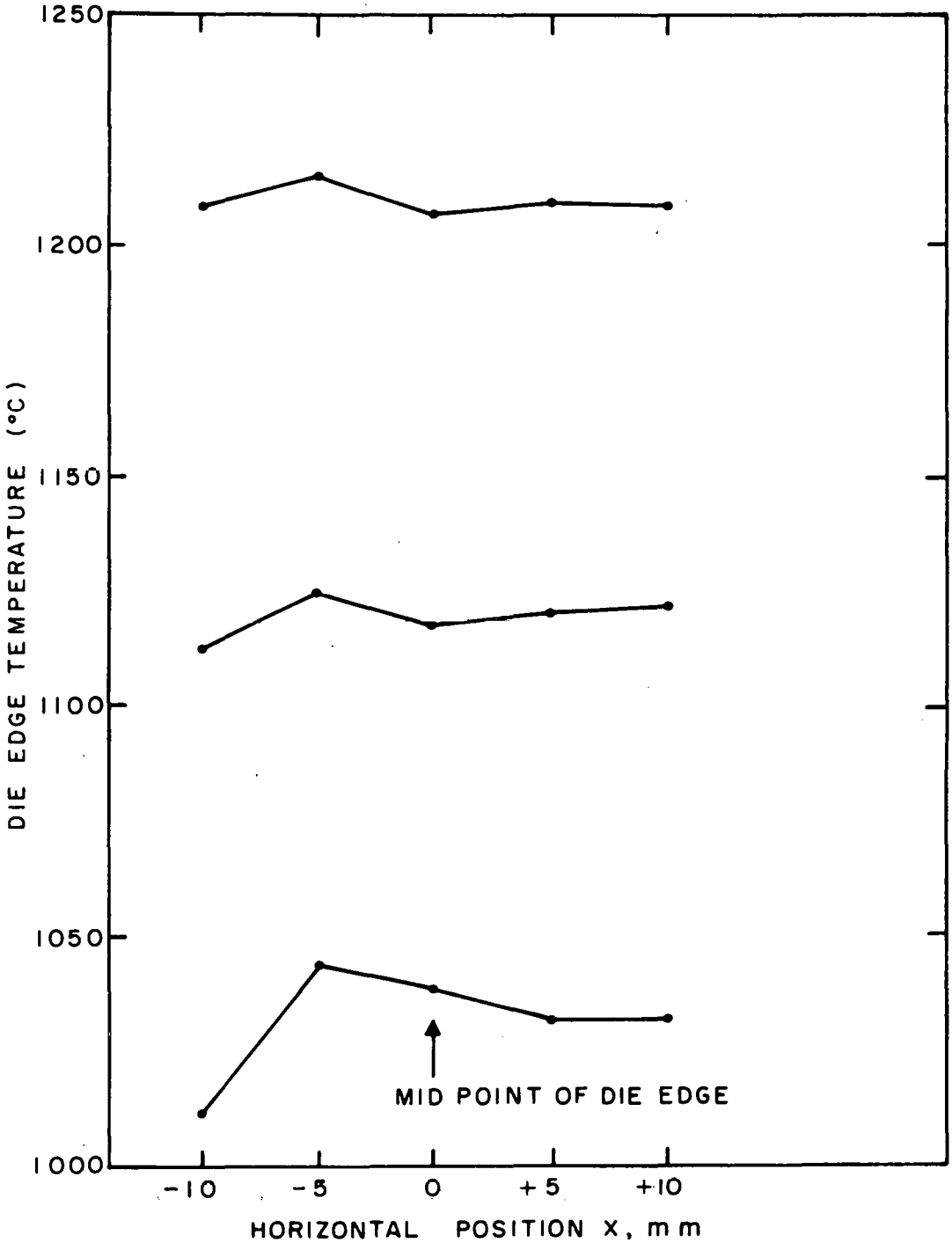

Figure 9. The horizontal temperature distribution at the edge of SiO_2 die slot at three different temperatures. The thermocouple was touching the edge of the fused silica which is positioned inside the V-shaped susceptor.

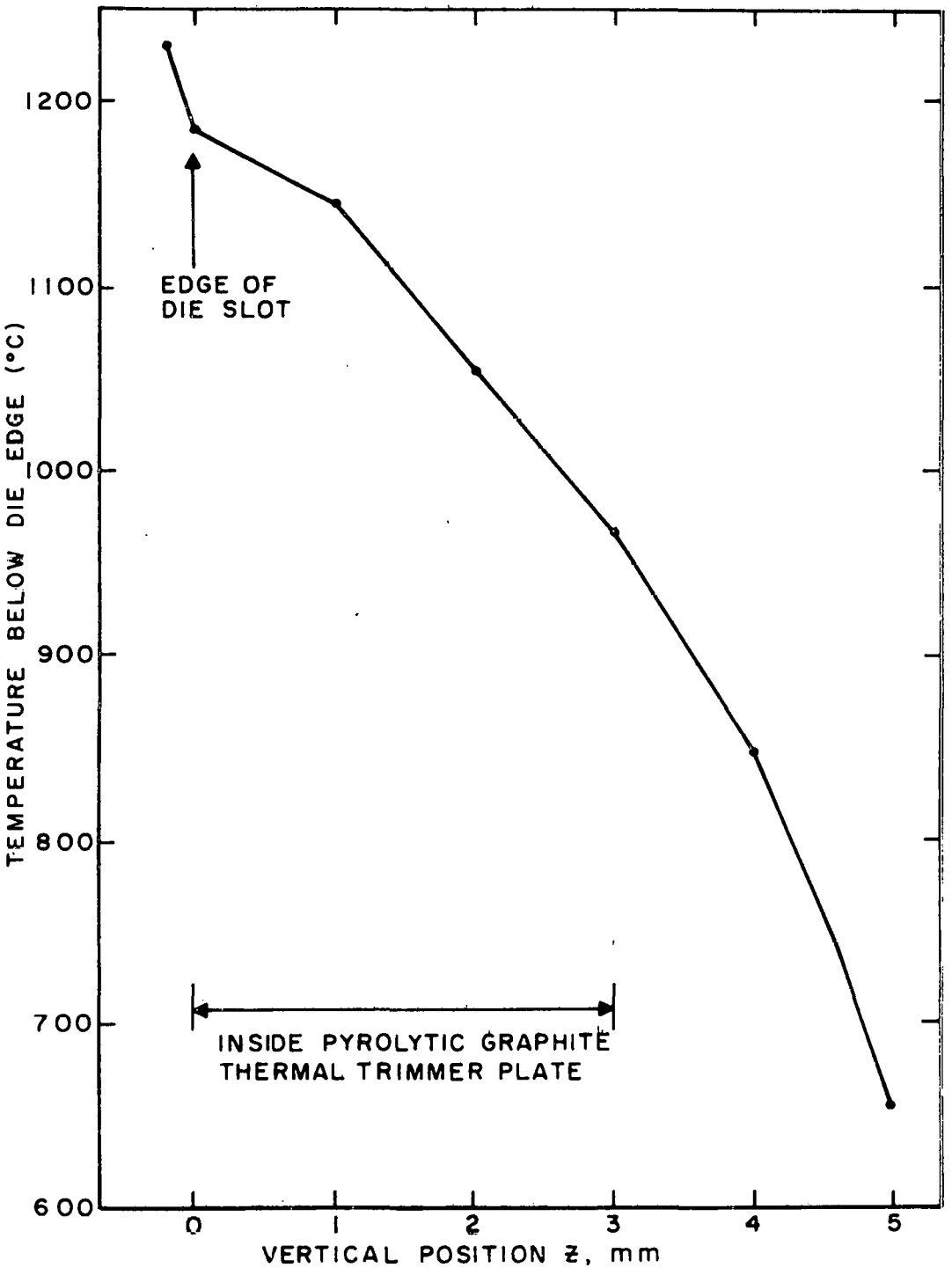

Figure 10. The vertical temperature distribution along the midpoint of the SiO_2 die slot. A thermal trimmer of 3-mm-thick pyrolytic plate is positioned underneath the V-shaped graphite susceptor.

silicon during the ribbon growth is executed by lowering a polycrystalline silicon bar (0.6 x 3.1 cm and 14 cm long) into the melt.

4. Seeding and Growth

After the silicon seed and the die-susceptor assembly with the thermal trimmer are positioned in the growth station within the quartz chamber, the silicon feed bar is attached, and the system is then closed. Titanium-gettered argon is introduced into the growth chamber at the bottom and exhausted at the top into a gas bubbler. After the system is flushed for 1 h, the power is turned on, and the die-susceptor assembly is slowly heated to allow out-gassing. In about 1/2 h, the temperature is raised at a more rapid rate, melting silicon in the die.

The silicon seed, which is about 1 cm away from the die during heating, is then brought up and inserted into the die slot with the aid of a stereoscope and the micromanipulator. The temperature is adjusted to a proper set point. Once a meniscus and the solid-liquid interface below the die are established, the silicon ribbon growth can be initiated.

SECTION IV

SILICON RIBBON GROWTH WITH THE INVERTED RIBBON GROWTH PROCESS

A. RIBBON GROWTH WITH NONWETTING DIES — THE INVERTED STEPANOV PROCESS

1. Growth Using Pyrolytic BN Die

The pyrolytic boron nitride (Union Carbide Corp., Chicago, IL) has a contact angle of 110° with the liquid silicon as measured by the sessile drop method. The BN has sufficient mechanical rigidity at the silicon growth temperature. Furthermore, it is relatively inert and durable in contact with the molten silicon, even though grown silicon ribbon is heavily doped with the boron at a level of $8 \times 10^{19}/cm^3$. BN particles (or particles of reaction products between Si and BN) were observed floating on the melt surface. Since these particles always rose to the surface, they were not incorporated into the growing crystal. A thin layer of β-Si_3N_4 forms on the BN die in contact with the liquid silicon. In the sense that the interior of the die slot becomes coated with a film wet by molten silicon, the process is similar to the EFG method. In the sense that the shape of the ribbon conforms to the interior dimensions of the die slot, the process is similar to the Stepanov method.

The pyrolytic BN has been employed both prior to and during this contract effort as a model die material in the inverted silicon ribbon growth to identify the important parameters and to examine any inherent limitations in ribbon thickness.

A flat plate die was used with a rectangular capillary slot, 2.5 cm w, 0.025 cm t, 0.08 cm h.* This was positioned inside a rectangular graphite susceptor on top of a pyrolytic graphite (PG) plate with a larger slot than the die. As is the case with the pyrolytic graphite, the pyrolytic BN exhibits an anisotropic thermal conductivity, i.e., 20 times higher in the "a-b" plane along the c-axis. Therefore, the "a-b" planes are positioned in the horizontal direction in order to contribute to the high vertical temperature gradient and flat horizontal isotherm desired for ribbon growth.

*In the remainder of this report, the convention for designating the slot dimensions is as follows. The slot width (w) is the long dimension in the horizontal plane and is listed first; the slot thickness (t) is the short dimension in the horizontal plane (i.e., the aperture or opening) and is listed second; the slot height (h) is the dimension in the vertical plane and is listed third. See Fig. 1.

A typical silicon ribbon grown with the flat BN die is shown in Fig. 11. The silicon ribbon grown to date is 2 cm wide, 0.05 to 0.08 cm thick, and 15 cm long. The length is limited by the stroke of the present apparatus, Model 1. Attempts to grow 0.025 cm thick ribbon with a flat die using slot dimensions of 2.5 cm w, 0.025 cm t, 0.03 cm h were not successful. The ribbon width decreased continuously (during growth) from the initial seed width of 2 cm. Since the various adjustments of the thermal gradients with the pyrolytic thermal trimmer did not alleviate this behavior, it is concluded that the decrease in the width was due to the lack of the sufficient replenishing of the liquid rather than to the thermal conditions at the growth interface. Slot heights less than 0.03 cm would enhance the feeding, but the slot is then mechanically not rigid in the flat-die configuration. In the "V" geometry, the BN die is sufficiently stiff even when the capillary height approached zero. Attempts were made to grow 0.025-cm-thick silicon ribbon with zero capillary height, but ribbon width decreased as in the case with the flat BN die. No further efforts were made to establish growth conditions to grow 0.025 cm or thinner ribbons with the BN die in order to pursue ribbon growth with SiO_2 and composite dies coated with CVD Si_3N_4.

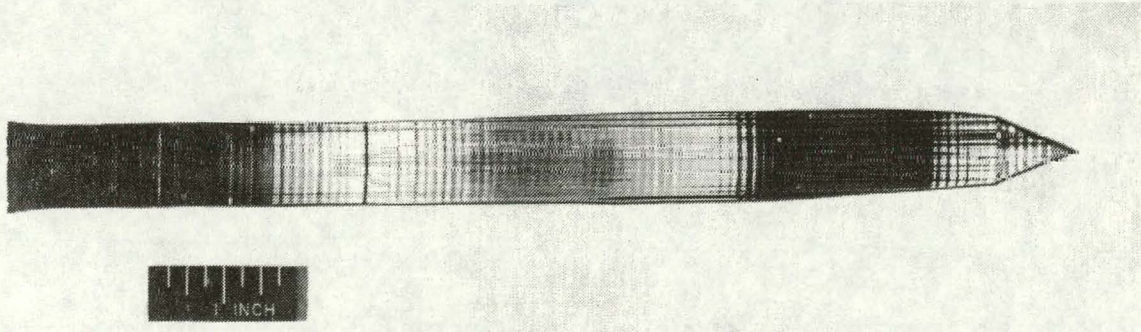

Figure 11. Photograph of a silicon ribbon grown by the inverted Stepanov process using a flat pyrolytic BN die. The growth axis and flat surface are $[\bar{1}1\bar{2}]$ and (110), respectively.

2. Growth Using SiO_2 Die

a. *Preliminary Observations and Modifications* - In the initial silicon ribbon growth attempts with SiO_2 die, a flat plate die or a rectangular crucible with a rectangular slot (2.0 cm w, 0.05 cm t, 0.1 cm h) was employed.

The slot was not filled with the liquid silicon. The melt height was 1 to 1.5 cm. When the slot was tapered, flow of the liquid silicon into the slot was enhanced but did not flow completely to the bottom edge of the die.

With the V-shaped crucible-die configuration described in Section III.A.4, the capillary slot (2.5 cm w, 0.05 cm w, 0.3 cm h) was filled with the liquid silicon completely to the edge. Figure 12 shows the cross section of the SiO_2 capillary slot filled with silicon.

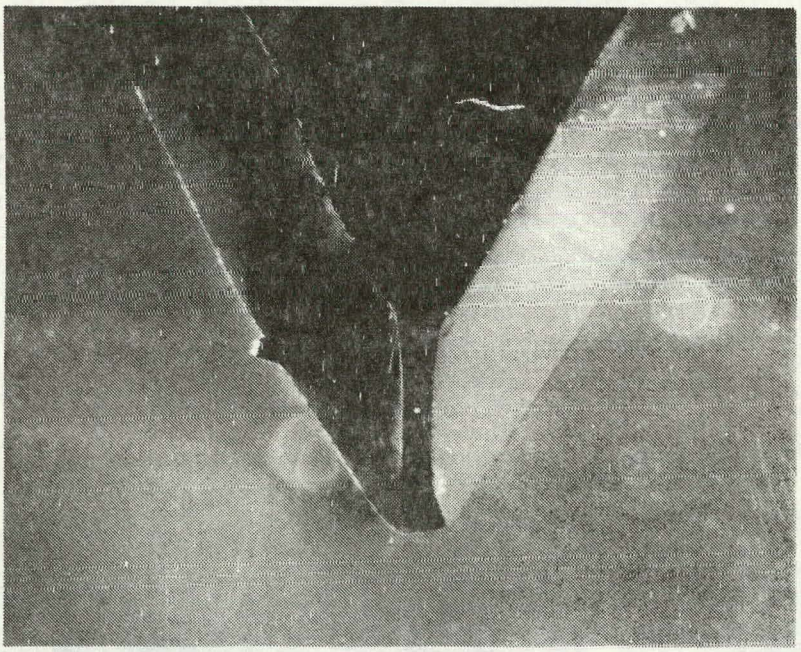

Figure 12. Photograph of the SiO_2 capillary slot filled with silicon in the V-shaped crucible-die configuration Mag. 10X.

During the growth, the ribbon thickness increased immediately after the growth started, with the result that the meniscus height decreased and freezing to the die occurred. At the same time, ribbon width decreased continually. This behavior recurred during the subsequent growth attempt when the meniscus was re-established by raising the temperature.

One common reason for growth instability is an unsatisfactory thermal gradient at the solid-liquid growth interface. Therefore, the thermal gradients at the die edge were modified using thermal trimmers (see Section III.B.1) in conjunction with the temperature profiling (see Section III.B.2).

In another attempt to alleviate the growth instability with SiO_2 die, the inner side of the die slot at the edge was beveled to 45°. This has been recommended in a design which takes into account the contact angle and the meniscus shape [5]. A flat die edge was also used to improve the mechanical rigidity. SiO_2 dies of the three different edge shapes are shown in Fig. 13. The size of the die slot was 2.5 cm w, 0.05 cm t, 0.3 cm h.

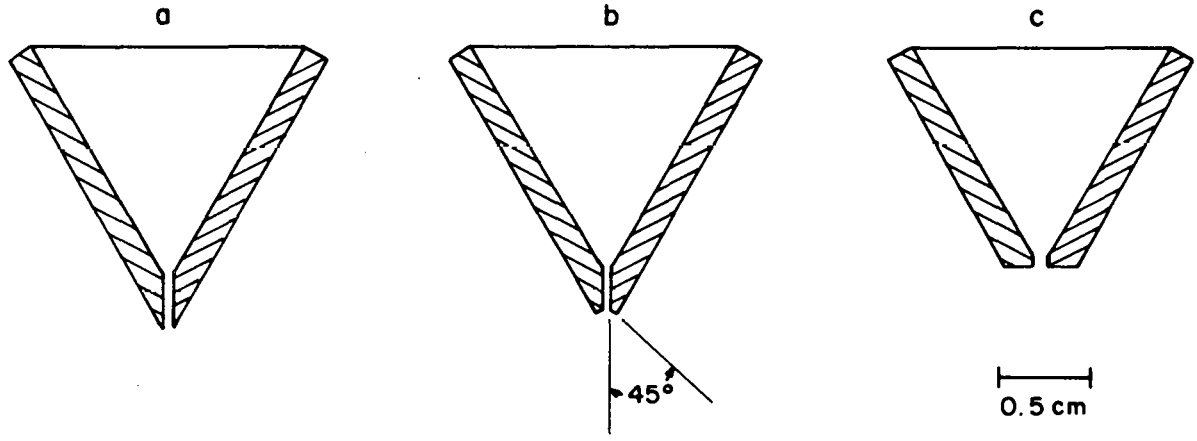

Figure 13. Cross section of fused silica dies of three different shapes at the die edge.

A pressure differential was applied between the melt surface and the die edge to bring the meniscus out of the die slot and to stabilize the ribbon growth. The hydrostatic pressure in the melt in the IS configuration supplies some pressure differential across the melt. By increasing the melt height above 1.0 cm, the pressure differential can be increased. However, since the present simple, efficient crucible-die design must be changed to accommodate a higher melt height, we adopted an alternative method to supply the auxiliary pressure differential by means of constricted gas flow.

A pyrolytic graphite plate with the "a-b" plane perpendicular to the ribbon growth axis was attached to the lower side of the susceptor/SiO_2 die assembly and positioned on top of a fused silica pedestal; this is provided

5. B. Chalmers et al., "Continuous Silicon Solar Cells," NFS Grant GI-37067X, Final Report, 1975.

with eight 0.15 cm diameter holes which can be constricted with fused silica rods, if necessary, to increase the pressure differential. Due to the argon flow from the upper space in the chamber through the leaks in the pedestal, a pressure differential was established. The pressure differential was measured by a U-type manometer filled with a low vapor pressure oil. At a flow rate of 5 ft^3/h, a pressure difference of 10 mm of oil (density = 0.96 g/cm^3) was measured. At 2- to 10-mm pressure difference, the meniscus protruded slightly outside the slot edge.

The silicon ribbon growth experiments with SiO_2 die in the V-configuration can be divided into two categories, depending on the susceptor. The first category is the ribbon growth with a standard V-shaped graphite susceptor, and the second is with a modified susceptor, the inner side of which is lined with pyrolytic graphite plate (see Fig. 14). In both cases, a pressure differential was applied.

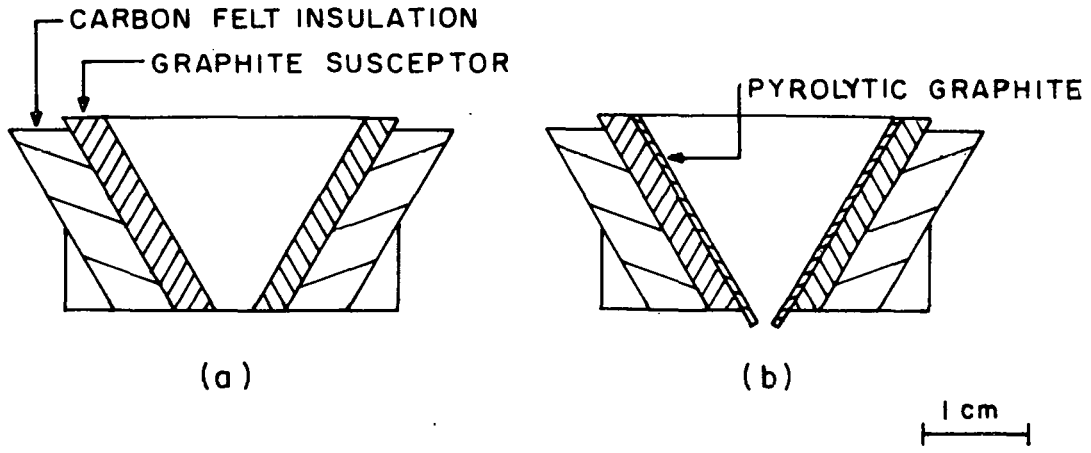

Figure 14. Cross-sectional view of the V-shaped graphite susceptor used with SiO_2 die, (a) a standard type and (b) a modified susceptor to decrease the vertical temperature gradient inside the susceptor.

b. *Ribbon Growth with the Standard V-Shaped Susceptor* - The V-shaped standard susceptor and a flat-edged silica die slot 0.05 cm high [see Fig. 13(c)] were used with a series of the thermal trimmers. The horizontal and vertical temperature gradients were measured, and ribbon growth was tried subsequently with the same configuration as was used for thermal profiling. Details of the temperature measurement have been described previously in Section III.B.2.

The gas flow for the pressure differential was the same both during the profiling and the ribbon growth. Previously, a quartz pedestal with a controlled gas leak was used to generate the pressure differential, and the die-susceptor assembly was positioned on top of the pedestal. This arrangement was not sufficiently versatile, however, to accommodate various types of thermal trimmers (such as L-shaped graphite). We have modified the arrangement by inverting the quartz pedestal and positioning it on top of the die-susceptor assembly.

The application of a pressure differential across the melt helped to bring the melt out of the slot and suppressed (to some extent) the mechanical vibration. The mechanical vibration is not, however, completely suppressed by the pressure differential, and the melt is continually in vertical motion both prior to seeding and during the ribbon growth after the meniscus was established outside the slot. It appeared that the vibration of the melt was caused by the formation and evolution of the silicon monoxide. This results in an oscillatory change of the contact angle.

The measured horizontal temperature distribution along the die edge and the vertical gradient below the die are given in Table 1. With the use of pyrolytic graphite trimmers such as T-1a, T-1b, and T-1c (see Fig. 7), and PG plates positioned inside a rectangle susceptor (T-2a, T-2b, and T-2c), the horizontal temperature gradients were a few degrees per mm at the midpoint of the slot. This low gradient should be within the range needed to maintain the variation of the meniscus height constant enough for stable growth (see Section V.A.3).

The vertical thermal gradient was between 22 and 75°C/mm, depending on the selection of the thermal trimmer. With high vertical gradients (57°C/mm or higher), a relatively high heat input was necessary to establish a meniscus along the seed. The ribbon growth instabilities which already seriously limited the ribbon growth with the lower vertical gradients became more pronounced with the increased gradient due to the increased SiO formation. The continuous increase of the ribbon thickness, decrease of width, and freeze-over of the meniscus to the die edge are commonly experienced when SiO_2 is used as the die material.

TABLE 1. HORIZONTAL AND VERTICAL TEMPERATURE GRADIENTS MEASURED AT THE DIE EDGE AND SOME RESULTS OF THE RIBBON GROWTH RUNS USING THE STANDARD V-SHAPED SUSCEPTOR AND SiO_2 DIE.

	Horizontal Temperature (°C) at							
Run No.	-10mm	-5mm	Midpoint	+5mm	+10mm	Vertical Temp. Gradient (°C/mm)	Thermal Trimmer in Fig. 7	Ribbon Growth Results
10-5-76 10-8-76*	1206	1204	1209	1204	1206	46	T-1b	Temp. measurement Grew ribbon 0.1 thick x 0.5 cm wide
10-4-76 10-19-76*	1210	1213	1214	1212	1208	30	T-1c	Temp. measurement Grew ribbon 0.1 thick x 0.4 cm wide
9-30-76	1210	1211	1209	1212	1213	26	T-2b	Temp. measurement
9-23-76 9-24-76*	1208	1211	1213	1208	1202	22	T-2c	Temp. measurement Meniscus size increased and melt ran out.
9-21-76 9-27-76*	1169	1163	1164	1164	1165	59	T-2a	Temp. measurement Ribbon thickness increased and froze over to die.
9-17-76	1210	1206	1202	1201	1198	65	T-2a	Temp. measurement
9-15-76	1190	1188	1184	1180	1180	75	T-1a	Temp. measurement

*Ribbon growth was carried out with the same configuration profiled above.

Because of the higher rf coupling of the upper section of the V-shaped susceptor, the vertical temperature gradient inside the susceptor led to overheating of the silica. This aggravated the growth instabilities due to the increased SiO evolution. Therefore, susceptors were modified as will be described in the following section.

c. *Ribbon Growth with a Modified V-shaped Susceptor* - In an effort to minimize the formation of SiO and improve "pinning" the meniscus at the die edge by decreasing the hysteresis, the V-shaped susceptor was modified to decrease the vertical gradient inside the susceptor and to avoid any unnecessary overheating of the fused silica and the liquid silicon.

Figure 14(b) shows the cross-sectional view of the modified susceptor in the ribbon growth configuration. The pyrolytic graphite plates (0.05 cm thick) were attached to the inner side walls of the susceptor. The high conductivity "a-b" plane of the pyrolytic graphite was parallel to the susceptor wall. Since the thermal conductivity along the "a-b" plane is about 200 times as high as along the c-axis, lining the susceptor with the PG plates should have decreased the vertical gradient inside the susceptor. At the same time gradients in the horizontal direction inside the susceptor should have been minimized. The thermal gradient inside the susceptor was not measured, but with the modified susceptor the vertical gradient in the melt within the susceptor was clearly low, since during the ribbon growth the surface of the melt (melt height, 1 cm) started to freeze when the temperature at the ribbon growth interface was lowered only a few degrees below the melting point.

To further enhance "pinning" the meniscus at the die edge, a fused silica die with sharp edges [see Figs. 12 and 13(a)] was employed. A pressure differential across the melt was also applied. The SiO formation was considerably less with the modified susceptor, but the hysteresis of the contact angle and the vertical vibration of the melt were still present and continued to be major causes for the growth instability. Only a short ribbon (4 mm long) was grown. The width was decreased, while the thickness became larger than the gap of the die slot.

To date, adjustment of the thermal gradients by using different thermal trimmers and beveling the inner capillary edge to 45° have not alleviated the growth instabilities.

It has been concluded, having established conditions suitable for growth with other die materials, that the key factor which contributes to the growth instabilities is the erratic wetting behavior of the liquid silicon with the fused silica. It has been observed that the silicon melt in the crucible and the die slot is in constant motion in the vertical direction. This is not observed in the pyrolytic BN crucible-die positioned in the same configuration. The formation and evolution of silicon monoxide apparently cause the erratic wetting behavior and the mechanical vibration in the melt.

Such erratic wetting behavior and mechanical vibration of the liquid silicon inside the narrow die slot affect the stability of the meniscus shape. Similar erratic wetting behavior has been reported in the preliminary shaped silicon growth employing fused silica capillary [5].

B. RIBBON GROWTH WITH WETTING DIES — THE INVERTED EFG PROCESS

1. Reactivity of the Molten Silicon with Die Materials Coated with CVD Si_3N_4 and CVD SiO_xN_y

Die materials, such as RS Si_3N_4, hot-pressed Si_3N_4, BN, and quartz have been coated with CVD Si_3N_4 or CVD SiO_xN_y. Of these, the CVD Si_3N_4/RS Si_3N_4 combination has been most frequently used in attempts to grow silicon ribbon; the CVD Si_3N_4/BN combination has been used to a lesser extent. Fig. 15(a) shows a photograph of a cross section of a CVD Si_3N_4/RS Si_3N_4 die that has been used for pulling silicon ribbon. The photograph corresponds to an end-on view near the bottom of the die and shows the central solidified silicon column bounded by the CVD Si_3N_4 layers and the shaped outer RS Si_3N_4. The cut face was lapped and the silicon slightly etched to help provide contrast between the different regions. An enlarged view of one of the CVD Si_3N_4 layers at the bottom of the die is shown in Fig. 15(b). Some chipping at the lower edge occurred during cutting. The CVD film remains continuous after about 2 h in contact with molten silicon. Similar dies have been reused for ribbon growth experiments without apparent dissolution of the CVD layer.

Experiments were conducted with CVD Si_3N_4/RS Si_3N_4 and CVD SiO_xN_y/RS Si_3N_4 composites, in which a molten silicon drop, 20 to 30°C above the melting point, was supported by the CVD coating for extended periods of time in a helium ambient. The samples were subsequently sectioned through the frozen silicon droplet and mounted in epoxy for lapping, etching, and profile examination. Figure 16(a) shows a photograph of a Si/CVD Si_3N_4/RS Si_3N_4

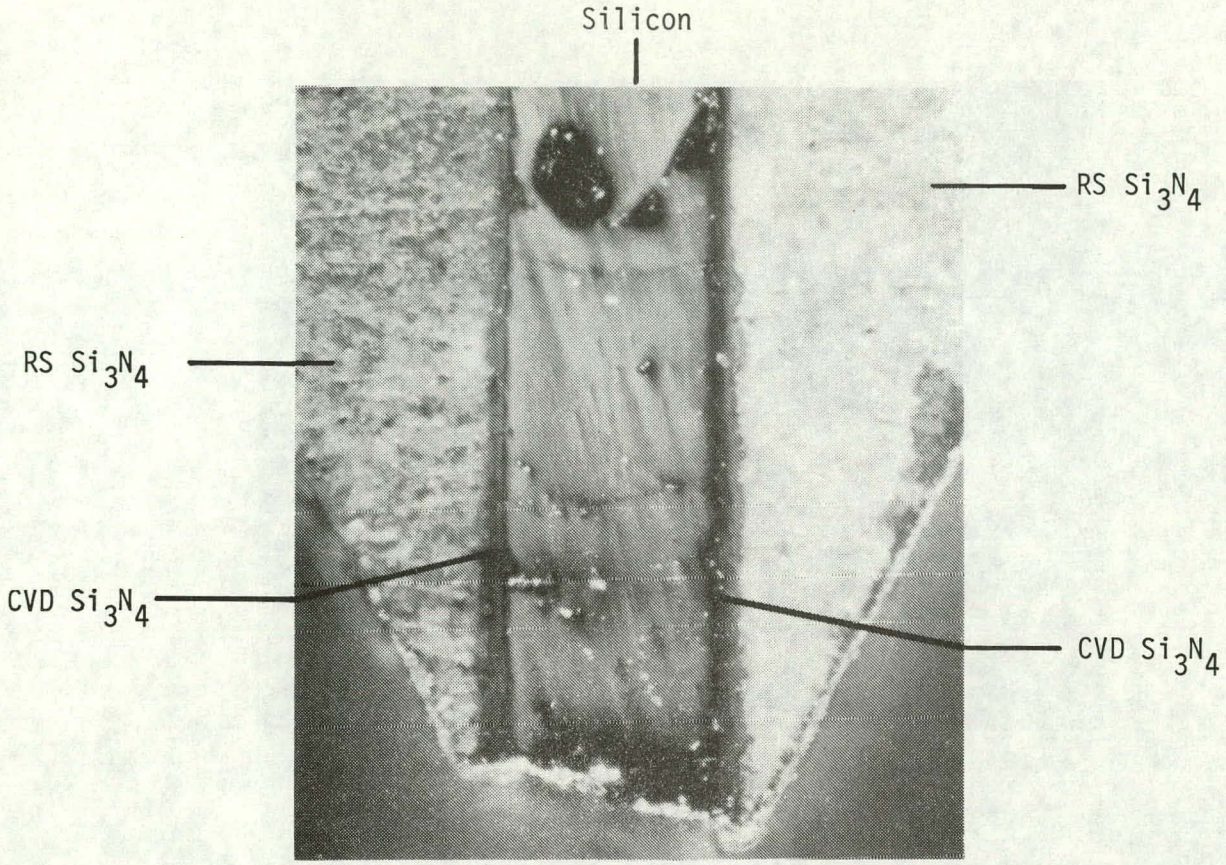

(a) ~50X

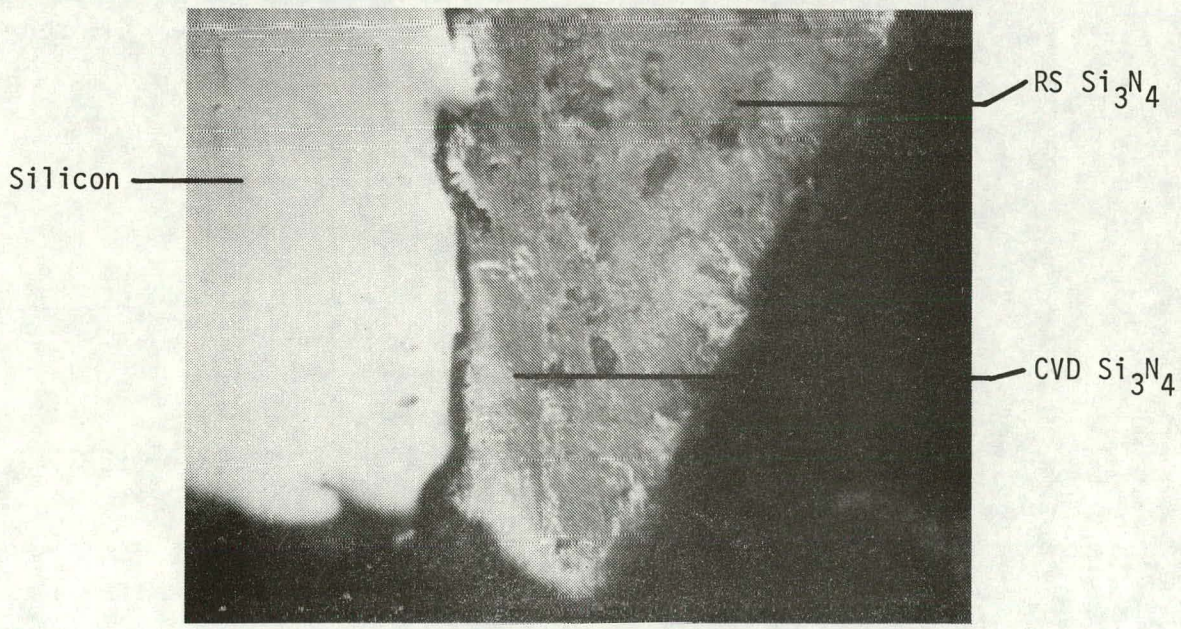

(b) ~260X

Figure 15. Cross-sectional view of a silicon ribbon die showing (a) solidified silicon column bounded by CVD Si_3N_4 and outer RS Si_3N_4 shaped die and (b) enlarged view of CVD Si_3N_4 layer. The die was maintained at liquid-silicon temperatures for about 2 h.

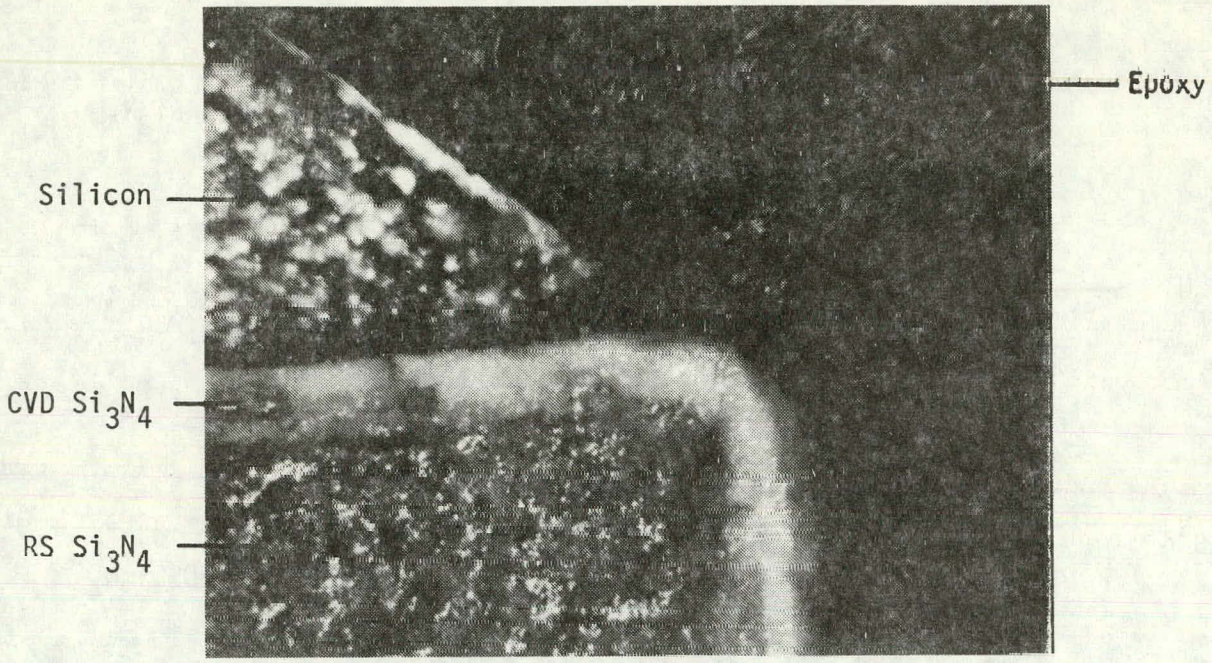

(a) ~260X

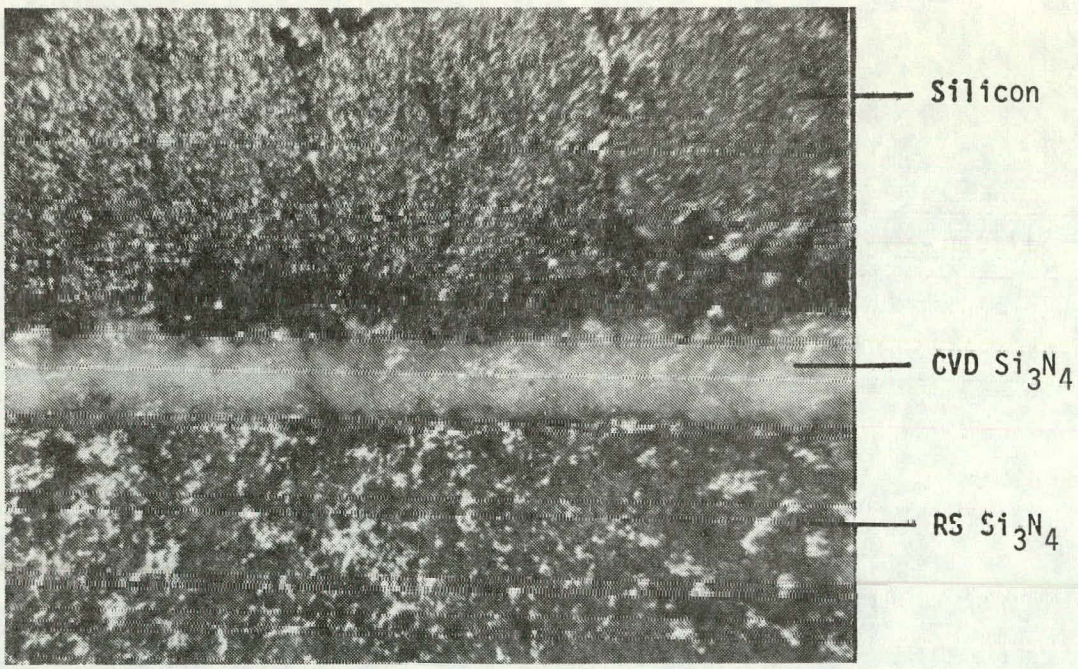

(b) ~260X

Figure 16. Photograph of a section of Si/CVD Si_3N_4/RS Si_3N_4 sample showing film continuity (a) near edge of silicon droplet and (b) under droplet after 1 h at 1440°C.

sectioned sample at the edge of the silicon drop, and Fig. 16(b) shows the profile toward the center of the drop. The heating time was 1 h at approximately 1440°C. The continuity of the film appears intact between the silicon and substrate and also around the edge of the substrate. Figures 17(a) and (b) show similar profiles for a sample heated at approximately 1450°C for 4 h. There is evidence of film fracture during the cutting operation [Fig. 17(a)]. The original thickness of the film appears unchanged, but the mechanical strength of the film has apparently deteriorated as evidenced by results of a scratch test on the CVD nitride layer after the silicon was etched off. Similar photographs for the case of a Si/CVD SiO_xN_y/RS Si_3N_4, heated simultaneously with the latter sample at 1450°C for 4 h, are shown in Figs. 18(a) and (b). Again, film continuity is maintained, and, in this case, no deterioration in mechanical strength was observed from a scratch test performed after the silicon was etched off.

Other observations are as follows: when silicon is etched from the film/substrate composite, the area from which the silicon was removed has a brown color. Microscopic examination shows the presence of well-defined crystallites in a shallow surface brown coating. Two types of crystallites are apparent: elongated brown-colored needles and small dark crystallites. On CVD Si_3N_4 surfaces, x-ray analysis has shown the presence of crystalline β-Si_3N_4 and β-SiC. On CVD SiO_xN_y surfaces, x-ray analysis has shown the presence of α-Si_3N_4, β-SiC, and a crystalline phase not identifiable at this time. It should be indicated that there has been some controversy about the composition of "α-Si_3N_4," as to whether it is a phase of Si_3N_4 or an oxynitride. The systems used here have contained graphite which could account for the formation of β-SiC by carbon transport if O_2 were present as an impurity in the gas stream. Likewise, β-Si_3N_4 could also be accounted for if N_2 were present in the gas stream. These are preliminary results with commercially available materials, and no effort has been made to control the impurity content. We believe that the impurity content in the starting materials has a major impact on the compatibility of all contact materials examined in this program. For example, CVD Si_3N_4 films on BN have shown greater reactivity with molten silicon than CVD Si_3N_4 on RS Si_3N_4 die materials. In turn, hot-pressed Si_3N_4 has provided a very poor substrate for CVD coatings with a large emission of impurities at liquid silicon temperatures. RS Si_3N_4 also emits considerable amounts of impurities at these temperatures.

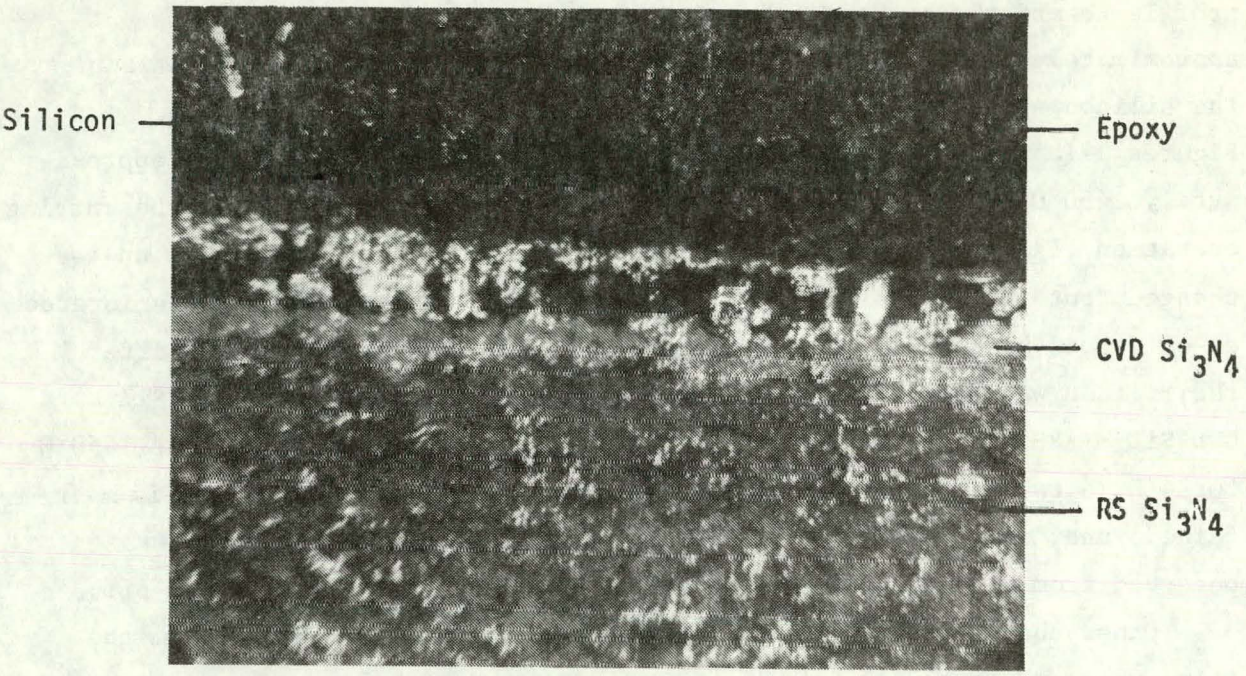

(a) ~260X

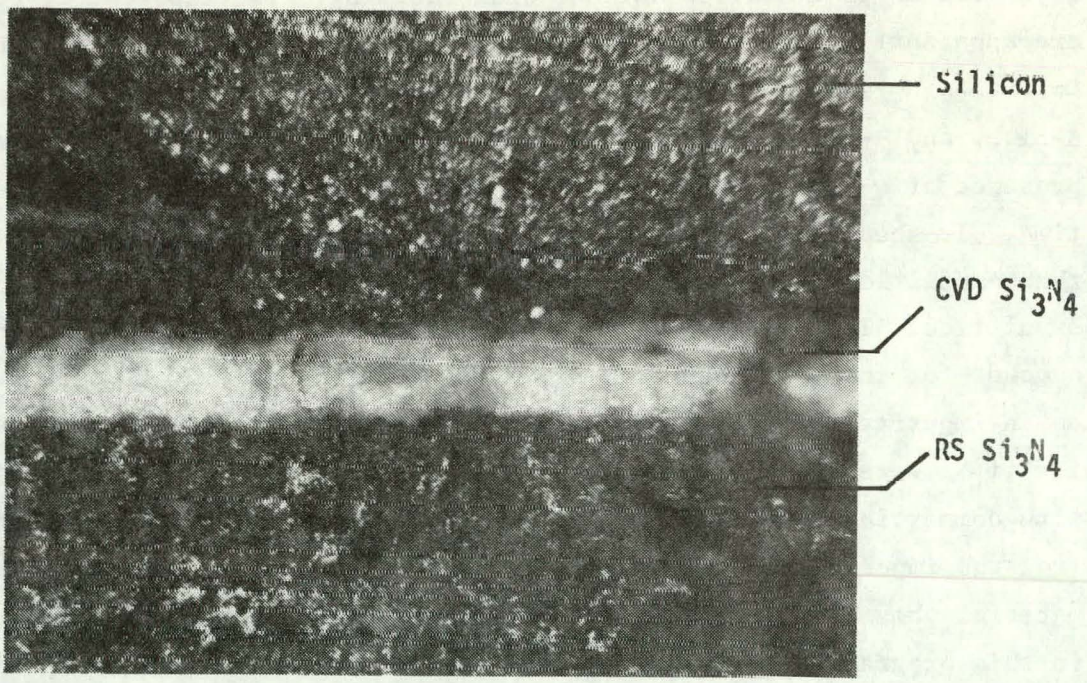

(b) ~260X

Figure 17. Photograph of a section of Si/CVD Si_3N_4/RS Si_3N_4 sample showing film thickness continuity (a) near edge of silicon droplet and (b) under silicon droplet after 4 h at 1450°C. Some fracture of the CVD film as a result of the cutting action is apparent.

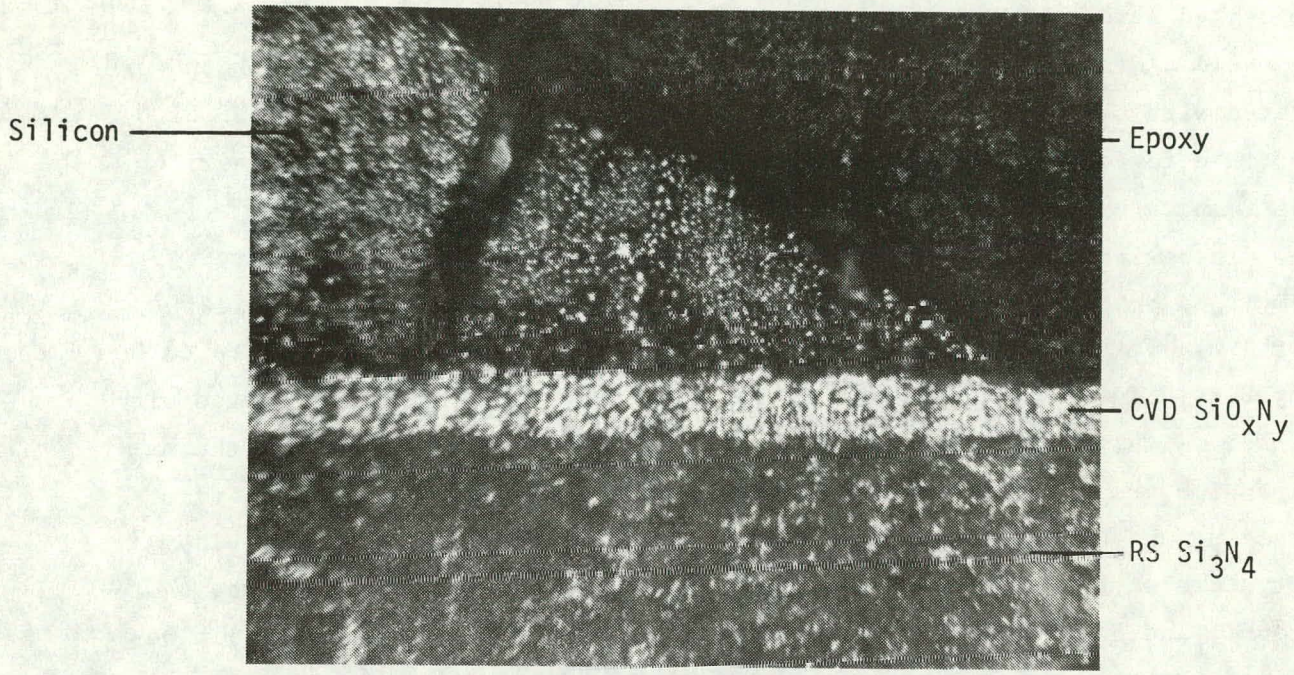

(a) ~260X

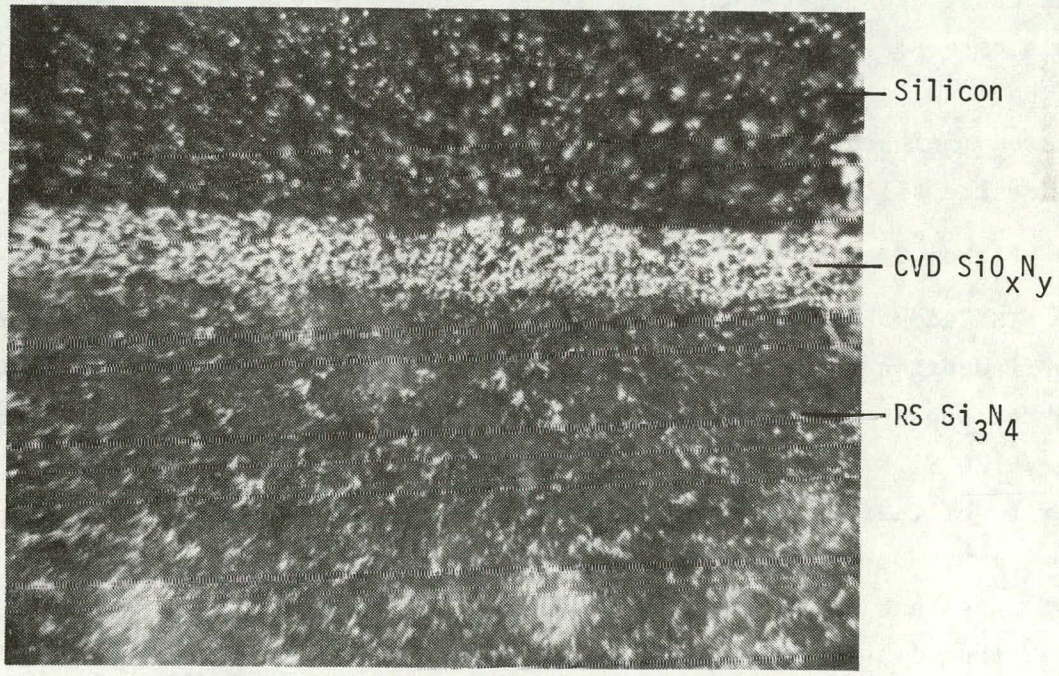

(b) ~260X

Figure 18. Photograph of a section of Si/CVD SiO_xN_y/RS Si_3N_4 sample showing film thickness continuity (a) near edge of silicon droplet and (b) under silicon droplet after 4 h at 1450°C. No film fracture was observed.

Current efforts are directed toward realizing higher purities in the deposited layers and the substrates.

All of the dies used in the recent attempts to grow silicon ribbon were coated with CVD Si_3N_4. The die substrate material was principally RS Si_3N_4, and in a few cases BN. The CVD layers appear to remain continuous during the temperature cycle of the growth process.

In peripheral experiments, various grades of graphite were coated with CVD Si_3N_4 or SiO_xN_y and subjected to a silicon sessile drop test at 1450°C for 1 h. Figure 19(a) is a photograph of six graphite samples (Ultra Carbon Corp., Bay City, MI), with corresponding designations, which have been coated with Si_3N_4. With the exception of UT-8, all samples show a mismatch in thermal expansion properties between the film and the substrate, leading to film cracking and absorption of the silicon droplet into the substrate. The curvature of the samples is apparent from the shadowing effect in the photograph. The Si_3N_4/UT-8 composite was only slightly curved and the film remained intact. The graphite substrates had a CVD coating on one side only.

Figure 19(b) shows a corresponding set of samples for CVD SiO_xN_y with the substrates coated on both sides. Sample UT-8 was the least affected in this case also. All specimens remained flat because of the CVD layer on both sides. The film on UT-2-S, UT-6, and UT-6ST displayed some cracks when viewed microscopically. The cracking occurred during the cooling process since the silicon droplets remain on the composites.

2. Ribbon Growth with Composite Die Coated with CVD Si_3N_4

Silicon ribbon growth has been carried out in the inverted Stepanov configuration using the V-shaped crucible-die assembly coated with CVD Si_3N_4. As the substrate material for the CVD coating, two kinds of Si_3N_4 were used, i.e., RS Si_3N_4 and hot-pressed Si_3N_4 (Cerac, Inc., Milwaukee, WI). The purity of these substrate materials is low. Table 2 shows semi-quantitative emission spectrographic analyses of both kinds of Si_3N_4. Analysis of the CVD Si_3N_4 and hot-pressed Si_3N_4 from a different source (Atomergic Chemical Co., Long Island, NY) is also given in Table 2. It is of interest to note that the CVD Si_3N_4 is much purer than the other Si_3N_4; the purity of the CVD material can be further improved. The density of the substrate silicon

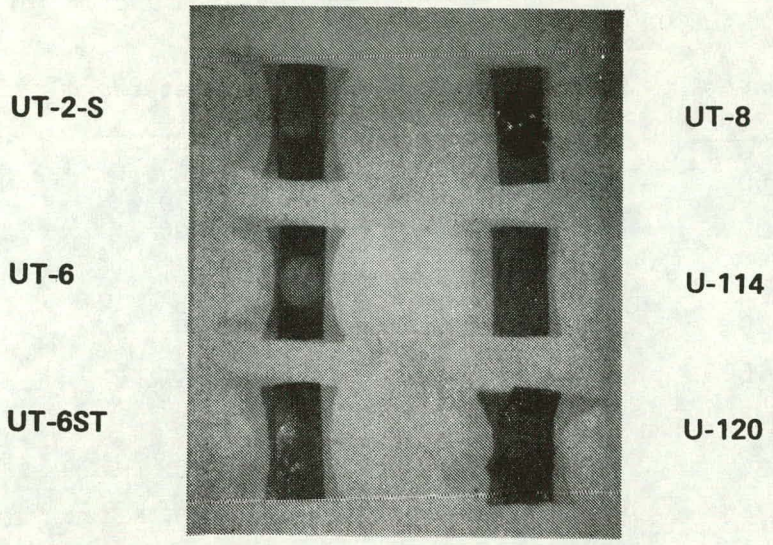

(a)

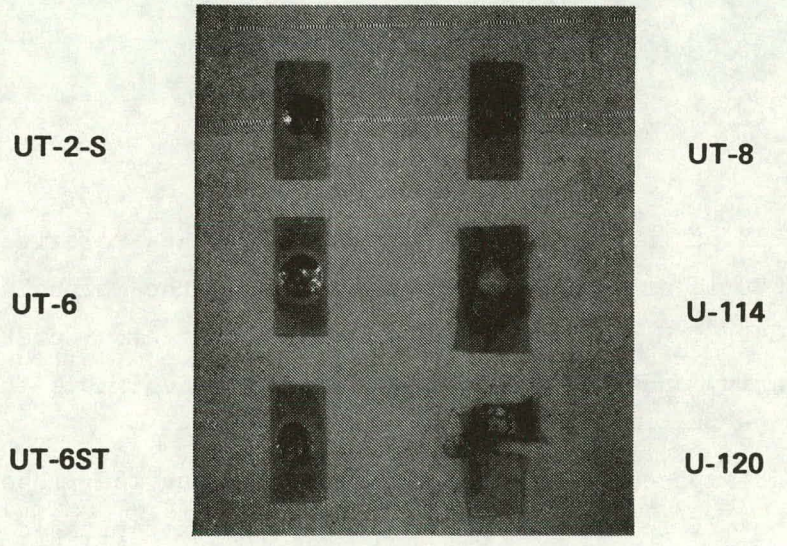

(b)

Figure 19. Silicon sessile drop test on (a) Si_3N_4/graphite composites, CVD coating on one side of each substrate and (b) SiO_xN_y/graphite composites, CVD coating on both sides of each substrate.

TABLE 2. EMISSION SPECTROGRAPHIC ANALYSIS OF VARIOUS SILICON NITRIDES (ppmw)

	Hot-Pressed (Atomergic)	Hot-Pressed (Cerac)	Reaction-Sintered (Cerac)	CVD Film
Cu	6-60	60-600	60-600	0.1-1
Ti	30-300	300-3000	300-3000	-
V	-	20-200	20-200	-
Ba	1-10	100-1000	10-100	-
B	15-150	60-600	6-60	10-100
Si	S	S	S	S
Mg	0.3%-3%	0.3%-3%	30-300	1-10
Mn	1-10	100-1000	100-1000	0.3-3
Cr	-	100-1000	60-600	-
Fe	30-3000	60-600	500-5000	0.3-3
Al	0.6%-6%	1%-10%	1%-100%	3-30
Be	-	3-30	0.6-6	-
Mo	-	3-30	30-300	-
Ca	30-300	600-6000	300-3000	-
Ni	3-30	60-600	100-1000	-

nitrides was about 75% of the theoretical density, and thus relatively porous. Since the CVD layer conforms rather closely to the morphology of the substrate, the CVD Si_3N_4 coating was not completely flat. Substrate materials of high purity and high density are therefore desirable for the improvement of the CVD coating.

The die surfaces exposed to the liquid silicon during the ribbon growth were coated with from ~25 to ~100 μm of CVD Si_3N_4. The hot-pressed Si_3N_4 has a second phase, and CVD-coated dies made of this material out-gas severely at the ribbon growth temperature. On the other hand, RS Si_3N_4 is single phase, and there is less out-gassing during ribbon growth. Therefore, RS Si_3N_4 is being employed as the CVD substrate material for the die. The size of the die slot opening was 0.05 x 2.5 cm and 0.3 cm high. Typically, the $(110)[11\bar{2}]$ silicon seeds were 0.04 cm thick, 1.2 to 2.0 cm wide, and ~5 cm long.

A number of thermal trimmers have been employed in the V-shaped crucible-die configuration. With a pyrolytic graphite plate trimmer, which is similar to the trimmer-1a in Fig. 7, it has been possible to achieve a stable and sustained growth of narrow ribbons. Figure 20 shows two silicon ribbons, 0.05 to 0.06 cm thick and 0.3 to 0.5 cm wide, which have been grown with the CVD-coated Si_3N_4 die. The ribbon width is small compared with the width of the seed and the die aperture. The narrowing of the grown ribbon is considered to be the result of an unsatisfactory thermal gradient at the solid-liquid (s-ℓ) ribbon growth interface. Both ribbons in Fig. 20 were grown at a rate of 10 cm/h. By increasing the growth rate and decreasing the temperature, it has been possible to increase the ribbon width to some extent (see the right-hand section of the lower ribbon in Fig. 20).

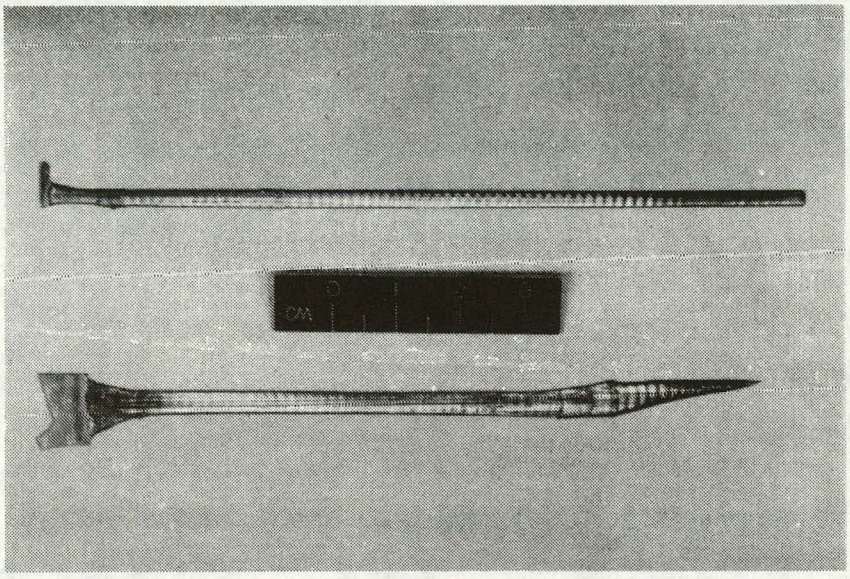

Figure 20. Photograph of silicon ribbons grown with RS Si_3N_4 die coated with CVD Si_3N_4.

After we established a stable and sustained ribbon growth, experiments were continued with the major emphasis on increasing the ribbon width. The sizes of the die aperture and seed were kept the same as in the earlier experiments. Silicon seeds were of the (110)[11$\bar{2}$] orientation. Thermal trimmers similar to trimmers-1a and 2a in Fig. 7 were applied. The first trimmer is a PG plate with a dogbone-shaped opening parallel to the die

aperture, and the thickness of the PG plate tapers off toward both ends. The second trimmer consists of a PG plate positioned inside a thin rectangular graphite susceptor. Most growth runs were conducted with the first type of thermal trimmer.

With both types of trimmers, the width of the silicon ribbon continually decreased as the growth proceeded. Figure 21 is a photograph of a typical silicon ribbon grown with the width instability. The growth direction was downward in the photograph, as indicated by the arrow. Instantaneous s-ℓ growth interface shapes are delineated by the horizontal striations on the ribbon surface (see Fig. 21). The interface shape at the lower end corresponds to the initial seed-ribbon junction. The other two striations represent the interface shapes when the growth was restarted, after the ribbon froze over momentarily to the die and then meniscus was re-established by an increase in temperature of the growth system. The delineated interface shapes are convex toward the melt, which indicated that the meniscus height at the ribbon end was higher than along the side of the ribbon. Such convex interface shape in the ribbon growth with flat die edge is certainly not suitable for the stable ribbon growth of constant width, as has been analyzed [6] in detail for the EFG, inverted Stepanov, and inverted EFG process. For the stable growth of wide ribbons, the meniscus height at the ribbon ends should be smaller than along the ribbon side. In other words, the favorable meniscus shape should be slightly concave toward the melt. This originates physically from the fact that one of the two principal radii of curvature of the meniscus undergoes a discontinuous change in the ribbon growth geometry, i.e., from infinity at the ribbon sides to about half the ribbon thickness at the ends. It is of interest to point out that according to an analysis of Surek [6], the stability vs the meniscus height is more favorable in the inverted configuration for both the Stepanov and the EFG processes (see Section V.C).

The s-ℓ growth interface shape is controlled by both the horizontal temperature distribution in the die aperture prior to seeding and the heat loss through the seed when the meniscus is seeded. In turn, the horizontal

6. T. Surek, J. Appl. Phys. 47, 4384 (1976).

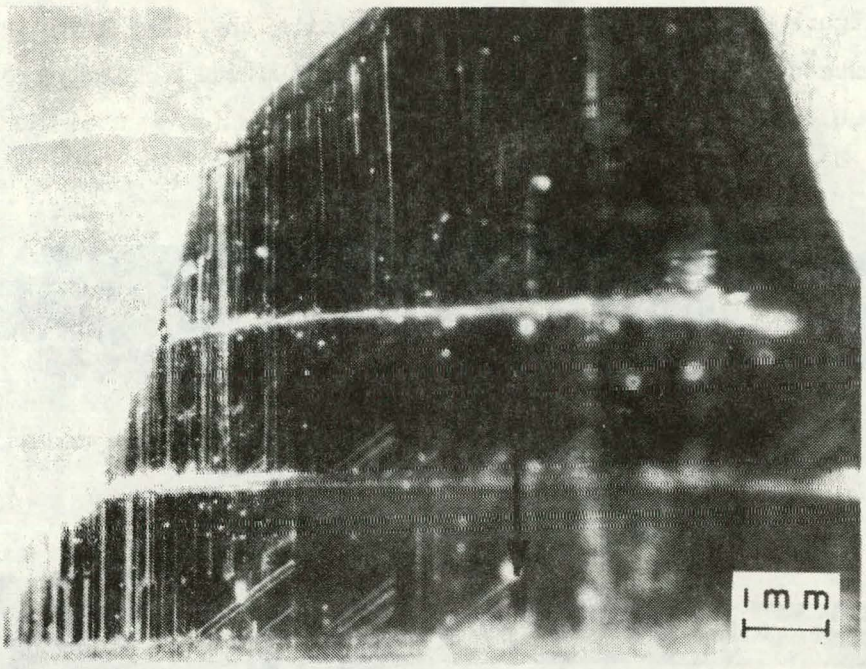

Figure 21. Photograph of a typical silicon ribbon grown with the width instability. The s-ℓ growth interface shapes, convex toward the melt, are revealed by the striations. The growth direction is indicated by the arrow.

temperature profile is controlled by the thermal distribution in the susceptor, melt, and thermal trimmer. In our ribbon growth configuration with the thermal trimmers mentioned above, the horizontal temperature gradient prior to seeding is ~8°C/cm, the ends being colder than the midpoint. This estimate is based on the observation of the onset of freezing of the melt inside the die aperture as the set-point of the temperature controller is lowered in small steps corresponding to about 1°C.

Thus, even though the isotherm in the die aperture prior to seeding was concave, a convex interface shape was established after seeding. This is due to the substantial increase of the heat drain at the seeded meniscus, which is calculated to be more than ten times the drain which exists before seeding (see Section V.A.3); the enhanced drain through the seed reverses the isotherm from the concave to a convex shape after seeding.

Use of curved dies resulted in substantial stabilization of the ribbon growth. We have achieved stable growth of 1.0- to 2.0-cm-wide ribbons using

curved dies. Figure 22 shows two ribbons grown with the UT-8 (AG)* and RS Si_3N_4 composite dies. Silicon seeds were of (110)[11$\bar{2}$] orientation, and 0.04 x 1.2 to 2.0 cm wide. The radius of curvature was 8.9 cm. The size of

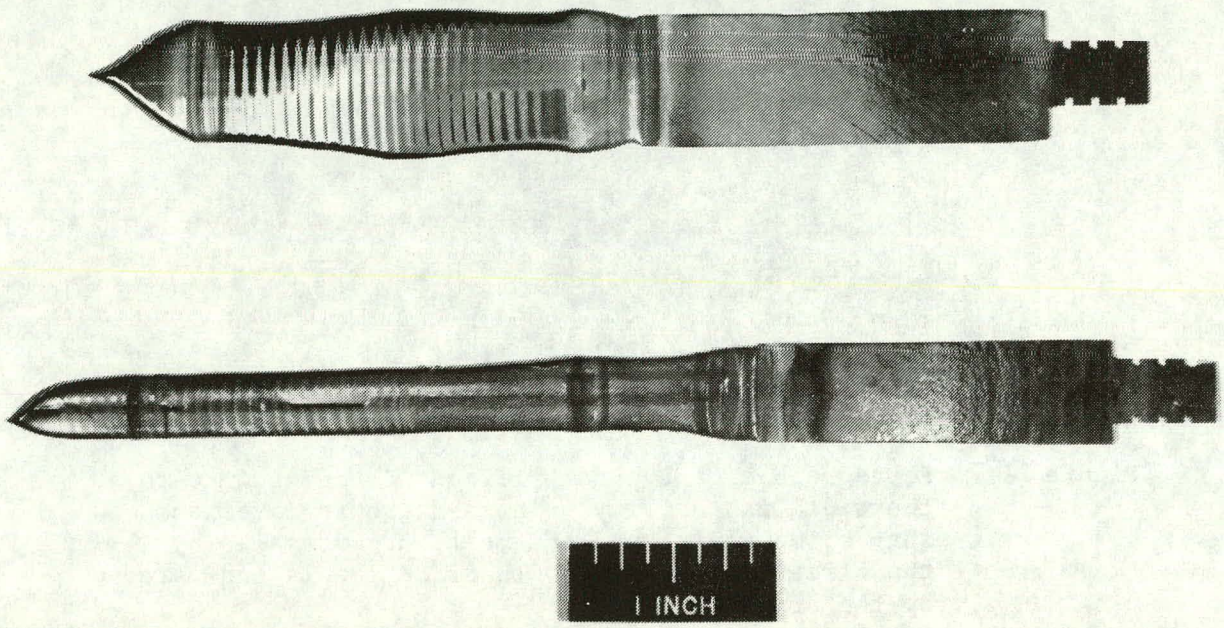

Figure 22. Photograph of silicon ribbons grown with curved dies. The section on the right is the seed ribbon. The upper ribbon was grown using a CVD Si_3N_4/UT-8 (AC) die. The lower ribbon was grown using a CVD Si_3N_4/RS Si_3N_4 die. The radius of curvature of both dies was 8.9 cm.

the die aperture was 0.05 x 2.5 cm. As the result of curvature, the height of the die slot was not the same along the die aperture, i.e., 0.3 cm at the ends and 0.25 cm at the midpoint. The outer die edges were elliptical in shape with a width of 0.05 to 0.06 cm at the midpoint and zero at both ends. The contact angle of liquid silicon with CVD Si_3N_4 is 53°, and thus the ribbon thickness with the composite dies is controlled, as in EFG, by the

* UT-8 graphite (Ultra Carbon Co.) has anisotropic coefficients of thermal expansion, i.e., 3.46 and 2.38 x 10^{-6} deg^{-1} in the "Against Grain" (AG) and in the "With Grain" directions, respectively. We find from the use-test in ribbon growth experiments that only UT-8 (AG) is suitable as the CVD die substrate.

outer dimension of the die edge. The thickness of the ribbons in Fig. 22 is 0.15 to 0.18 cm, while the die slot was 0.05 cm thick. Efforts are in progress to grow thin ribbons (0.025 to 0.05 cm thick as a near-team goal) by providing narrower die edges. In the V-shaped configuration, this requires curvature of the die in two directions. The length of the grown ribbon was 7 to 10 cm, and was limited by the amount of the feed melt used in these runs. Longer ribbons will be grown by increasing the melt volume and by continuous feeding. The ribbon growth rate was 10 to 50 cm/h.

SECTION V

ANALYSIS OF THE INVERTED SILICON RIBBON GROWTH PROCESS

A. THERMAL ANALYSIS WITH COMPUTER MODELING

1. Introduction

To control the growth of single crystal silicon ribbon using the inverted silicon ribbon growth process it is important to have some knowledge of the thermal conditions which exist along the growing ribbon and some insight into the impact of the thermal environment and the ribbon dimensions on the growth velocity which might be achieved. The aim of this portion of the investigation has been to develop a computer simulation of the thermal aspects of the inverted silicon ribbon growth process and systematically examine the effect of the various experimental parameters on the thermal profile along the ribbon and, in particular, on the growth velocity. We have also considered the effect of the choice of the ambient temperature profile and growth chamber configuration in reducing the curvature in the temperature profile along the growing ribbon, thus minimizing the thermal stress to which the growing crystal is subjected.

Many of the results discussed below appear in ref. [7]. We have also included in this summary our thermal model of the laser-supported ribbon to ribbon growth process [8].

2. Mathematical and Computational Aspects

In Fig. 23 we illustrate the dominant factors that determine the heat transfer and thus the temperature profile within the growing silicon ribbon in the inverted ribbon growth process. In order to form the molten zone the temperature of the die, T_D, is maintained a few degrees in excess of the melting point of silicon. Heat is drawn from the die by conduction

7. A. E. Bell, RCA Review 38, 109 (1977).
8. R. W. Gurtler and A. Baghdadi, "Laser Zone growth in a Ribbon-to-Ribbon (RTR) Process," Quarterly Report No. 1, ERDA/JPL/954376-76/1, March 1976.

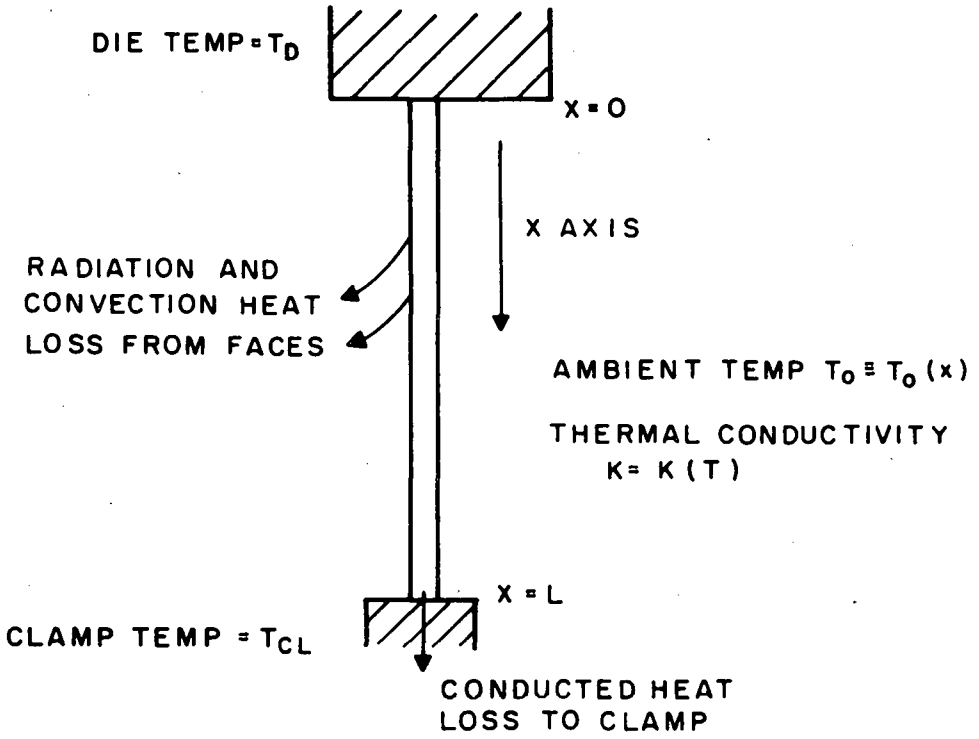

Figure 23. One-dimensional thermal model for the inverted ribbon growth process.

and also by convective transport* since the ribbon is growing with a constant velocity V-cm/s, and, consequently, molten silicon must flow from the die. This heat flux, together with the latent heat of fusion generated at the freezing interface of the molten zone, passes down the ribbon where dissipation to the ambient occurs via radiation and gas convection. In addition to these heat losses there are conductive and convective losses to the clamp that supports and withdraws the growing crystal. We will assume that the clamp temperature is held at a constant value T_{CL}.

In general, the ribbon will be grown with a width in excess of 2 cm and a thickness of 0.05 cm or less. In this case, the surface-area contribution from the ribbon edges, and therefore the associated surface

*We use the term convective transport to refer to that heat energy transport due solely to the motion of the hot silicon ribbon relative to the die and the growth chamber.

heat loss, will represent less than a few percent of the total surface area of the ribbon. This implies that we can safely neglect the ribbon edge losses and solve the heat-diffusion equation in two dimensions only — along the growth direction (x-axis, Fig. 23) and through the ribbon thickness (y-axis). The dissipation of heat through radiation and convection from the surface of the ribbon to the ambient results in a temperature gradient normal to these faces given by

$$K \left(\frac{dT}{dy} \right)_{surf} = \dot{Q}_R + \dot{Q}_C \tag{1}$$

where K is the thermal conductivity of silicon and $\dot{Q}_R$ and $\dot{Q}_C$ are the heat loss rates by radiation and gas convection, respectively. As we shall see, the radiative term dominates, so that the maximum value of the temperature gradient normal to the surface can be estimated to be

$$\left(\frac{dT}{dy} \right)_{surf} \lesssim \frac{\sigma\epsilon}{K} \left(T_M^4 - T_0^4 \right) \tag{2}$$

where T_M is the melting point of silicon, ϵ is the emissivity, σ is the Stefan-Boltzmann constant, and the ambient temperature T_0 is given the lowest practical value of room temperature, 300°K. Under these conditions

$$\left(\frac{dT}{dy} \right)_{surf} \lesssim 115°K/cm \tag{3}$$

Since the thickness of the ribbon is 0.05 cm or less, we can now estimate the temperature differential between the ribbon center and its surface as

$$\Delta T \lesssim \frac{t}{2} \left(\frac{dT}{dy} \right)_{surf} = 3°K \tag{4}$$

In view of this small maximum value for the temperature differential we can reasonably approximate the ribbon to be isothermal through its thickness and thus simplify the model further to a solution of the heat-diffusion equation [9] in one dimension only, along the growth axis of the ribbon, i.e.,

9. H. S. Carlsaw and J. C. Jaegar, *Conduction of Heat in Solids* (Clarendon Press, Oxford, England, 1959).

$$\frac{d}{dx}\left[K\frac{dT}{dx}\right] = \frac{2(w+t)}{wt}\left[\sigma\varepsilon(T^4 - T_0^4) + G\,(T - T_0)\right] + VS\frac{dT}{dx} \qquad (5)$$

where w is the width of the ribbon, t is the thickness of the ribbon, G is the gas convection heat transfer coefficient, and S is the volume specific heat of silicon. The final term VS(dt/dx) in Eq. (5) arises from the convective transport of heat resulting from the motion of the growing single crystal ribbon relative to the die and the stationary mesh-point grid (x-axis) upon which the temperature profile is computed. (This terminology should not be confused with the convective heat loss from the ribbon surfaces to the ambient of the growth chamber.)

The numerical values of the physical constants in Eq. (5) above are well known [10,11] except for the gas convection heat transfer coefficient, G. We have estimated G using an expression appropriate to natural convection heat loss from a vertical plate in air [12] and find $G \approx 1.5 \times 10^{-3}$ W cm^{-2} K^{-1} for $T_0 = 300°K$ and $G \approx 0.5 \times 10^{-3}$ W cm^{-2} K^{-1} for $T_0 = 1500°K$. Both of these values are uncertain to within a factor of two, and we have used a typical figure $G = 1.10^{-3}$ W cm^{-2} K^{-1} for the calculations that follow. Fortunately, the gas convection heat loss is a small fraction of the total dissipation so that this uncertainty does not have a large impact on the results of these calculations (Table 3).

In order to correctly account for the discontinuous change in thermal conductivity that occurs on melting (K = 0.22 W cm^{-1} K^{-1} for solid silicon and K = 0.64 W cm^{-1} K^{-1} for liquid silicon at the melting point), we have used a heat flux conserving discretization scheme in the numerical analysis. Rewriting Eq. (5) with the heat flux $\phi = K(dT/dx)$,

$$\frac{d\phi}{dx} = \frac{2(w+t)}{wt}\left[\sigma\varepsilon(T^4 - T_0^4) + G\,(T - T_0)\right] + VS\frac{dT}{dx} \qquad (6)$$

10. M. Neuberger et al., "Silicon," Hughes Aircraft Co., Culver City, Colorado, AD698342.
11. Y. S. Touloukian et al., Eds., *Thermophysical Properties of Matter* (IFI/Plenum Press, New York, 1970).
12. A. I. Brown and S. M. Marco, *Introduction to Heat Transfer* (McGraw-Hill Book Co., New York, 1969).

On the ith mesh point of a grid running from x = 0 to x = L (Fig. 23) with point spacing ΔX Eq. (6) becomes

$$\frac{\phi_{i+1/2} - \phi_{i-1/2}}{\Delta X} = \frac{2(w + t)}{wt} [\sigma\varepsilon(T_i^4 - T_{Oi}^4) + G (T_i - T_{Oi})] + VS \frac{(T_{i+1} - T_{i-1})}{2\Delta X} \tag{7}$$

where

$$\phi_{i+1/2} = K_{i+1/2} \frac{(T_{i+1} - T_i)}{\Delta X} \tag{8}$$

$$\phi_{i-1/2} = K_{i-1/2} \frac{(T_i - T_{i-1})}{\Delta X} \tag{9}$$

and $K_{i\pm1/2}$ is the thermal conductivity of the silicon at a temperature midway between that on the ith and the $(i\pm1)$th mesh-points. Substituting Eq. (8) and Eq. (9) into Eq. (7), the temperature on the ith mesh point is given by

$$T_i^4 + \alpha T_i - \beta = 0 \tag{10}$$

where

$$\alpha = \frac{C\Delta X^2 + K_{i+1/2} + K_{i-1/2}}{R\Delta X^2} \tag{10a}$$

$$\beta = T_{Oi}^4 + \frac{C}{R} T_{Oi} + \frac{K_{i+1/2}T_{i+1} + K_{i-1/2}T_{i-1}}{R\Delta X^2} - VS \frac{(T_{i+1} - T_{i-1})}{2R\Delta X} \tag{10b}$$

$$R = \frac{2(w + t)G}{wt} \sigma\varepsilon \tag{10c}$$

$$C = \frac{2(w + t)G}{wt} \tag{10d}$$

We have solved Eq. (10) iteratively on each mesh point using the Gauss-Seidel method with an over-relaxation factor of 1.8 to 1.95 to speed

the convergence [13]. The liberation of latent heat of fusion at the freezing boundary of the molten zone was taken into account in the following manner. On each successive iteration of the mesh the temperature profile was examined to determine the location of the freezing boundary and the index of the mesh point closest to this boundary position. A quantity of heat just equal to $\dot{Q}_F$, the rate of liberation of latent heat, was then included as a heat gain term at this mesh point during the subsequent iteration of the computation. $\dot{Q}_F$ depends only on the growth velocity and the cross-sectional area of the ribbon, and is easily calculated from

$$\dot{Q}_F = VwtL \tag{11}$$

where L is the latent heat of fusion in joules/cm^2 for silicon.

The convergence of the computer temperature profile to its steady-state value was monitored by evaluating the energy imbalance

$$\Delta = \frac{Q^+ - Q^-}{Q^+} \tag{12}$$

where Q^+ is the heat input to the ribbon via conduction and convective transport at the die plus the latent heat of fusion generated at the molten zone and Q^- is the total heat loss from the ribbon surface and also through conduction and convective transport to the ribbon clamp. Since Δ is computed directly from the calculated temperature profile, it provides a useful means for physical validation of the profile by ensuring that conservation of energy is maintained. In general, we were able to obtain a convergence to $\Delta \lesssim 0.02$.

3. Results of the Model

a. *Growth Rate* - To illustrate the effect of the convective heat transport term, VSdt/dx, on the temperature profile, we computed the profile for a 3.0 cm long, 1.0 x 0.0375 cm ribbon growing with a velocity of 0.11 cm/s in a 300°K uniform ambient, both with and without the inclusion

13. B. Carnahan, H. A. Luther, and J. O. Wilks, *Applied Numerical Methods* (John Wiley and Sons, New York, 1969).

of the convective term. The results are shown in Fig. 24, and we see that when the convective term in included, there is a general evaluation of

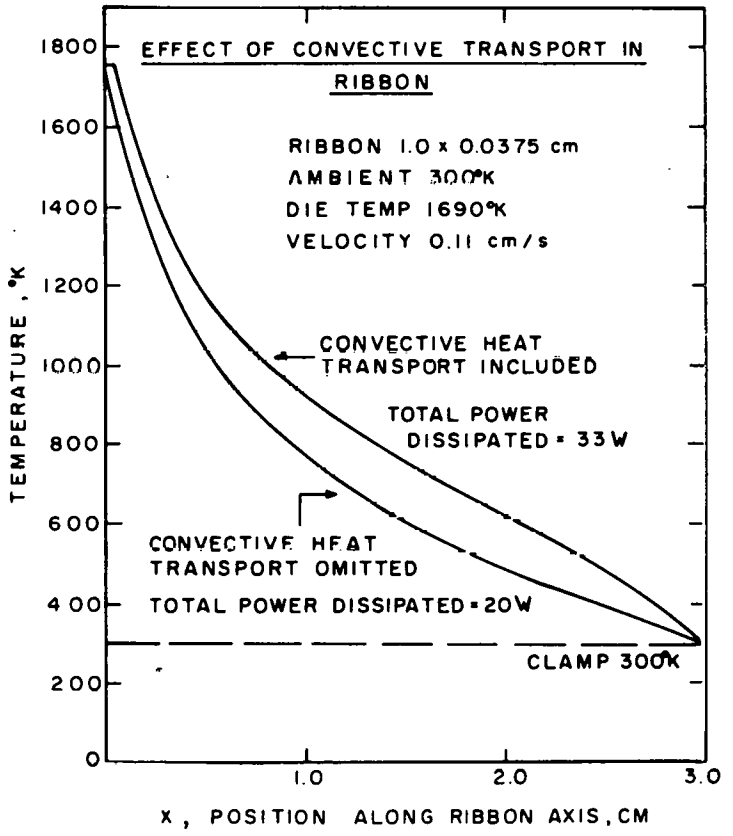

Figure 24. Effect of convective heat transport on the temperature profile of a growing ribbon.

the temperature profile along the ribbon in order to dissipate the additional heat input arising from convective transport from the die in the form of the liquid silicon which is drawn from the die. The net convective heat input to the ribbon is given by

$$P_C = SV(T_D - T_{CL})wt \tag{13}$$

where T_D is the die temperature and T_{CL} is the clamp temperature. P_C is 11.6 W for the case shown in Fig. 24, and the distribution of the heat loss by mode of dissipation is shown in Table 3.

TABLE 3. EFFECT OF THE CONVECTIVE TRANSPORT TERM ON THE TOTAL POWER DISSIPATION AND ITS DISTRIBUTION BETWEEN THE VARIOUS MODES OF DISSIPATION

Parameter	No convective transport (W)	Convective transport included (W)
Total power dissipated	19.7	33.3
Radiation loss	15.88	22.64
Convection loss	2.44	3.50
Clamp conduction loss	1.38	4.29
Clamp convective loss	0.00	2.86

In Fig. 25 we show the temperature profile in the neighborhood of the molten zone as a function of the ribbon growth velocity. In all cases the ribbon geometry (0.0375 x 1.0 cm, 3.0 cm long), die temperature (1690°K) and ambient temperature (300°K, uniform along ribbon) remain unchanged and only the growth velocity is varied. The position of the freezing boundary of the molten zone is given by the point at which the gradient of the temperature profile dT/dx undergoes an abrupt change in value. This feature is a direct consequence of the liberation of the latent heat of fusion Q_F [Eq. (11)] and the discontinuous change in the thermal conductivity of silicon at the melting point, since conservation of energy across the freezing boundary demands that

$$-K_S \left(\frac{dT}{dx} \right)_{x_B+\delta_x} = -K_L \left(\frac{dT}{dx} \right)_{x_B-\delta_x} + \dot{Q}_F \qquad (14)$$

where x_B is the position of the freezing interface. Since the heat conducted away from the freezing interface $-K_S(dT/dx)_{x_B+\delta_x}$ wt is limited by the rate at which heat can be dissipated from the remainder of the ribbon ($x > x_B$) to the ambient and to the clamp, we expect that as the velocity is increased, the magnitude of the latent heat term in Eq. (14) will increase, and the temperature gradient in the liquid silicon $(dT/dx)_{x<x_B}$ must decrease. This effect is evident in Fig. 25 and leads to a reduction in the heat drain

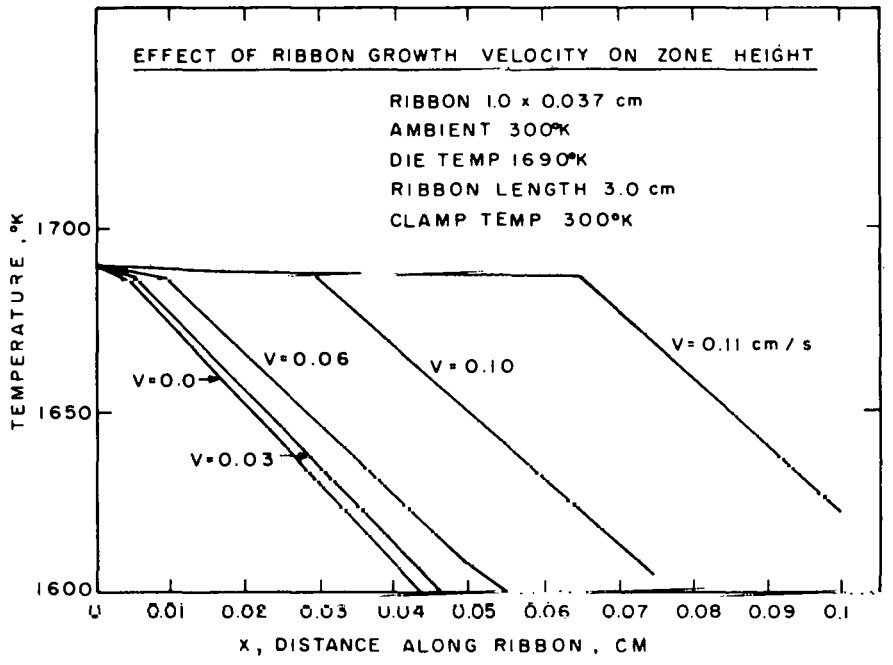

Figure 25. Temperature profile in the vicinity of the molten zone as a function of growth velocity in uniform 300°K ambient.

on the die due to conduction into the molten zone. On the other hand, increasing the growth velocity will lead to increased heat drain on the die due to the convective transport of heat retained in the molten silicon supplied from the die aperture. The dependence of these quantities on the ribbon growth velocity for the case shown in Fig. 25 is indicated in Table 4.

The most notable feature of Fig. 25 is the increase of the zone height with the ribbon growth velocity. The molten zone height, normalized to the ribbon thickness, is shown in Fig. 26 directly as a function of growth velocity for the data in Fig. 25, and we see an initially slow rate at increase of the zone height, which becomes ever more rapid as the growth velocity approaches and exceeds about 0.1 cm/s (140 in./h). Clearly, the surface tension of the liquid silicon cannot support an indefinitely large molten zone height, and even before a catastrophic collapse of the zone occurs, a zone height that is large relative to the ribbon thickness is expected to affect the geometry of the growing single crystal. Thus, the divergence of the zone height above the critical

TABLE 4. INFLUENCE OF GROWTH VELOCITY ON THE THERMAL CHARACTERISTICS OF GROWING RIBBON FOR 300°K AMBIENT AND 1690°K DIE TEMPERATURE

Die Temp. T_D (°K)	Ambient Temp. (°K)	Growth Velocity V (cm/s)	(in./min)	Zone Height H (cm)	$\frac{H}{t}$	Latent Heat Input Q_c (W)	Net Convective Input P_c (W)	Power Conducted From Die P_D (W)	Total Power Dissipated (W)	Mode of Power Dissipation % Radiation	Convection	Conduction	Convective Transport
1690	300	0.0	0.0	0.006	0.17	0.0	0.0	19.5	19.0	80	13	7	0
1690	300	0.03	0.71	0.007	0.18	4.66	3.17	13.8	21.7	76	12	9	3
1690	300	0.06	1.42	0.012	0.31	9.31	6.32	8.46	24.9	73	11	10	6
1690	300	0.10	2.36	0.037	0.99	15.5	10.52	2.76	30.4	71	10	12	7
1690	300	0.11	2.60	0.067	1.79	17.1	11.6	2.88	33.3	71	10	12	7

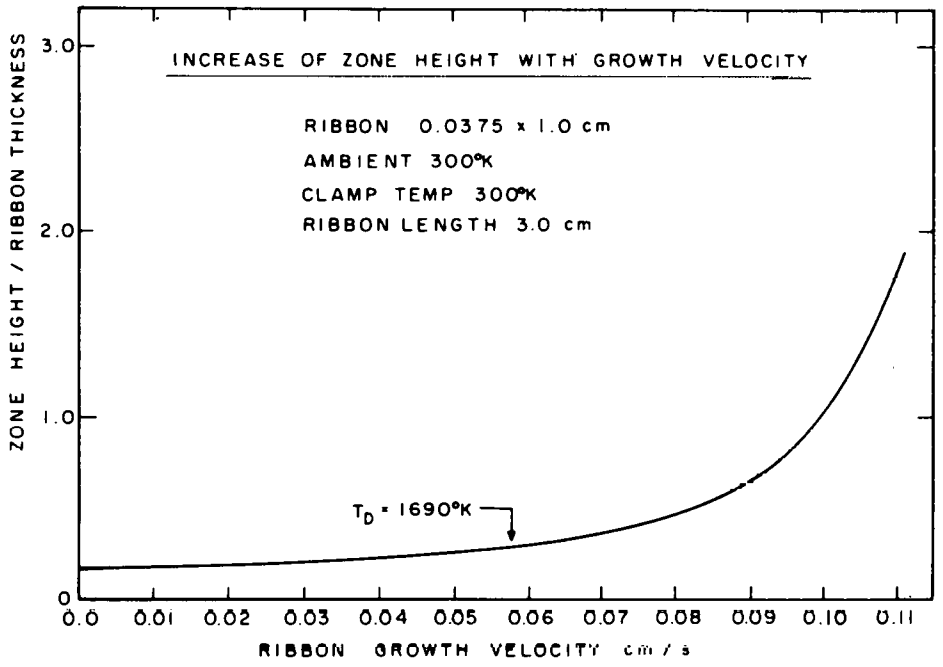

Figure 26. Zone height, normalized to the ribbon thickness, as a function of growth velocity taken from the data of Figure 25.

velocity in effect limits the maximum growth rate for the ribbon for a given set of ambient conditions.

In Fig. 27 we show the temperature profile in the neighborhood of the molten zone as a function of the growth velocity for a 0.0375 x 1.0 cm ribbon, 3.0 cm long in an elevated uniform ambient of 1300°K for a die temperature of 1690°K (T_M = 1683°K). The elevated ambient temperature reduces the rate at which heat can be dissipated from the ribbon to the ambient and the ribbon clamp to about 11 W (V = 0) compared with about 19 W (V = 0) for the 300°K ambient. Moreover, we note that the mode of dissipation is shifted even more toward the radiative mode (compare Tables 4 and 5). The reduction in power dissipation in the 1300°K ambient reduces the temperature gradient in the solid adjacent to the molten zone $(dT/dx)_{x_B+\delta_x}$, and in view of Eq. (14) we expect the reduction of the temperature gradient in the liquid, and the consequent increase in the zone height, to occur at lower growth velocities. This is apparent in Fig. 27 where the zone height has already grown quite large for a velocity of only 0.065 cm/s.

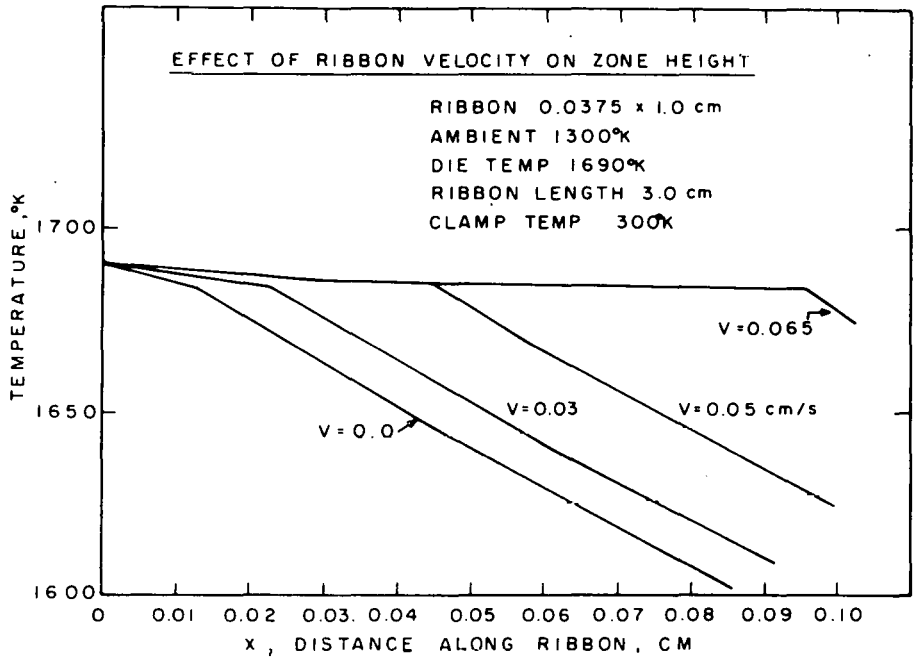

Figure 27. Temperature profile in the vicinity of the molten zone as a function of growth velocity in a uniform 1300°K ambient (die temperature 1690°K).

The zone height is related to the temperature gradient in the liquid zone and the temperature of the die by

$$H \approx \frac{T_D - T_M}{(dT/dx)_{x<x_B}} \tag{15}$$

therefore, some reduction in the zone height under conditions of constant growth velocity and ambient temperature should be possible by reducing the elevation of the die temperature above the melting point. In Fig. 28 we show the temperature profile for the same ribbon and ambient as in Fig. 27 but with the die temperature reduced to 1685°K. The change in the zone height at constant growth velocity is shown most clearly in Fig. 29, where we note that despite the apparent reduction in the zone height at the lower velocities, the maximum practical growth rate is increased by perhaps only 20% due to the rapid divergence of the zone height in both instances as the critical velocity is approached. As the critical

TABLE 5. INFLUENCE OF GROWTH VELOCITY ON THERMAL CHARACTERISTICS OF A GROWING RIBBON FOR 1300°K AMBIENT WITH DIE TEMPERATURES OF 1690°K and 1685°K

Die Temp. T_D (°K)	Ambient Temp. (°K)	Growth Velocity V (cm/s)	Growth Velocity V (in./min)	Zone Height H (cm)	Zone Height $\frac{H}{t}$	Latent Heat Input Q_c (W)	Net Convective Input P_c (W)	Power Conducted From Die P_c (W)	Total Power Dissipated (W)	Mode of Power Dissipation (&) Radiation	Convection	Conduction	Convective Transport
1690	1300	0.0	0.0	0.014	0.36	0.0	0.0	11.0	10.7	98	2	0	0
1690	1300	0.03	0.71	0.024	0.63	4.66	0.94	6.3	14.5	78	2	0	20
1690	1300	0.05	1.18	0.046	1.23	7.76	1.48	3.95	17.6	70	2	0	28
1690	1300	0.065	1.54	0.096	2.57	10.1	1.94	3.37	21.3	68	2	0	30
1685	1300	0.0	0.0	0.0007	0.02	0.0	0.0	10.4	10.2	98	2	0	0
1685	1300	0.03	0.71	0.0036	0.10	4.66	0.87	5.57	13.7	76	2	0	22
1685	1300	0.06	1.42	0.019	0.50	9.31	1.75	1.12	17.7	65	2	0	33
1685	1300	0.07	1.65	0.064	1.70	10.9	2.03	1.52	20.6	65	2	0	33

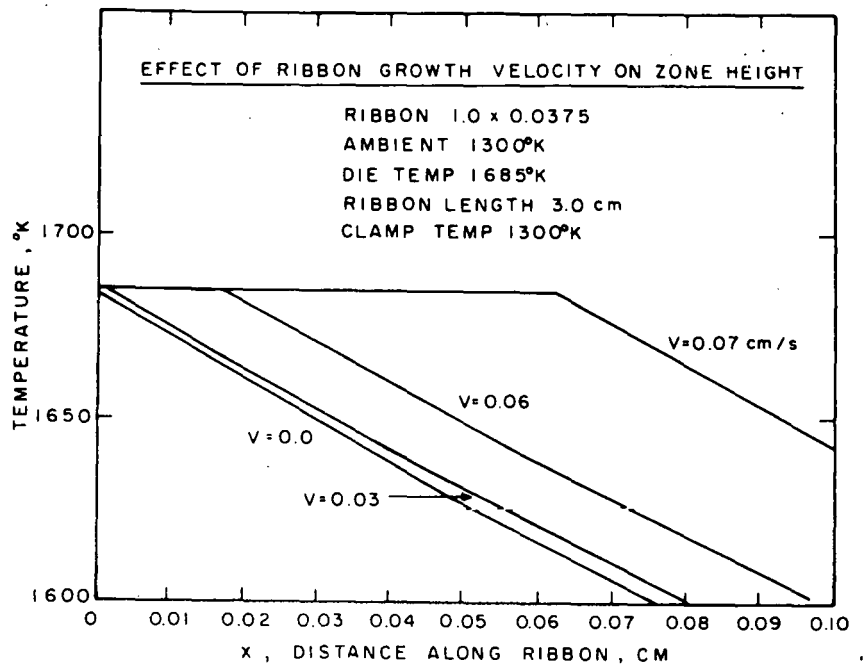

Figure 28. Temperature profile in the vicinity of the molten zone as a function of growth velocity in a uniform 1300°K ambient (die temperature 1685°K).

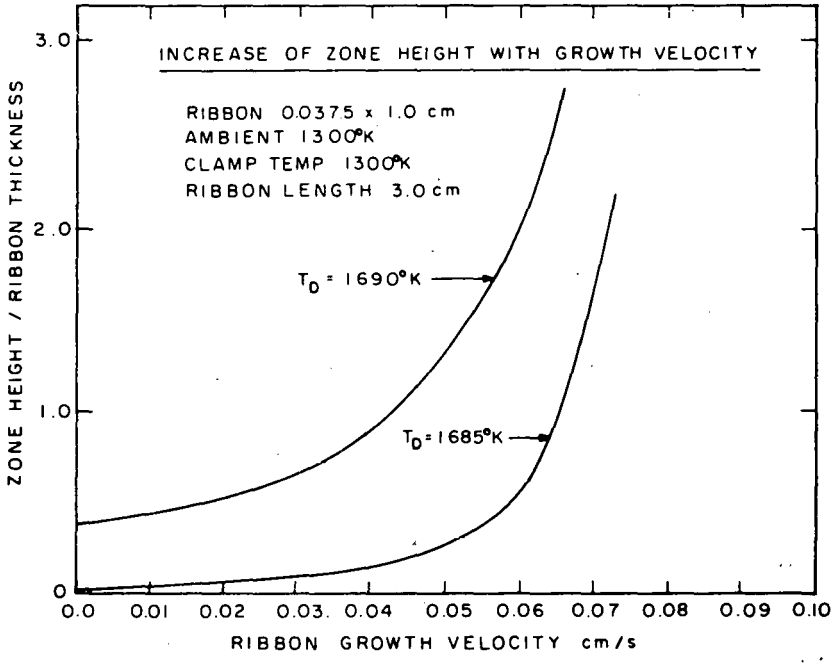

Figure 29. Zone height, normalized to the ribbon thickness as a function of growth velocity taken from the data of Figs. 27 and 28.

velocity is approached, the temperature gradient in the liquid zone tends to zero so that Eq. (14) becomes

$$-K_S \left(\frac{dT}{dx} \right)_{x_B+\delta_x} = Q_F = VwtL \tag{16}$$

where V is the critical velocity. $-K_S(dT/dx)_{x_B+\delta_x}$ is equal to the rate at which heat is dissipated from the ribbon at $x > x_B$, so that the maximum growth rate is seen to be that velocity that generates latent heat of fusion at a rate equal to the rate at which heat can be dissipated from a stationary ribbon, P_S. (The increase in dissipated power seen in Tables 4 through 6 for a moving ribbon serves only to balance the extra convective heat input, and does not aid in the dissipation of latent heat.) Thus, for given ambient conditions

$$V \lesssim \frac{P_S}{Lwt} \tag{17}$$

Reducing the die temperature will help to maintain a lower zone height at subcritical growth rates, but since reducing the die temperature under otherwise constant ambient does not greatly affect P_S (see Table 5), the critical growth rate remains essentially unchanged.

Equation (17) suggests that some increase in the critical growth rate may be achieved by reducing the ribbon thickness, t, thereby reducing the rate of liberation of latent heat at constant growth velocity. In Fig. 30 we investigate this possibility by showing the temperature profile near the molten zone for a ribbon whose thickness is reduced to one-half (0.0187 cm) of the previous ribbon thickness. The ambient temperature is still maintained at 300°K, and we see that, for a given growth velocity, the zone height for the thinner ribbon is indeed smaller than that for the 0.037 cm thick ribbon shown in Fig. 25. When the reduced zone height is normalized to the reduced ribbon thickness as shown in Fig. 31 and the maximum growth velocities of the 0.0375-cm-thick and 0.0187-cm-thick ribbons are determined for the same H/t criterion (for example H/t $\approx$ 2), then we see that the 50% reduction in ribbon thickness gains $\sim$35% increase in growth velocity, to yield a figure of 0.15 cm/s for the thinner ribbon. In Table 6 we observe that the reduction in ribbon thickness has lowered

TABLE 6. INFLUENCE OF GROWTH VELOCITY ON THERMAL CHARACTERISTICS OF 0.0187 x 1.0 cm GROWING RIBBON FOR 300°K AMBIENT AND 1690°K DIE TEMPERATURE

Die Temp. T_D (°K)	Ambient Temp. (°K)	Growth Velocity V (cm/s)	Growth Velocity V (in./min)	Zone Height H (cm)	Zone Height $\frac{H}{t}$	Latent Heat Input Q_L (W)	Net Convective Input P_C (W)	Power Conducted From Die P_D (W)	Total Power Dissipated (W)	Mode of Power Dissipation % Radiation	% Convection	% Conduction	% Convective Transport
1690	300	0.00	0.00	0.005	0.27	0.00	0.00	13.7	13.3	83	14	3	0
1690	300	0.06	1.42	0.005	0.27	4.64	3.15	10.1	10.1	77	14	5	4
1690	300	0.10	2.36	0.010	0.53	7.74	5.26	18.3	18.3	75	13	6	6
1690	300	0.15	3.54	0.043	2.30	11.60	7.90	22.9	22.9	74	12	7	7
1690	300	0.16	3.78	0.063	3.37	12.4	8.39	24.2	24.2	74	11	7	8

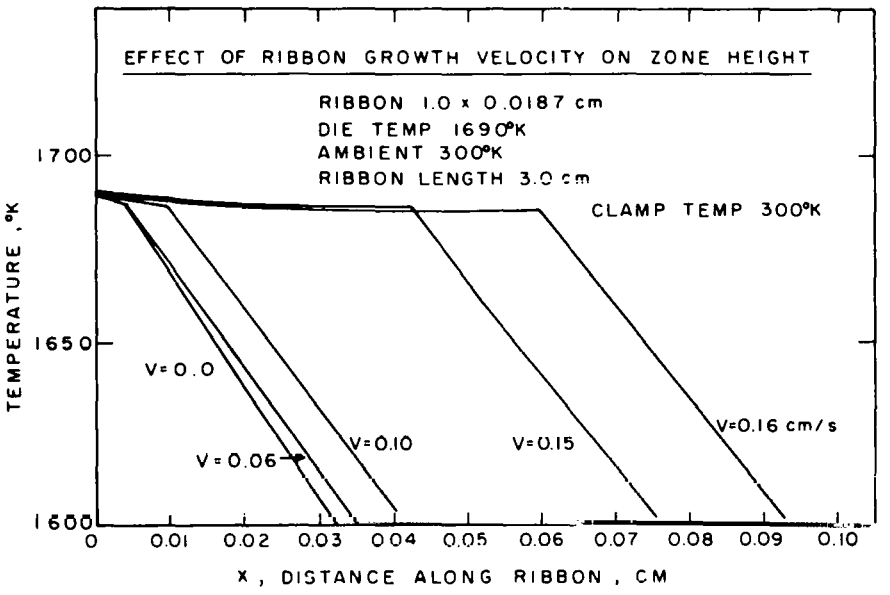

Figure 30. Temperature profile in the vicinity of the molten zone as a function of growth velocity for a ribbon with 50% reduction in thickness (uniform ambient 300°K).

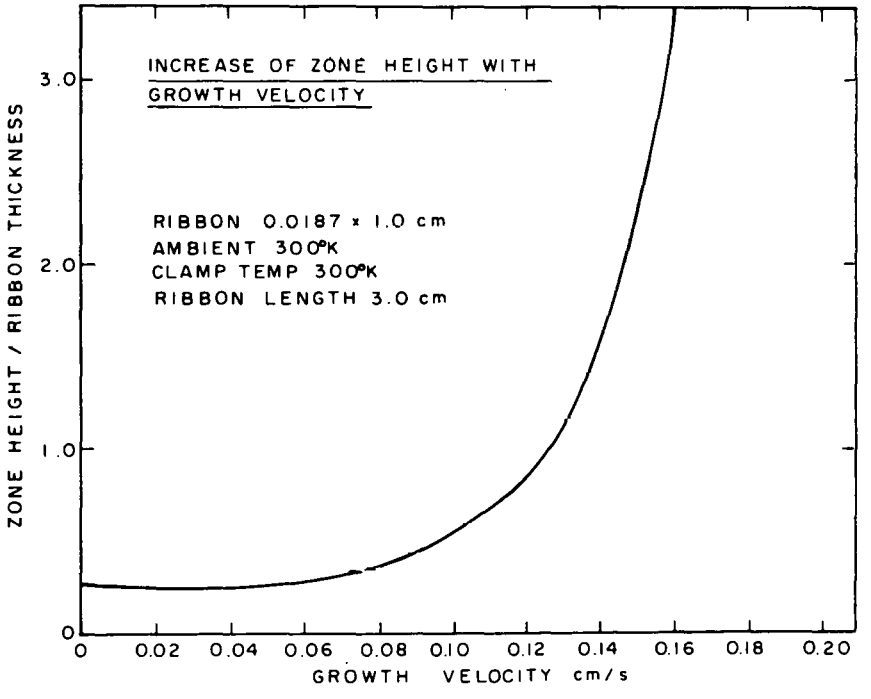

Figure 31. Zone height, normalized to ribbon thickness, as a function of growth velocity, taken from the data of Fig. 30.

the thermal conductance of the ribbon so that P_s, the power dissipated to the ambient by a stationary ribbon, has been reduced from 19 W where t = 0.0375 cm (Table 4) to 13.3 W where t = 0.0187 cm in the same ambient conditions. Thus, while it is evident that a thinner ribbon will have a higher maximum growth velocity, some of the advantage of the reduced generation of latent heat will be offset by the reduced thermal conductance of the ribbon and the consequently smaller value of heat dissipation from ribbon to ambient.

To summarize the results of the model concerning the effect of ambient thermal conditions and ribbon geometry on the growth rate:

(1) For a given ribbon geometry and ambient conditions, the zone height increases with the growth velocity and does so more and more rapidly as the critical (maximum) growth velocity is approached.

(2) The critical growth velocity is given approximately as that velocity that leads to the generation of latent heat of fusion at a rate just equal to the rate at which heat can be dissipated from the ribbon when stationary in the same ambient.

(3) The highest growth rates will be achieved with the coolest ambient temperatures, by increasing the convective heat transfer coefficient, G, or reducing the separation of the die from the ribbon clamp so as to increase the conducted heat loss from the ribbon.

(4) At a given growth rate and under otherwise constant conditions, reduction of the die temperature will reduce the zone height.

(5) The maximum growth rate for thinner ribbon is increased, but by an amount that is less than proportional to the reduction in the thickness.

b. *Thermal Stress* — For an isotropic medium the thermal stress is clearly zero if the temperature distribution through the medium is uniform. However, it can be shown in general that if the temperature distribution has a constant temperature gradient, dT/dx, there will be no thermal stresses. In other words, for an isotropic medium the thermal stress depends only on the curvature, d^2T/dx^2, of the temperature profile and its higher order spatial derivatives. In view of this result, in order to grow silicon ribbon with a minimum of thermal stress it is necessary to manipulate

the thermal environment of the ribbon to produce a temperature profile in the ribbon itself which is as linear as possible. This requirement is particularly important for those regions of the ribbon where the temperature during growth exceeds the plastic temperature and even low thermal stress will cause irreversible strain, resulting in intrinsic stress at room temperature. In our analysis we have not attempted to calculate the thermal stress quantitatively, but have examined the effect of the thermal ambient of the ribbon on the curvature in the ribbon temperature profile since this will be a measure of the thermal stress.

In Fig. 32, curve I, we show the temperature profile along a 3.0-cm ribbon with a 1.0 x 0.0375 cm cross section growing with V = 0.10 cm/s. In this case the ambient temperature was uniform along the ribbon at 300°K, and the ribbon clamp is also fixed at 300°K. Considerable curvature of the isotherm is evident, and the magnitude of d^2T/dx has a maximum value of 2×10^4°K/cm^2 at the zone boundary and falls progressively in regions closer to the ribbon clamp. In Fig. 32, curve II, the profile for the same ribbon in a uniform ambient of 1300°K is shown. Since the higher ambient temperature reduces the heat loss from the ribbon to the ambient, the temperature gradient at the molten zone interface and, therefore, the maximum growth velocity are reduced, and this profile was generated when the velocity was set to 0.05 cm/s. The magnitude of the curvature shows a general reduction of only about a factor of two as it is noted by comparing with the 300°K ambient case (curve I). Curve III in Fig. 32, which is significantly more linear than the others, results when the ambient temperature itself is linearly reduced from 1650°K at the die aperture to 300°K at the ribbon clamp. The magnitude of d^2T/dx^2 is reduced by about an order of magnitude from that generated in the uniform 300°K ambient case. However, the general increase in the ambient temperature now limits the rate at which heat may be dissipated from the ribbon surfaces to about one-quarter of that in the 300°K uniform ambient; thus, in order to linearize the temperature profile, the growth rate has suffered and is limited to about 0.03 cm/s in the linear ambient temperature environment.

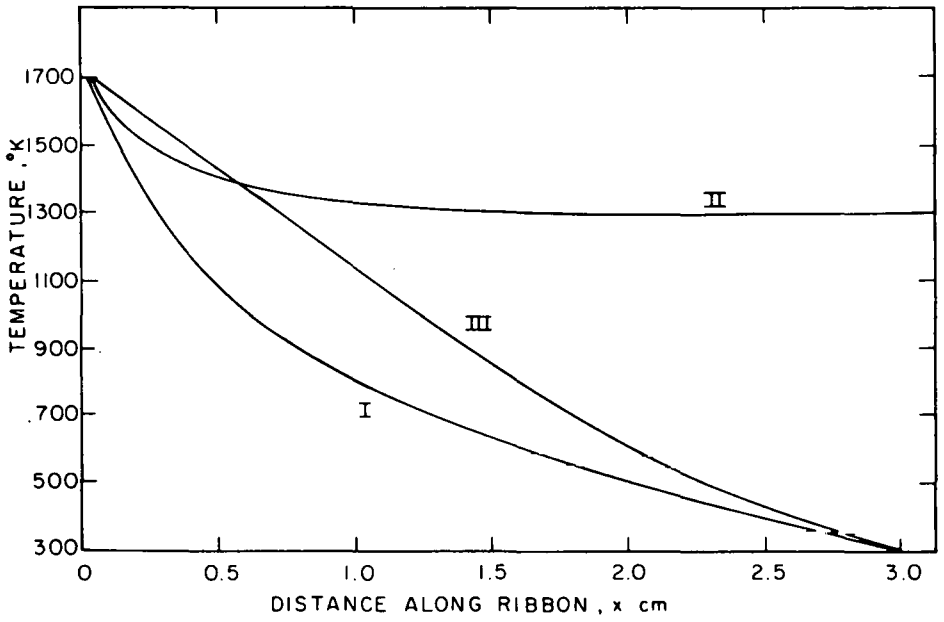

Figure 32. Ribbon temperature profiles for 0.0375 x 1.0 cm ribbon, ribbon clamp 3.0 cm from die. Curve I: 300°K uniform ambient V = 0.10 cm/s. Curve II: 1300°K uniform ambient V = 0.05 cm/s. Curve III: Linear ambient from 1650°K at the die to 300°K at the clamp, V = 0.03 cm/s.

The thermal gradient at any point, x, along the ribbon is given by

$$\frac{dT}{dx} = \frac{Q}{KA} \tag{18}$$

where Q is the heat flux at that point, K is the thermal conductivity, and A is the cross-sectional area. The thermal conductivity of silicon is a function of the temperature and increases as we move from the hotter regions close to the floating zone down to the cooler regions close to the clamp. At the same time the heat flux in the ribbon reduces as we go toward the clamp due to the heat lost via radiation and convection from the ribbon surfaces to the ambient. As we have seen in Fig. 32, curve I, these two effects combine to progressively reduce the temperature gradient down the ribbon and introduce a positive curvature into the profile. Even if the ribbon were insulated to prevent heat loss to the ambient and keep Q constant all along the ribbon, curvature would still exist due to

the increasingly large thermal conductivity towards the clamp. This curvature, due solely to the temperature dependence of the thermal conductivity, is shown in Fig. 33, curve I. In order to obtain a linear temperature, gradient heat must be added to the ribbon as we move towards the clamp in just the right quantity to compensate for the increasingly large thermal conductivity. As we have seen, heat may be added to the ribbon by arranging for the ambient temperature profile to exceed that of the ribbon itself; however, this will tend to reduce the heat conducted from the floating zone boundary, and therefore limit the growth rate. We can, however, add heat to the ribbon from the ambient and simultaneously maintain the growth rate by increasing the conducted heat loss to the ribbon clamp. This is achieved by reducing the separation between the die aperture and the clamp. In Fig. 33 the separation has been reduced from the 3 cm used in Fig. 32 to only 0.5 cm, and the clamp temperature is maintained at 800°K. Figure 33, curve IV, shows the profile in the ribbon with a growth velocity of 0.08 cm/s when the ambient temperature varies linearly from 1600°K at the die aperture (x = 0.0 cm) to 1400°K at the ribbon clamp (x = 0.5 cm). The curvature in this case is now negative, indicating that the heat input from the ambient is overcompensating for the increasing thermal conductivity. A more linear profile results when the ambient varies linearly from 1600 to 1300°K, and this case is shown in curve III of Fig. 33 for a ribbon velocity of 0.08 cm/s. Due to the proximity of the ribbon clamp in this case the conducted heat loss to the clamp is increased to 25 W compared with only 11 W for the linear temperature ambient when the ribbon is clamped 3 cm from the die aperture. The resultant increase in the temperature gradient at the zone boundary permits an increase of the maximum growth velocity from 0.03 cm/s to 0.08 cm/s.

In summary, we can see that in principle it is possible to achieve a high growth rate simultaneously with a linear ribbon temperature profile by shortening the distance between the die aperture and the ribbon clamp, thereby increasing the heat flux from the molten zone boundary by increasing the conducted loss to the ribbon clamp. The radiative and convective heat transfer can then be adjusted by tailoring the ambient temperature profile to result in a linear temperature variation along the ribbon, compensating for the temperature dependence of the thermal conductivity of the silicon.

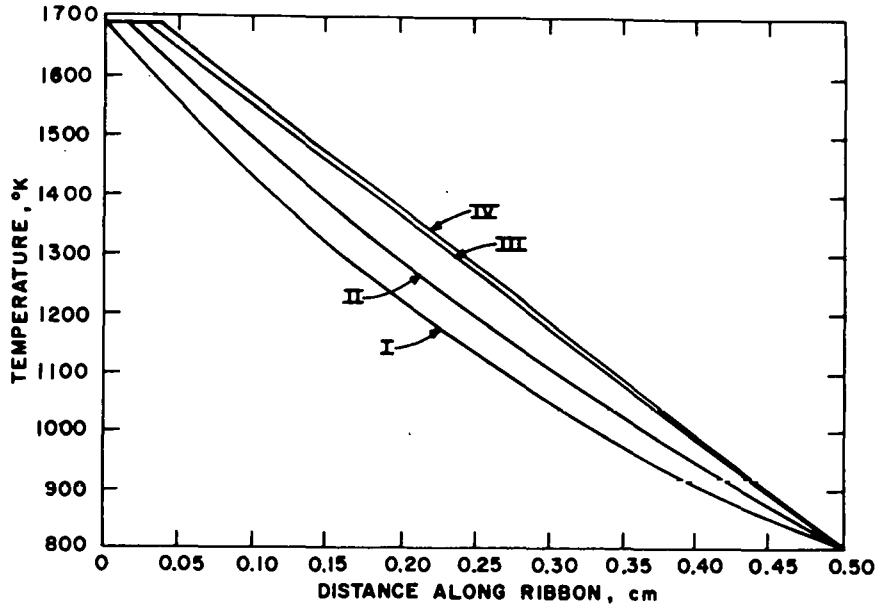

Figure 33. Temperature profile along 0.0375-cm-thick ribbon for various ambient conditions and growth rates. In all cases the ribbon is clamped at 800°K at a distance of 0.5 cm from the die aperture. Curve I: V = 0.0, no radiation or convection heat loss. Curve II: uniform ambient 800°K, V = 0.125 cm/s. Curve III: linear ambient 1600°K at x = 0, 1300°K at x = 0.5 cm, V = 0.08 cm/s. Curve IV: linear ambient 1600°K at x = 0, 1400°K at x = 0.5 cm, V = 0.08 cm/s.

B. RIBBON GROWTH STABILITY — RIBBON THICKNESS VS THE MENISCUS HEIGHT UNDER POSITIVE PRESSURE

The equilibrium shape of the meniscus can be calculated using the Laplace capillary equation. The Laplace equation relates the pressure difference ΔP inside and outside the meniscus to the radius of curvature and the interfacial tension γ between the molten silicon and the ambient gas phase, i.e., $\Delta P = \gamma (1/R_1 + 1/R_2)$. Here R_1 and R_2 are the first and the second principal radii of curvature of the meniscus.

The Laplace equation is a second-order differential equation. The analytical solution of the equation for the ribbon growth geometry is, however, rather difficult. The reason is that near the ends of the ribbon the radius of curvature (R_2) changes from minus infinity along the side of

the ribbon to approximately minus half the ribbon thickness -t/2 at the ribbon ends. The solution for the meniscus shape in the ribbon growth geometry is approximated by a combination of two solutions, i.e., a solution for meniscus against a vertical flat plate and that against a vertical cylinder of radius t/2 [5].

Results of the approximate solutions regarding the effect of the hydrostatic pressure in the meniscus on the shape stability [6] will be described here briefly. The steady-state s-t dependence (s, the meniscus height) for various values of the hydrostatic pressure was established. The s-t relationships applying at the ribbon side and at the ends of the ribbon were found. It is of interest to note that the hydrostatic pressure is negative in EFG or the Stepanov process, while this is positive in the inverted EFG or inverted Stepanov process.

A lesser degree of dependence of the ribbon thickness on changes in the meniscus height is desirable for the stable ribbon growth. Fluctuations in the meniscus height can be caused during ribbon growth by temperature fluctuations or mechanical vibrations in the growth system. In other words, a lower absolute value of the slope, $|dt/ds|$, in the s-t relationship is a quantitative measure of the ribbon growth stability. The shape stability of the ribbon side is enhanced under the positive pressure compared with the case under the negative pressure. Under positive pressure, as in the inverted Stepanov and inverted EFG process with sufficient melt height, shape stability increases within limit, as the meniscus height increases; for instance, at a hydrostatic pressure of 2 cm, the limit of stability $|dt/ds| = 0$ is reached at $s \approx t$. The stability at the ribbon ends is also enhanced under the positive pressure.

C. STABILITY OF SEEDING WITH NONWETTING DIES

The static stability of the meniscus after seeding is one of the key requirements for stable and successful crystal growth. This stability problem is particularly important in the inverted Stepanov process (IS), where the geometry of the silicon ribbon is controlled primarily by the physically shaped meniscus in a narrow rectangular slot of a nonwetting die.

Conventionally, the equilibrium shape of the meniscus after seeding and the capillary rise problems are treated by solving the Laplace equation which relates to the pressure difference across the interface between melt and the ambient gas phase.

We have taken an alternative approach to the problem of the stability of seeding by evaluating the surface-free energies of the system prior to and after the seeding. This approach allows one to include explicitly in the stability conditions such dimensional parameters as the height of the capillary slot (h) and the thickness of the silicon sheet (t).

The analysis was carried out by using a model represented schematically in Fig. 34. For the growth of a ribbon of constant cross section employing a nonwetting shaping guide, Gaulé and Pastore [14] found that the relative cross-sectional dimensions of the capillary slot and the ribbon must be interrelated, i.e., $t \approx t_o$ and $\omega \approx \omega_o$, where t and ω are the thickness and width of the ribbon, and t_o and ω_o the corresponding dimensions of the capillary slot.

The surface-free energy before seeding (F_1) and after seeding (F_2) can be expressed as follows:

$$F_1 = \gamma\, \omega_o t_o + 2\gamma_d h\, (\omega_o + t_o) + \gamma_{Si} + \omega \tag{19}$$

$$F_2 = \gamma\, (\omega_o t_o - \omega t) + \gamma_{s\ell}\omega t + 2\gamma_{d\ell} h\, (\omega_o + t_o) \tag{20}$$

Here h is the capillary height, γ and γ_{Si} the surface tension of liquid and solid silicon, respectively, $\gamma_{s\ell}$ the interfacial free energy between the liquid and solid silicon, and $\gamma_{d\ell}$ the interfacial free energy between the liquid silicon and die. In the above expression it was assumed that the meniscus height below the die is negligible, and the work done to increase the melt volume after seeding is supplied by the external means, i.e., by increasing power input.

14. G. K. Gaulé and J. R. Pastore, in *Metallurgy of Elemental and Compound Semiconductors*, R. O. Gruble, Ed., (Interscience Publ., Inc., New York, 1961).

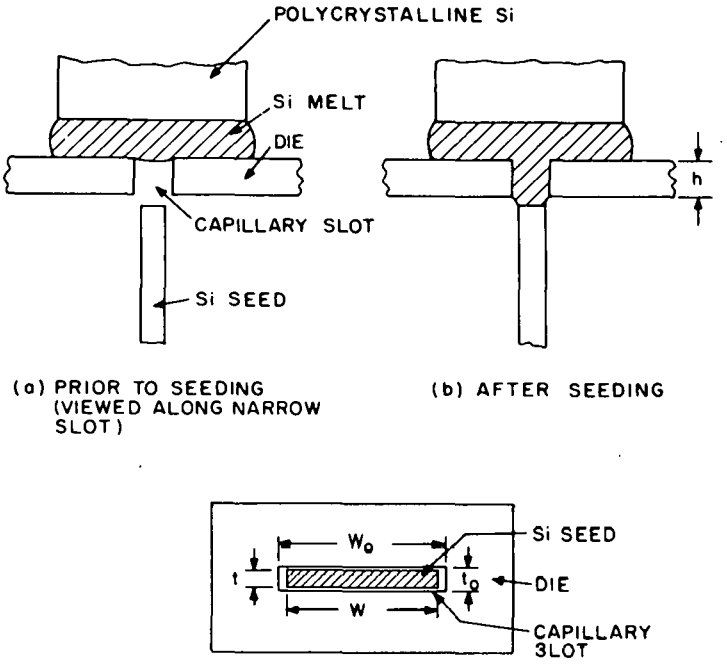

Figure 34. A schematic of the configuration employed for the analysis of stability of seeding in the inverted ribbon growth with nonwetting die.

For the system to be stable energetically after the seeding, the total surface-free energy at this state must be lower than before seeding:

$$F_2 - F_1 \leq 0 \tag{21}$$

From Eqs. (19), (20), and (21), and using the relationship $\gamma \cos \alpha = \gamma_d - \gamma_{d\ell}$ we find

$$h \leq \frac{\omega t(\gamma + \gamma_{Si} - \gamma_{s\ell})}{2(\omega_o + t_o)\ (-\gamma \cos \alpha)} \approx \frac{t(\gamma + \gamma_{Si} - \gamma_{s\ell})}{2\gamma(-\cos \alpha)}$$

or

$$h \leq \frac{t(\gamma + \gamma_{Si} - \gamma_{s\ell})}{2\gamma(-\cos \alpha)} = \frac{(0.96)(t)}{(-\cos \alpha)} \tag{22}$$

Here γ = 720 dyne/cm, γ_{Si} = 1000 dyne/cm [15], and $\gamma_{s\ell}$ = 350 dyne/cm [16] were used. The relationship between the capillary height (h) and the thickness of the silicon ribbon (t) given in Eq. (22) applies in IS only when the contact angle is larger than 90°. The allowed capillary height for the stable seeding can be higher than the values from Eq. (22) when the hydrostatic pressure head due to the melt height is taken into account in the real case.

A die material for which the relationship of Eq. (22) applies is the pyrolytic boron nitride, where the contact angle between molten Si and BN is 110°. The h-t relationship for the BN die will be

$$h \leq (2.78)(t) \tag{23}$$

In the silicon growth experiment with the flat BN die (as described in Section IV.A.1), the ratio of h/t for the stable growth was found to be in the range of 0.5 to 1.0 when the ribbon thickness was larger than 0.05 cm. This ratio is close to the value expected from the relationship of Eq. (23). However, for the growth of ribbons less than 0.025 cm in thickness, the ratio approaches zero.

When the contact angle is smaller than 90°, as in the case using SiO_2 dies, a new h-t relationship must be found by taking into account the capillary rise before seeding.

One of the important parameters in the shaped crystal growth with a die is the capillary rise (h_o), which is a function of the contact angle (α) and the capillary thickness (t_o) for a given liquid. The capillary rise, h_o, can be expressed as follows:

$$h_o = \frac{1}{\rho g} \cdot \frac{2\gamma \cos \alpha}{t_o} \tag{24}$$

where g, ρ, and γ are the gravitation constant, density, and surface tension of the melt, respectively.

15. R. J. Jaccodine, J. Electrochem. Soc. 110, 524 (1963).
16. D. Turnbull, J. Appl. Phys. 21, 1022 (1950).

In the inverted Stepanov silicon ribbon growth using a die with contact angle larger or slightly smaller than 90°, h_o can be negative (capillary depression) or slightly positive (capillary rise). Calculated values of h_o for SiO_2 and pyrolytic BN dies of various capillary thickness are reproduced in Table 7 along with the h_o values for carbon die for comparison.

TABLE 7. CAPILLARY RISE OF THE LIQUID SILICON IN SiO_2, PYROLYTIC BN, AND CARBON DIE

Die	α (degree)	t_o (cm)	h_o (cm)
SiO_2	87	0.05	0.7
		0.025	1.3
		0.01	3.3
Pyrolytic BN	110	0.05	- 4.3
		0.025	- 8.6
		0.01	-21.6
Carbon	30	0.05	10.9
		0.025	21.8
		0.01	54.6

For instance, in the case of the pyrolytic BN die with $\alpha \approx 110°$, there is a capillary depression which amounts to $h_o = -4.3$ cm for a slot thickness of 0.05 cm. The interfacial free energy between the liquid and solid silicon ($\gamma_{s\ell}$) is less than one-half the liquid surface tension (γ), i.e., 350 vs 720 dyne/cm. As discussed in this section, the low interfacial free energy is a driving force to partly overcome the capillary depression in the pyrolytic BN die and thus to bring the meniscus into or out of the die slot depending on the height of the slot, when the melt is seeded with the silicon seed crystal. The capillary rise due to the seeding as a function of the capillary thickness can be estimated by Eq. (22). The hydrostatic pressure in the melt due to the gravity reinforces this driving force in the IS silicon ribbon growth.

It is of interest to mention that the viscous pressure drop for the melt flow through the capillary slot needed to sustain the ribbon growth is low for typical silicon ribbon growth [5]. A pressure drop of 3 μm in liquid silicon is calculated, for instance, in a ribbon grown at a pull rate of 2.4 cm/min using a die with a slot 0.02 cm thick and 0.05 cm high.

SECTION VI

CHARACTERIZATION OF THE SILICON RIBBONS GROWN BY THE INVERTED RIBBON GROWTH PROCESS

A. RIBBONS GROWN WITH PYROLYTIC BN DIE

1. X-Ray Topographic Investigation

The crystallinity and defect structure of silicon ribbons grown with the flat pyrolytic BN die were investigated by x-ray topography and chemical etching. The properties of a typical silicon ribbon which was 1.4 cm wide and 0.04 cm thick are described in this section. The nominal growth orientation was $(110)[\bar{1}1\bar{2}]$.

A $(\bar{1}11)$ projection topograph is reproduced in Fig. 35, which was taken using a Lang camera and MoK_α radiation. A $(\bar{3}33)$ topograph, which is more sensitive to long range strains, was also taken. A regular array of spot defects is imaged at the right side of Fig. 35 and is visible over the full height of the topograph. Many of the defects have generated local dislocation arrays. The regular periodicity of these defects suggests they are related to a regular variation in the ribbon growth procedure. In addition, Fig. 35 shows planar defects imaged as parallelograms with a fringe contrast across the area of defects. This appearance in the $(\bar{1}11)$ topograph (Fig. 35) and the no-contrast of the defects in the $(\bar{3}33)$ topograph are consistent with identifying these planar defects as stacking faults.

The section topograph of the same specimen as shown in Fig. 35 is reproduced in Fig. 36. Note the planar defect extending through the crystal. Also, the images are often not uniform from one surface to the other, but instead go out of contrast along a well-defined line. This indicates low-angle grain boundaries cutting the wafer at these lines.

In general, the ribbons were composed of long grains along the growth direction. Often a single grain would not extend from one surface of the ribbon to the other. The misorientation between grains varied from less than 0.1° to over 1°. There was no evidence that the grains were twin related.

The change in orientation of the ribbon due to the presence of grains was determined by finding the orientation of the ribbon for diffraction from

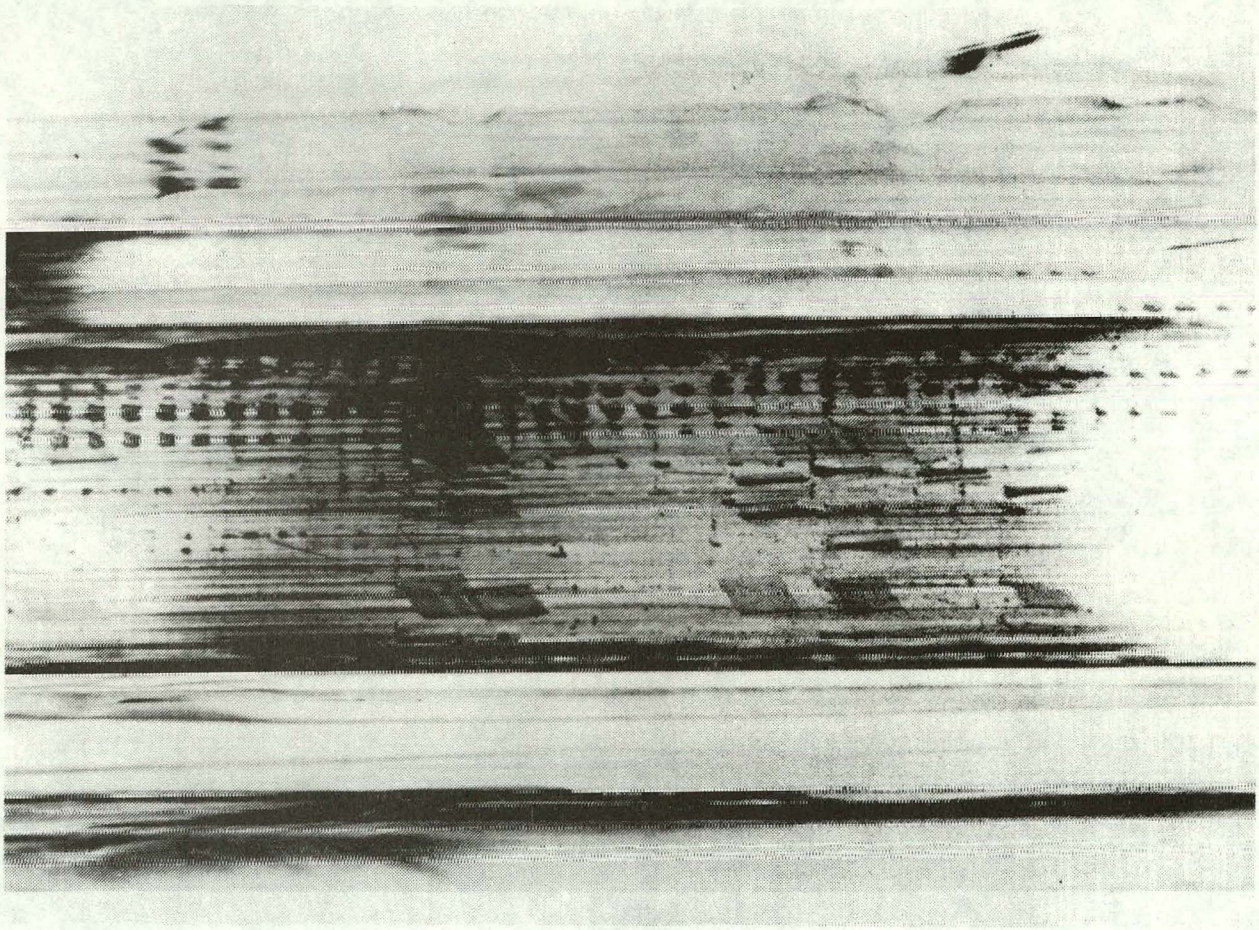

Figure 35. A ($\bar{1}11$) projection topograph of a silicon ribbon grown with a flat pyrolytic BN die (#9-26-75, Section 3). Mag. 8X.

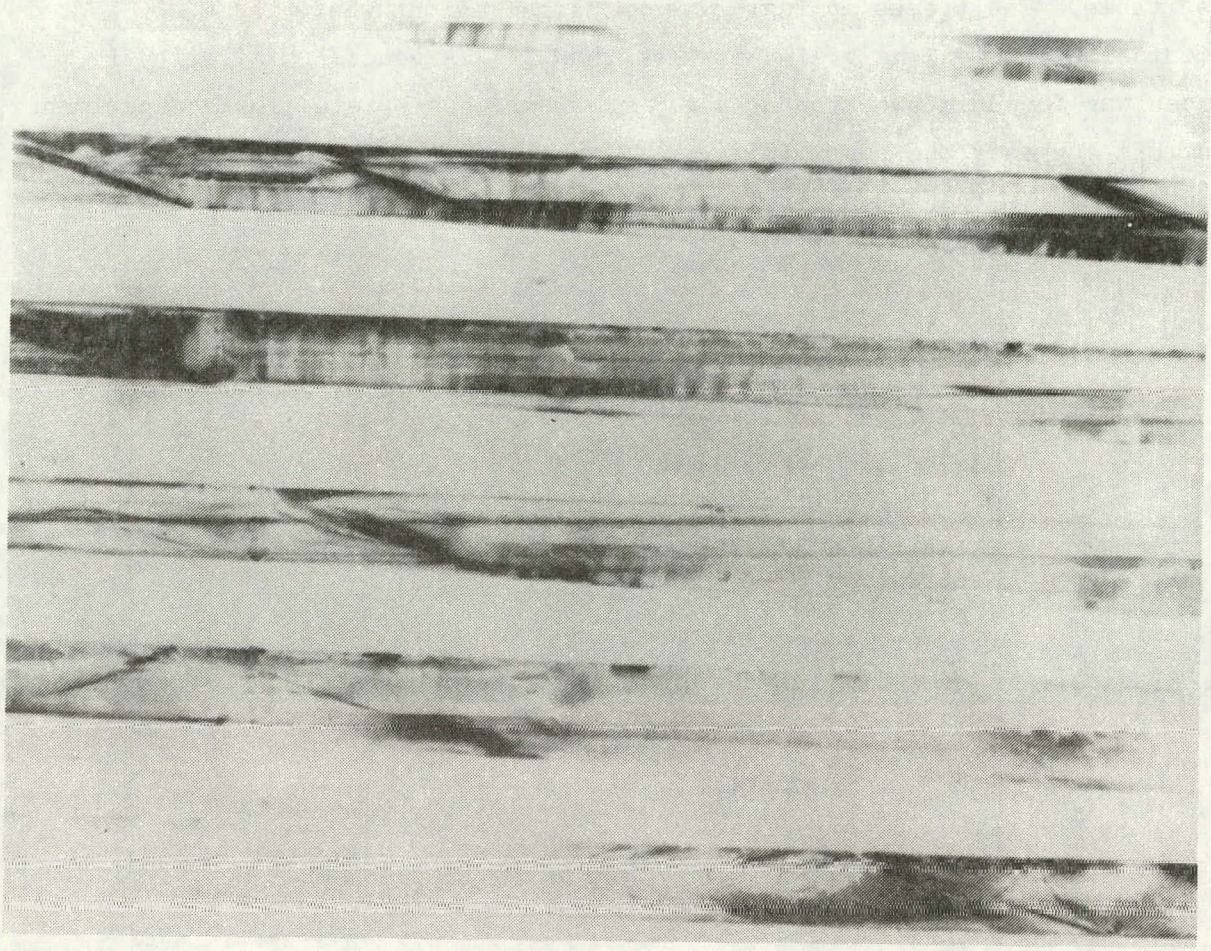

Figure 36. A $(\bar{3}33)$ section topograph of a silicon ribbon shown in Fig. 35. Mag. 28X.

($\bar{3}33$) planes at 0.25-mm intervals across the ribbon. Figure 37 shows the change in orientation in the specimen (#9-26-75, Section 3). The x-ray beam used was only 0.5 mm high and collimated by the 20-μm slit used for section topography. Changes in orientation less than 0.01° are easily observable. The traces in Fig. 37 show large regions where the misorientation between the grains is less than 2°. A general similarity in traces was found in two ribbon specimens from two separate growth experiments, and this suggests the possibility that irregularities in the growth procedure (such as the nonuniformity in the capillary slot) may contribute to the grain structure.

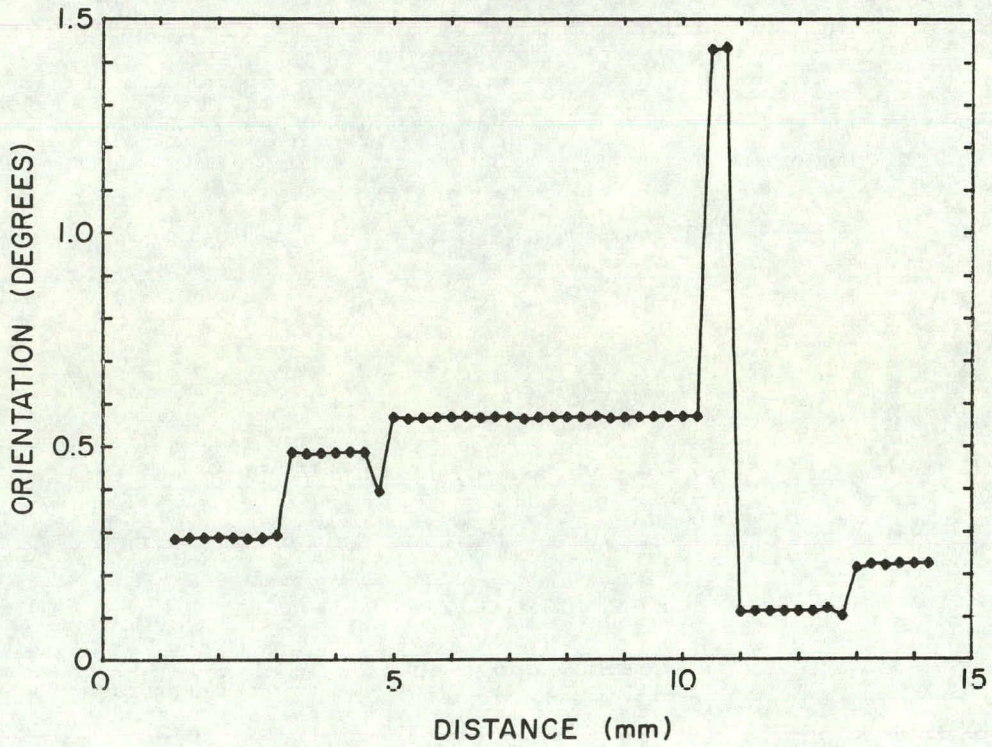

Figure 37. The change is orientation as a function of distance across the silicon ribbon shown in Fig. 35.

The silicon ribbon investigated by the x-ray topography (#9-26-75, Section 3) was Sirtl etched. Photomicrographs were taken from the middle

region of the ribbon, where the defect structure was revealed in the ($\bar{1}11$) projection topograph (see Fig. 35). Typical defects are as follows:

- Grain boundaries parallel to the growth axis [Fig. 38(a)];
- Twin lines parallel to the axis [Fig. 38(b)];
- Surface inclusions which are not associated with defects in the vicinity [Fig. 38(c)];
- Surface inclusions which are associated with line defects [Fig. 38(d)].

In addition to these defects, randomly distributed dislocation etch pits were revealed; the etch pit density was about $6 \times 10^3/cm^3$. Localized defects with associated localized dislocation arrays were observed in the ($\bar{1}11$) topograph (see Fig. 35), but a similar etch pit distribution was not observed. This indicates that the local dislocation arrays do not intersect the ribbon surface.

The origin of the grain and defect formation such as twinning, dislocation, and stacking faults is not understood completely. Systematic investigation of this problem is required with x-ray methods, chemical etching, and other physical characterization techniques.

2. Solar Cells Fabricated in Epitaxially Deposited Silicon

There has been a good deal of discussion and investigation concerning the possibility of fabricating solar cells in epitaxial layers of silicon deposited on ribbon silicon. The rationale is that not all the defects characteristic of the ribbon silicon are propagated into the epi layer. Significantly improved cell efficiencies have been realized by this process [17]. It was also recently reported [18] that a 13% efficient cell has been fabricated in epitaxial silicon deposited on heavily boron-doped ($1 \times 10^{19}/cm^3$) Czochralski silicon. In IS ribbon grown using BN dies, the boron doping has prevented direct use of the ribbon in solar cells. We have not proposed that epitaxial growth be employed with the IS ribbon, and indeed the overall objective of this program is to improve the structure of

17. H. Kressel, R. D'Aiello, P. Robinson, and S. H. McFarlane, "Epitaxial Silicon Technology for Low-Cost Solar Cells," NSF Grant AER 74-15532, Second Interim Report, October 1975.
18. B. F. Williams, at Fourth Project Integration Meeting on Low-Cost Silicon Solar Array Project, ERDA/JPL, Pasadena, Calif., October 27-28, 1976.

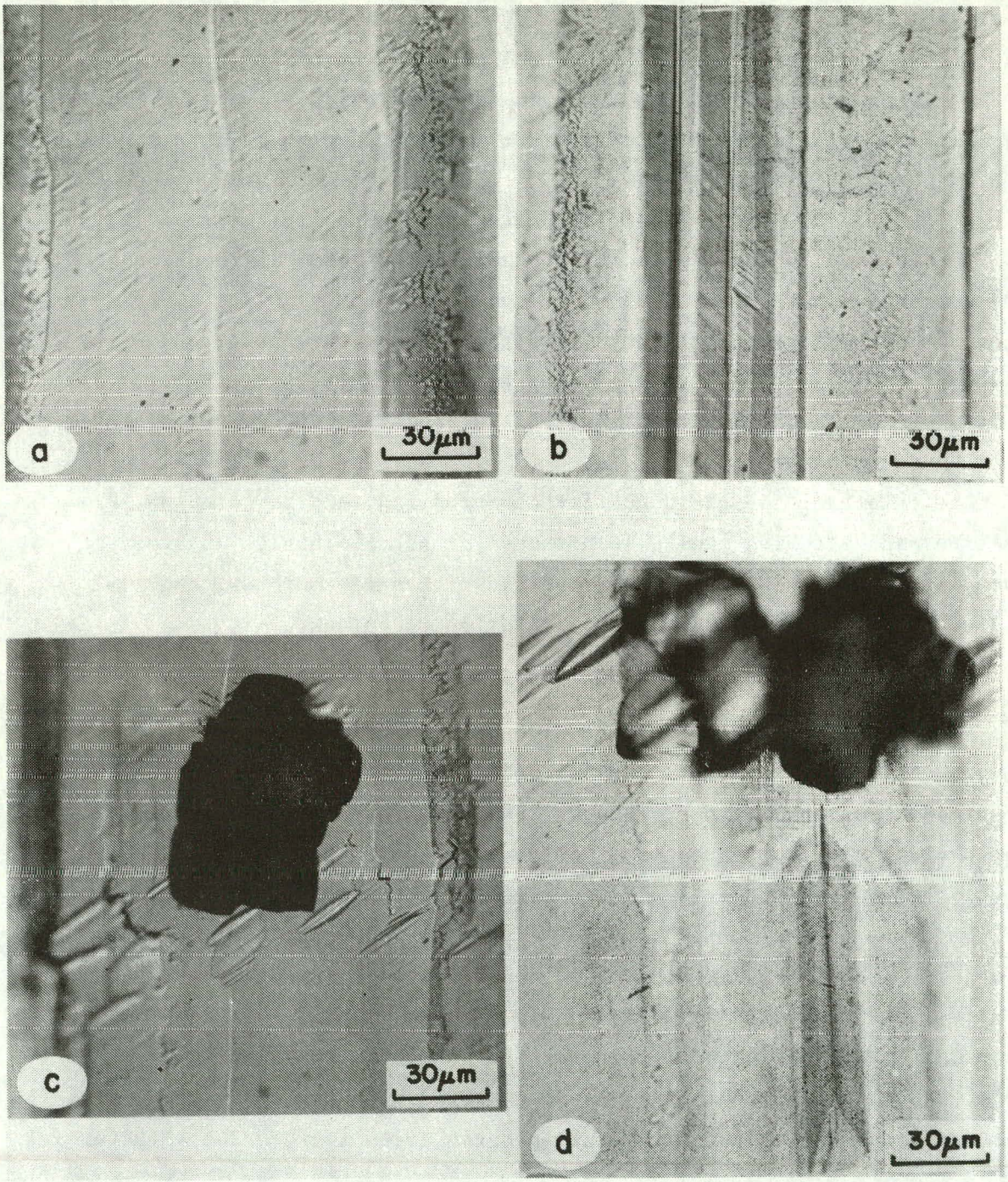

Figure 38. Photomicrographs of a Sirtl etched silicon ribbon investigated in Fig. 35 showing (a) grain boundaries, (b) twins, (c) a recessed inclusion on the surface without related linear defects, and (d) a surface inclusion with a linear defect.

the ribbon by avoiding contamination from the die. There is a real possibility, however, that epitaxy costs can be very significantly reduced. Therefore, we thought it would be interesting to compare characteristics of cells fabricated in silicon deposited on boron-contaminated IS ribbon with the characteristics previously realized in cells fabricated in silicon deposited on EFG ribbon and in silicon deposited on heavily boron-doped Czochralski silicon.

Figure 39 shows one of the two cells fabricated on a 1.5 x 3 cm section of the same ribbon. A 50 μm p-layer (1 x 10^{15} cm^{-3}) was deposited and was followed by 1 μm n-layer (1 x 10^{18} cm^{-3}). An antireflection coating (Ta_2O_3) was applied. The I-V characteristics of the solar cells on the IS and Czochralski reference wafer are plotted in Fig. 40. The measured data of the cell parameters are reproduced in Table 8. The efficiencies of the two IS cells (AM1) were 8.1 and 8.2%, while the Czochralski cell had an efficiency of 10.2%.

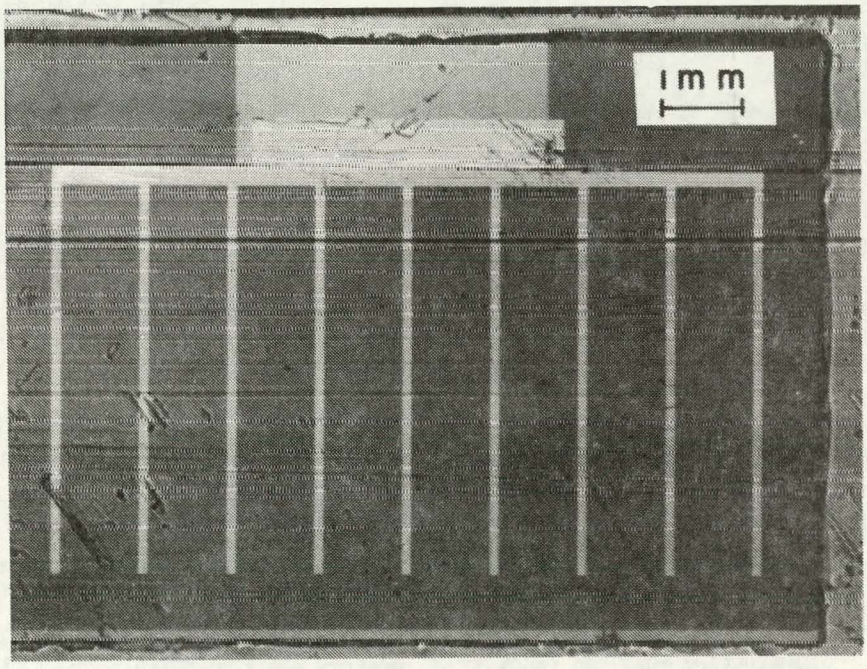

Figure 39. Photomicrograph of a solar cell fabricated in the epitaxially grown layer on a silicon ribbon grown with BN die.

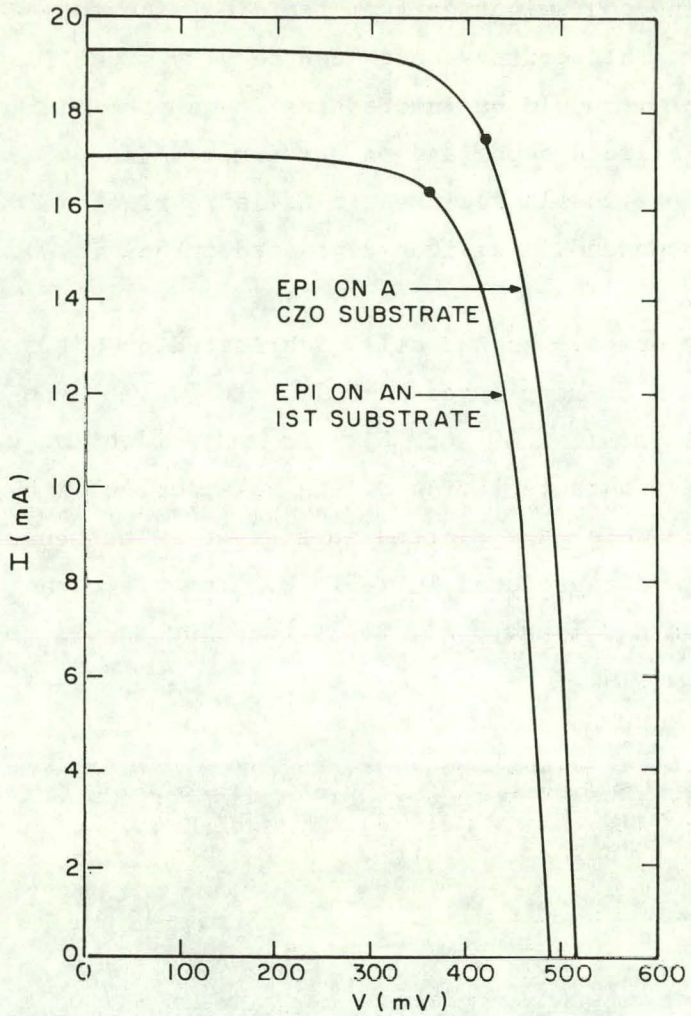

Figure 40. I-V characteristics of the epitaxial solar cells on a silicon ribbon grown with BN die and a Czochralski silicon wafer.

TABLE 8. MEASURED VALUES OF THE SOLAR CELL PARAMETERS

Sample/Cell	J_{SC} (mA/cm^2)	V_{OC} (mV)	P_{MAX} (mW/cm^2)	F.F.	η (%)
Epi IS Cell 1	22.8	488	7.9	0.708	8.2
Epi IS Cell 2	22.8	492	7.8	0.694	8.1
Czochralski	25.7	514	9.8	0.742	10.2

The epitaxial cell structure was not optimized. The efficiencies can be improved by grading the doping level. It has been established that the carrier collection and cell efficiency can be increased by building in the impurity gradient in the base region to provide a drift field for enhanced carrier transport to the collecting p-n junction [17]. The efficiencies of the epitaxial solar cells on the EFG silicon ribbons with the similar structure are reported to be about 8% on the average [17]. The minority carrier lifetime was 0.3 to 0.5 μs and 0.8 μs for the IS and Czochralski based cells, respectively.

B. RIBBONS GROWN WITH COMPOSITE DIES COATED WITH CVD Si_3N_4

The crystalline structure of the silicon ribbons grown using composite CVD Si_3N_4 coated dies was characterized by x-ray topography. Projection and section topographs were taken by using MoK_α radiation.

Figure 41 is an x-ray projection topograph of a silicon ribbon grown using a composite die of UT-8 (AG) coated with ~50 μm CVD Si_3N_4. The ribbon surface is (011) and the growth direction is $[\bar{2}11]$, vertically upward on the page. Topograph (a) was taken with the $(\bar{1}1\bar{1})$ diffracting plane which is parallel to the growth direction and perpendicular to the surface. Topograph (b) was taken with the $(11\bar{1})$ diffracting plane which is ~70° from the growth direction and perpendicular to the surface. The vertical white grains in (b) are twinned regions which are not evident in (a), since the twin plane is also the diffracting plane in (a). The same region of the ribbon is shown in both topographs. The major feature of the ribbon is a series of parallel grains running along the growth direction. The misorientation of the grains should be small, within 0.1°, since the Bragg condition for diffraction is met to give the contrast. Some grains have resolvable dislocation structure, while some have a level of strain which obscures any further detail.

Figure 42 shows section topographs of the same silicon ribbon as in Fig. 41. Topographs in (a) were taken with the $(\bar{1}1\bar{1})$ diffracting plane. Different grains of the ribbon are imaged, and the quality of the ribbon varies among the grains. Topographs in (b) were taken with the $(11\bar{1})$ diffracting plane, and each topograph cuts across several grains of the

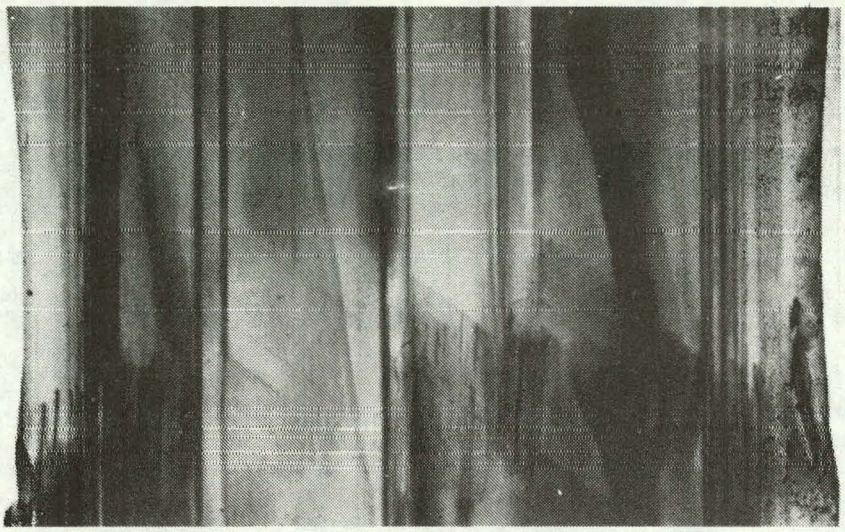

(a)

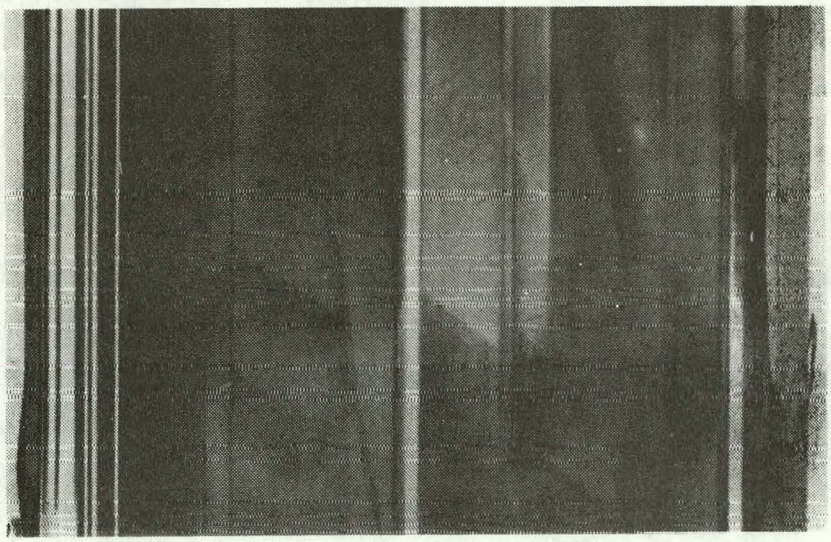

(b)

Figure 41. X-ray projection topograph of a silicon ribbon grown with a composite die coated with CVD Si_3N_4 on UT-8 (AG). (a) [1̄1̄1], and (b) [111] diffraction. Mag. 5X.

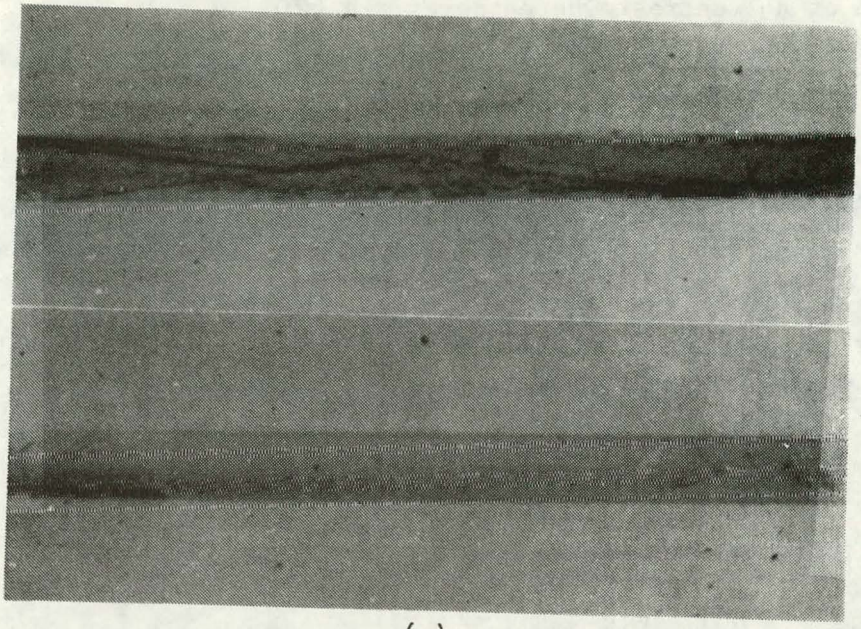

(a)

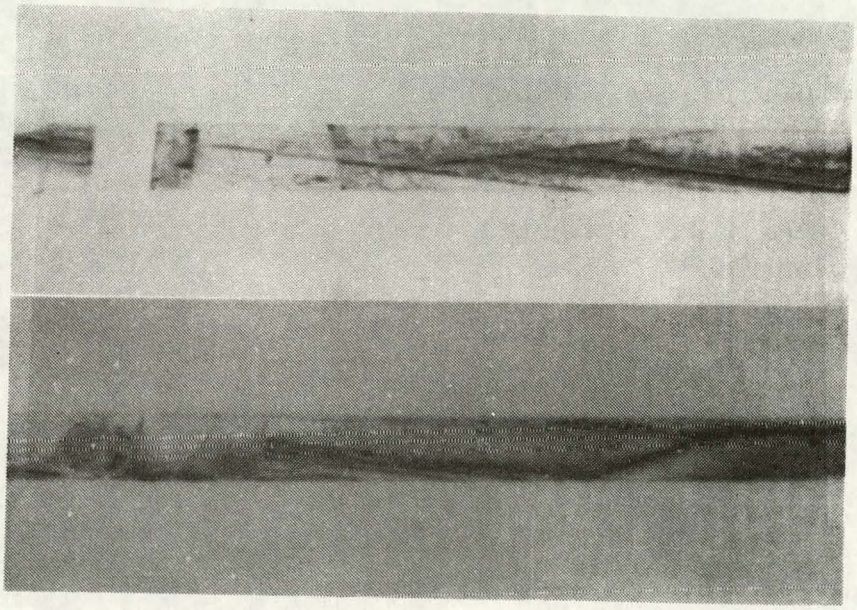

(b)

Figure 42. X-ray section topograph of a silicon ribbon shown in Fig. 41. (a) [111], and (b) [11$\bar{1}$] diffraction. Mag. 5X.

ribbon. The relative good and bad quality of the grains is evident as well as the region of no contrast where there is a twin.

The resistivity of the silicon ribbons grown with the composite dies is 0.02 to 0.2 ohm-cm. The low resistivity is the result of the contamination of our growth system. Thin plates of pyrolytic BN plate are used as the insert between the V-shaped crucible-die and the inner susceptor wall (see Section III.A.4). This is a precautionary measure to prevent contact of the liquid silicon with the susceptor as the result of a leak. The BN insert is a major source of contamination. More recently we have been able to maintain the melt in the system at a level of 80 ohm-cm (p-type) by removal of all BN parts.

SECTION VII

CONCLUSIONS

The feasibility of growing silicon ribbons by the inverted ribbon growth process has been established using both nonwetting BN dies and wetting composite dies with a CVD Si_3N_4 surface. Both a flat die and a V-shaped crucible-die configuration have been employed. Ribbon growth using nonwetting and wetting dies in the inverted configuration can be identified as the inverted Stepanov and inverted EFG process.

Use of the nonwetting SiO_2 die in the inverted Stepanov configuration was more difficult than originally anticipated. Even though the SiO_2 die slot in the V-shaped crucible-die arrangement was readily filled with the liquid silicon, ribbon growth was not stable. Immediately after the ribbon growth was initiated, the ribbon thickness increased, and the width decreased. Extensive modifications of the growth conditions did not completely alleviate the growth instabilities. These modifications included thermal trimming, application of the hydrostatic pressure and various die designs. The problems experienced in the use of the SiO_2 dies are associated primarily with the formation and evolution of SiO at the interface between the liquid silicon and silica die. The SiO evolution causes the hysteresis of the contact angle and vibration at the melt surface and meniscus. This prevents shaping or "pinning" the meniscus at the die edge. While the growth instabilities with SiO_2 die are not necessarily insurmountable, we felt that the investigation of other die materials in the inverted ribbon growth configuration would be more productive within the time frame of the overall JPL program, particularly for the growth of thin ribbons.

The reactivity of the liquid silicon with various die materials has been investigated. This effort was initiated under a separate in-house program and was folded into the contract effort in December 1976. CVD Si_3N_4 and CVD $Si_3O_xN_y$ were found to be promising as die materials and are considerably more resistant to reaction with and/or dissolution in the molten silicon than other materials examined to date. CVD Si_3N_4 has a contact angle of 53° with the liquid silicon. Reaction-sintered Si_3N_4 and graphite, such as UT-8 (AG), proved to be suitable as the substrate material to coat with CVD Si_3N_4. Stable growth of silicon ribbons

(2 cm wide, ~0.05 cm thick) was achieved by the inverted EFG process using curved dies coated with the CVD Si_3N_4. The radius of the curvature at the die edge was 8.9 cm.

The growth orientation of the silicon ribbons is (011)[$\overline{2}11$]. Low angle grains with misorientations within 0.1° and twins parallel to the growth axis were observed in the ribbons grown with the composite CVD Si_3N_4 coated dies. The resistivity of the ribbons was low (~0.020 ohm-cm); this was due to the contamination of the growth system, which can be eliminated. Because of the low resistivity, it was not feasible to construct solar cells directly in the grown ribbon.

Solar cells made in the epitaxially deposited silicon on a silicon ribbon grown by the inverted Stepanov process with the BN flat die had an efficiency of 8.2%, while the efficiency in the Czochralski control wafer was 10.2%. The minority carrier lifetime was 0.3 to 0.5 μs and 0.8 μs for the IS and Czochralski based cells, respectively.

The results of our thermal model for the inverted Stepanov growth process show that for a given set of ambient conditions and ribbon geometry, as the growth velocity increases, so does the height of the molten zone. The maximum growth velocity is that velocity which leads to the generation of latent heat of fusion at a rate just equal to the rate at which heat can be dissipated from the ribbon to the ambient. Our model shows that as this velocity is approached, at constant die temperature, the height of the molten zone diverges rapidly. The particular numerical values for the maximum growth velocity which our model predicts are, of course, specific to the particular ambient conditions which have been defined for the model. In practice, the maximum growth rates may be increased, primarily by design of the growth chamber which would lead to increased convective heat transfer or increased conducted heat loss to the ribbon clamp. In such a case excessive curvature in the ribbon temperature profile may lead to excessive stress in the ribbon; however, with the thermal model it can be seen that in principle the thermal profile can be linearized by adjusting the ambient temperature profile in the growth chamber.

REFERENCES

1. A. V. Stepanov et al., Bull. Acad. Sci. USSR, Phys. Series 33, 1826 (1969); A. V. Stepanov, Transl, Soviet Phys. Technical Physics 29, 339 (1959).

2. J. C. Schwartz, T. Surek, and B. Chalmers, J. Electronic Mat. 4, 555 (1975); H. E. Bates, F. H. Cocks, and A. I. Mlavsky, "Thick Film Silicon Growth Techniques," NAS7-100/JPL-953365, First Quarterly Progress Report, July 1972.

3. T. F. Ciszek, Mat. Res. Bull. 7, 731 (1972).

4. P. C. Goundry and J. C. Boatman, "Investigation of Single Crystal Si Ribbon," AFAL-TR-66-312, Part I, Sept. 1966, and Part II, Oct. 1967.

5. B. Chalmers et al., "Continuous Silicon Solar Cells," NSF Grant GI-37067X, Final Report, 1975.

6. T. Surek, J. Appl. Phys. 47, 4384 (1976).

7. A. E. Bell, RCA Review 38, 109 (1977).

8. R. W. Gurtler and A. Baghdadi, "Laser Zone Growth in a Ribbon-to-Ribbon (RTR) Process," Quarterly Report No. 1, ERDA/JPL/954376-76/1, March 1976.

9. H. S. Carlsaw and J. C. Jaeger, *Conduction of Heat in Solids* (Clarendon Press, Oxford, England, 1959).

10. M. Neuberger et al., "Silicon," Hughes Aircraft Co., Culver City, Colorado, AD698342.

11. Y. S. Touloukian et al., Eds., *Thermophyscial Properties of Matter* (IFI/Plenum Press, New York, 1970).

12. A. I. Brown and S. M. Marco, *Introduction to Heat Transfer* (McGraw-Hill Book Co., New York, 1942).

13. B. Carnahan, H. A. Luther, and J. O. Wilks, *Applied Numerical Methods* (John Wiley and Sons, New York, 1969).

14. G. K. Gaulé, and J. R. Pastore, in *Metallurgy of Elemental and Compound Semiconductors*, R. O. Gruble, Ed., (Interscience Publ., Inc., New York, 1961).

15. R. J. Jaccodine, J. Electrochem. Soc. 110, 524 (1963).

16. D. Turnbull, J. Appl. Phys. 21, 1022 (1950).

17. H. Kressel, R. D'Aiello, P. Robinson, and S. H. McFarlane, "Epitaxial Silicon Technology for Low-Cost Solar Cells," NSF Grant AER 74-15532, Second Interim Report, October 1975.

18. B. F. Williams, at Fourth Project Integration Meeting on Low-Cost Silicon Solar Array Project, ERDA/JPL, Pasadena, Calif., October 27-28, 1976.

☆U.S. GOVERNMENT PRINTING OFFICE: 1978-740-094/1373